

INVESTIGATION OF STATISTICAL SEISMOLOGY IN THAILAND-LAOS-MYANMAR BORDERS



A Thesis Submitted in Partial Fulfillment of the Requirements

for the Degree of Master of Science in Geology

Department of Geology

FACULTY OF SCIENCE

Chulalongkorn University

Academic Year 2021

Copyright of Chulalongkorn University

การสำรวจวิทยาคลื่นไหวสะเทือนเชิงสถิติบริเวณชายแดนประเทศไทย-ลาว-พม่า



วิทยานิพนธ์นี้เป็นส่วนหนึ่งของการศึกษาตามหลักสูตรปริญญาวิทยาศาสตรมหาบัณฑิต

สาขาวิชาธรณีวิทยา ภาควิชาธรณีวิทยา

คณะวิทยาศาสตร์ จุฬาลงกรณ์มหาวิทยาลัย

ปีการศึกษา 2564

ลิขสิทธิ์ของจุฬาลงกรณ์มหาวิทยาลัย

Thesis Title INVESTIGATION OF STATISTICAL SEISMOLOGY IN
 THAILAND-LAOS-MYANMAR BORDERS
By Miss Manunchaya Neanudorn
Field of Study Geology
Thesis Advisor Professor Dr. SANTI PAILOPLEE

Accepted by the FACULTY OF SCIENCE, Chulalongkorn University in Partial
Fulfillment of the Requirement for the Master of Science

..... Dean of the FACULTY OF SCIENCE
(Professor Dr. POLKIT SANGVANICH)

THESIS COMMITTEE

..... Chairman
(Assistant Professor Dr. VICHAI CHUTAKOSITKANON)

..... Thesis Advisor
(Professor Dr. SANTI PAILOPLEE)

..... Examiner
(Professor Dr. MONTRI CHOOWONG)

..... External Examiner
(Dr. Songkhun Boonchaisuk)

มัญญา แน่นอุดร : การสำรวจวิทยาคลื่นไหวสะเทือนเชิงสถิติบริเวณชายแดนประเทศไทย-ลาว-พม่า. (INVESTIGATION OF STATISTICAL SEISMOLOGY IN THAILAND-LAOS-MYANMAR BORDERS) อ.ที่ปรึกษาหลัก : ศ. ดร.สันติ ภัยหลบลี้

วัตถุประสงค์ของการศึกษาคั้งนี้มุ่งเน้นที่การสำรวจวิทยาคลื่นไหวสะเทือนเชิงสถิติในบริเวณชายแดนไทย-ลาว-พม่า โดยสำรวจพฤติกรรมการเกิดแผ่นดินไหวและหาพื้นที่เสี่ยงต่อการเกิดแผ่นดินไหวในอนาคต ข้อมูลที่ใช้ในงานวิจัยนี้เป็นฐานข้อมูลแผ่นดินไหวจากกรมอุตุนิยมวิทยา หลังจากตรวจสอบและปรับปรุงข้อมูลในทางสถิติแล้วจึงนำมาใช้ การศึกษาพฤติกรรมการเกิดแผ่นดินไหว โดยประยุกต์ใช้สมการความสัมพันธ์การกระจายตัวความถี่-ขนาดแผ่นดินไหว ผลการศึกษาคือ บริเวณจังหวัดน่าน ประเทศไทย และ บริเวณทางตอนใต้ของเมืองหลวงพระบาง ประเทศลาวเป็นบริเวณที่พฤติกรรมการเกิดแผ่นดินไหวสูงที่สุด โดยสามารถเกิดแผ่นดินไหวขนาดใหญ่ที่สุดขนาด 5.1, 5.6, 6.3, 6.1 ในอีก 5, 10, 30, 50 ปี และมีคาบอุบัติซ้ำสำหรับแผ่นดินไหวขนาด 4.0, 5.0, 6.0 และ 7.0 ในอีก 1, 5, 20, และ 75 ปีตามลำดับและโอกาสเกิดแผ่นดินไหวขนาด 4.0, 5.0, 6.0 และ 7.0 คือ 100 %, 100 %, 70 – 100 % และ 20 – 60 %, ตามลำดับ การหาพื้นที่เสี่ยงต่อการเกิดแผ่นดินไหวในอนาคต โดยใช้สามวิธีคือ ความเค้นทางธรณีแปรสัณฐาน หรือ ค่าคงที่ b การเปลี่ยนแปลงอัตราการเกิดแผ่นดินไหว หรือ ค่าคงที่ Z และ ระเบียบพื้นที่-เวลา-ความยาวรอยเลื่อน หรือ คะแนน RTL จากการทดสอบทั้งหมดได้ตัวแปรและสัญญาณบอกเหตุที่สามารถระบุพื้นที่เสี่ยงภัยก่อนเกิดแผ่นดินไหวได้ และนำบริเวณพื้นที่เสี่ยงภัยจากทั้งสามสัญญาณบอกเหตุ มาซ้อนทับกันสามารถบอกได้ว่าบริเวณชายแดนประเทศไทย-พม่า และ บริเวณจังหวัดน่าน ประเทศไทย และ ทางตะวันตกของหลวงพระบาง ประเทศลาว เป็นพื้นที่เสี่ยงมากที่สุดที่สามารถเกิดแผ่นดินไหวได้ในอนาคต

สาขาวิชา ธรณีวิทยา

ปีการศึกษา 2564

ลายมือชื่อนิสิต

ลายมือชื่อ อ.ที่ปรึกษาหลัก

6270094423 : MAJOR GEOLOGY

KEYWORD: Seismic pattern, Earthquake activity, Precursory Seismic Quiescence,
Seismotectonic stress, Seismicity rate change

Manunchaya Neanudorn : INVESTIGATION OF STATISTICAL SEISMOLOGY IN
THAILAND-LAOS-MYANMAR BORDERS. Advisor: Prof. Dr. SANTI PAILOPLEE

The purpose of this research is to understand more about the statistical seismology of the Thailand-Laos-Myanmar border in order to monitor earthquake activity and locate potentially dangerous area. The seismicity data was collected from the Thailand Meteorological Department. Following that, the catalog's homogeneity and completeness were improved. The first step is to identify the earthquake activity by using the adaptive frequency-magnitude distribution. The results are that Nan province, Thailand, and south Luang Prabang, Laos are the highest activity areas which can generate a maximum magnitude of 5.1 M_L , 5.6 M_L , 6.3 M_L , and 6.7 M_L in 5, 10, 30, 50 years. The return period with the M_L of 4.0, 5.0, 6.0, and 7.0 was 1, 5, 20, and 75 years. The probability of the occurrence of the earthquake with the M_L of 4.0, 5.0, 6.0, and 7.0 was 100%, 100%, 70-100%, and 20-60%, respectively. Then, identify the prospective area using three methods: b value, Z value, and RTL algorithm. After performing iterative tests on three methods with the appropriate parameter, reasonable estimates of the anomalous precursors. Overlaying maps of those three methodologies makes it possible to identify prospective places for a coming major earthquake. The Thailand-Myanmar border region, Nan province, Thailand, and southwest of Luang Prabang, Laos are the most risk areas for the earthquake in the future.

Field of Study: Geology

Student's Signature

Academic Year: 2021

Advisor's Signature

ACKNOWLEDGEMENTS

Throughout the writing of this thesis and seminar, I have received a lot of help and guidance from the professor, family, and friends.

I would like to begin by expressing my gratitude to my advisor, Professor Dr. Santi Pailoplee, for his essential assistance in developing the study topics and methodology. His informative remarks pushed me to improve my thoughts and elevate my work. He is not only assisting me with this task, but also with my mental health during this auspicious time.

I would want to express my gratitude to all the lecturers in the Petroleum Geoscience program and the Department of Geology at Chulalongkorn University for their unwavering support and assistance during my time at university.

Additionally, I would like to express my gratitude to my parents for their wise guidance and sympathetic ear. They are always available to me. Last but not least, I could not have finished this thesis without the help and encouragement of my friends and coworkers.

Finally, I heartfelt thanks go out to my partner in crime who helped in the entire study directly and indirectly for his constructive advisory and endless support.

จุฬาลงกรณ์มหาวิทยาลัย
CHULALONGKORN UNIVERSITY

Manunchaya Neanudorn

TABLE OF CONTENTS

	Page
ABSTRACT (THAI).....	iii
ABSTRACT (ENGLISH).....	iv
ACKNOWLEDGEMENTS	v
TABLE OF CONTENTS	vi
LIST OF TABLES	x
LIST OF FIGURES	xi
CHAPTER 1 INTRODUCTION.....	18
1.1 Background.....	18
1.2 Study Area	30
1.3 Objective.....	31
CHAPTER 2 THEORY AND METHODOLOGY.....	32
2.1 Theory.....	32
2.1.1 Seismotectonic Stress (b value).....	32
2.1.2 Seismic Pattern (D_c value).....	33
2.1.3 Seismicity Rate Change (Z value)	34
2.1.4 Seismic Quiescence (RTL Algorithm).....	37
2.2 Literature Review.....	38
2.2.1 Earthquake Activities in the Thailand-Laos-Myanmar Border.....	38
2.2.2 Spatial and Temporal of b value Anomalies	39
2.2.3 Regional Variations and Correlations of Gutenberg–Richter Parameters and Fractal Dimension.....	39

2.2.4 Precursory Seismic Quiescence before the earthquake	41
2.2.5 Applied region–time–length algorithm.....	42
2.3 Methodology.....	44
2.3.1 Thesis Preparation	45
2.3.2 Completeness Data.....	45
2.3.3 Earthquake Activity.....	45
2.3.4 Seismotectonic Stress.....	45
2.3.5 Seismic Pattern.....	45
2.3.6 Seismic Quiescence.....	46
2.3.7 Discussion	46
2.3.8 Conclusion.....	46
CHAPTER 3 DATA COMPLETENESS	47
3.1 Collecting the Earthquake Catalogue	47
3.2 Earthquake Declustering.....	49
3.3 Genetic Network Analytic System.....	49
CHAPTER 4 EARTHQUAKE ACTIVITY	52
4.1 Earthquake Frequency-Magnitude Distribution	52
4.2 Maximum Magnitude	55
4.3 Return Period	57
4.4 Probability of Occurrence.....	59
CHAPTER 5 SEISMOTECTONIC STRESS AND SEISMIC PATTERN.....	61
5.1 Seismotectonic Stress	61
5.2 Seismic Pattern	67
CHAPTER 6 SEISMIC QUIESCENCE.....	69

6.1 Seismicity Rate Change	69
6.1.1 Temporal investigation	69
6.1.2 Spatial investigation.....	75
6.2 Region-Time-Length Algorithm	81
6.2.1 Temporal investigation	81
6.2.2 Spatial investigation.....	87
CHAPTER 7 DISCUSSION	92
7.1 Earthquake Activity	92
7.2 Seismic Pattern	95
7.3 Evolution of Stress Transfer.....	96
7.4 Tectonic Stress in Present Day.....	98
7.5 Quiescence Time Span of Z value	99
7.6 Present Quiescence Map from Z value.....	100
7.7 The Starting of Seismic Quiescence from Seismicity Rate Change(Z value).....	101
7.8 Stochastic of Z value.....	102
7.9 Quiescence time span of RTL Algorithm.....	103
7.10 Present Quiescence Map from RTL algorithm	104
7.11 The Starting of Seismic Quiescence of RTL Algorithm	105
7.12 Correlation Coefficient of RTL Score.....	106
7.13 Forecasting Prospective Area.....	109
CHAPTER 8 CONCLUSION.....	3
REFERENCES	6
VITA.....	13

LIST OF TABLES

	Page
Table 1.1. The classification of earthquake predictions.....	19
Table 1.2. Summary of active fault zone earthquake potential criteria used in seismic hazard assessments in Thailand and neighbouring areas.	22
Table 3.1. Example of Earthquake catalogue in TLMB.	47
Table 5.1. List earthquakes with a magnitude (M_L) greater than 5.0 that occurred along the TLMB between 2010 and 2020.	62
Table 6.1. The lists of strong-to-major earthquakes ($M_L \geq 5.0$) that occurred within the TLMB from 2010 to 2020, as well as the results from the Z value investigation using $N = 25$ events and $T_w = 1.5$ years.....	70
Table 6.2. The lists of strong-to-major earthquakes ($M_L \geq 5.0$) that occurred within the TLMB from 2010 to 2020 and the RTL algorithm investigation results using $r_0 = 90$ km and $t_0 = 2$ years.....	82
Table 7.1. Examples of correlation coefficients of the RTL scores obtained with different utilized r_0 and t_0 values for the M_L 5.2 earthquake on May 5 th , 2014. Case A represents the parameters utilized in this study, whereas case B represents the other nearby parameters recognized for correlation.....	107
Table 7.2. Legend of the map in Figure 7.18 showing the prospective area in TLMB... 1	

LIST OF FIGURES

	Page
Figure 1.1. A map shows mainland Southeast Asia along with the 13 seismic zones that have been established (A to M).The map shows the locations of the epicenters of completeness earthquakes with $m_b \geq 4.0$ reported from 1974 to 2010 (green circles), completeness earthquakes with $m_b \geq 7.0$ (blue circles), and important earthquakes mentioned in the text (red circles). Red lines denote the fault lines compiled by Pailoplee et al. (2009). Grey polygons represent the geometry of the postulated seismic source zones by Pailoplee and Choowong (2013).....	20
Figure 1.2. Maps of mainland Southeast Asia showing (a) Active faults in Thailand and neighbouring areas interpreted from remote sensing data (IKONOS, LANDSAT, and MODIS) and a previous study (b) an enlarged map was interpreting active faults in northern Thailand and neighbouring areas.....	21
Figure 1.3. The photo shows the damage established by The M_w -6.8 Tarlay earthquake on March 24 th , 2011, in Myanmar. (https://upload.wikimedia.org).....	25
Figure 1.4. The photo shows the damage establishment by The M_w -6.3 Mae Lao earthquake on May 5 th , 2014, in Chiang Rai, Thailand (https://www.asiaone.com/).....	25
Figure 1.5. Distribution of b value along the TLMB in (a) 1984-1995, (b) 1984-2000, (c) 1984-2005, and (d) 1984-2010.The red star indicates earthquakes greater than 5.0 that occurred after the data collection. (Pailoplee et al., 2013).	26
Figure 1.6. Distribution of b value along the Indonesian island chain between (a) 1980-2000 and (b) 1980-2005. The red star indicates earthquakes greater than 7.0 that occurred five years after the earthquake data collection (Pailoplee, 2014b).	27
Figure 1.7. (a) Topographic map of the study area with significant faults and earthquakes (b) Map of the spatial distribution of Z statistic before the 6.1 M_w earthquake in 2008 in South Iran.The white star indicates the epicenter of the 2008 Qeshm main shock. The red colour indicates a positive Z value, which corresponds	

to a drop in seismicity rate, whereas the blue colour indicates an increase in seismicity rate. (Sorbi et al., 2012)	28
Figure 1.8. The spatial distribution in the RTL algorithm at the Sumatra-Andaman. (a) from November 2002 to August 2004. (b) from April 1996 to October 1998.....	29
Figure 1.9. (a) Map of Thailand and neighbouring countries indicating the study area. (b) Map displays the complete seismicity catalogue epicenters distribution along TLMB from 2010 and 2020.	30
Figure 2.1. illustrates (a) a uniformity seismicity rate and (b) a cumulative number of earthquakes plot against time. (Bachmann, 2001)	35
Figure 2.2 illustrates (a) a uniformity seismicity rate with quiescence interval and (b) a cumulative number of earthquakes with quiescence interval plot against time.(Bachmann, 2001).....	35
Figure 2.3. Schematic explanation of how to calculate the Z value (Öztürk and Bayrak, 2011).....	36
Figure 2.4. The diagrams illustrating the spatial distribution of seismic quiescence at the position (x, y, z) show (a) the R_{max} , (b) The V_{RTL} curve, and (c) the seismic quiescence map in the shaded region (Puangjaktha and Pailoplee, 2016).....	38
Figure 2.5. The spatial distribution of b value and epicenters of earthquakes was reported by the USGS between January 1 st , 2000, and December 25 th , 2004. The stars indicate the positions of the two most significant shocks (before the December 26 th , 2004, earthquake) on October 24 th , 2002, the M_s -7.1 (upper star), and November 2 nd , 2002, the M_s -7.6 (lower star). b) Spatial distribution of b value. The magnitudes M_s (left) and M_w (right) were employed. Low b is represented by blue, whereas high b is represented by red. White dots show the epicentral sites. (Nuannin, 2005)	40
Figure 2.6. (a) The epicenters of earthquakes with a magnitude more than 3.5 for the last 50 years and 15 different seismogenic zones in Western Anatolia. (b) b values , and (c) D_c values (Bayrak and Bayrak, 2012).	41

Figure 2.7. Cumulative number (black line) and Z value (blue line) plots for anomalous areas at Tokachioki, Japan. (Katsumata, 2011).....	42
Figure 2.8. Temporal variation in the RTL function at the epicenter of the 1999 Chi-Chi earthquake. The bar chart depicts the incidence of earthquakes greater than 5.5 that occurred within a typical distance of $2r_0$ from the epicenter of the Chi-Chi main shock; the number next to each bar indicates the magnitude. Seismic activity began in 1993, while seismic quiescence began in 1997 (Chen and Wu, 2006).	43
Figure 2.9. A simplified flow chart illustrating the eight steps of the methodology used in this study.	44
Figure 3.1. The photos from the ZMAP program (Wiemer, 2001) show the histogram graph of the earthquake catalogue from TMD during 2007-2020 (a) magnitude histogram, (b) depth histogram, (c) date histogram, and d) hour histogram.....	48
Figure 3.2. The photos from the ZMAP program (Wiemer, 2001) show the details of the earthquake catalogue from TMD from 2007 to 2020 after declustering.....	50
Figure 3.3. The photos from the ZMAP program Wiemer (2001) show the details of the earthquake catalogue from TMD during the period 2007-2020 after declustering and GENAS.....	50
Figure 3.4. Cumulative number graph showing the (a) seismicity detected from TMD during period 2007-2020 (b) the earthquake catalogue after declustering and (c) the earthquake catalogue after declustering and GENAS.	51
Figure 4.1. FMD plot of the earthquake catalogue from TMD from 2007 to 2020. White squares show the cumulative number of earthquakes equal to or larger than each magnitude, Grey squares shows the number of earthquakes of each magnitude and solid lines are the lines of best fit, following Woessner and Wiemer (2005). M_c defined as the magnitude of completeness.....	52
Figure 4.2. Spatial distributions of the (a) a value, (b) value, (c) standard deviation of b value, and (d) Percent of the goodness fit of the FMD (white dots are earthquake epicenters).....	54

- Figure 4.3. Map of TLMB showing the maximum earthquake magnitude generated in the particular period of the next (a) 5, (b) 10, (c) 30, and (d) 50 years..... 56
- Figure 4.4. Map of the TLMB showing the recurrence interval of earthquakes with an individual M_L of (a) 4.0, (b) 5.0, (c) 6.0, and (d) 7.0 58
- Figure 4.5. Map of the TLMB showing probabilities of an earthquake with a magnitude of (a) 4.0, (b) 5.0, (c) 6.0, and (d) 7.0 M_L that could be generated in the next 50 years. 60
- Figure 5.1. Distribution of b value along the TLMB between (a) 2000-2012, (b) 2000-2014, (c) 2000-2016, and (d) 2000-2018. The red stars indicates earthquakes greater than 5.0 that occurred after the data collection and the white dots are the epicenters..... 64
- Figure 5.2. Distribution of Standard deviation of b value along the TLMB between (a) 2000-2012, (b) 2000-2014, (c) 2000-2016, and (d) 2000-2018. The black star indicates earthquakes with a magnitude greater than 5.0 that occurred after the period for gathering earthquake data and the white dots are the epicenters. 65
- Figure 5.3. Distribution of percent of goodness fit of b value along the TLMB between (a) 2000-2012, (b) 2000-2014, (c) 2000-2016, and (d) 2000-2018. The red star indicates earthquakes greater than 5.0 that occurred after the data collection and the white dots are the epicenters. 66
- Figure 5.4. The spatial distribution of D_c value with the radius 150 km from fractal dimension..... 67
- Figure 6.1. (a-m) the graph plot between the cumulative number of earthquakes (grey line) and Z value (black line) plotted against time. The black stars indicate the time of each earthquake occurrence. The transparent grey strip illustrates the Z value anomaly, which is recognized as the quiescence stage..... 74
- Figure 6.2. The spatial distribution of a-m the Z values for thirteen of nineteen large earthquakes (nos. 6-13 and 15-19 in Table 6.1) during the time slice of seismic quiescence determined from the temporal investigation are depicted on a map of

the TLMB. The colors red and blue represent a decrease (+Z) and an increase (-Z) in seismicity rate, respectively. Black stars show the epicenter of the earthquake case study.....	80
Figure 6.3. (a-i) Temporal variation of the RTL score (grey line) of nine strong-to-major earthquakes recognized in the retrospective test. The black square indicates the origin time of each strong-to-major earthquake.	86
Figure 6.4. (a-i) During each case study, the spatial distribution of RTL values along TLMB observed seismic quiescence. The epicenter of each earthquake is depicted as a black star.....	91
Figure 7.1. Comparative of (a) this study with (b) Pailoplee et al. (2013) showing maximum magnitude in 50 years in TLMB.....	94
Figure 7.2. Comparative of (a) this study with (b) Pailoplee et al. (2013) showing the distribution of return period of 5.0 along the TLMB.....	94
Figure 7.3 Comparative of (a) this study with (b) Pailoplee and Charusiri (2015) showing the distribution of the probability of occurrence of 5.0 along the TLMB.	95
Figure 7.4. Distribution of b value along the TLMB from (a) 2010-2012, (b) 2010-2014, (c) 2010-2016, (d) 2010-2018, and (e) 2010-2020. The red star indicates earthquakes with a magnitude $\geq 5.0 M_L$ that occurred after the data collection.	97
Figure 7.5. Comparative the spatial distribution of b value along the TLMB border of (a) the spatial distribution of b value this study from 2000-2020 with (b) the spatial distribution of the b value of Pailoplee et al. (2013) in 1984-2010. The red star indicates earthquakes with a magnitude ≥ 5.0 that occurred after the data collection.	98
Figure 7.6. Comparative of Puangjaktha and Pailoplee (2016) with this study showing the graph of time of seismic quiescence (Z_{max}) to the time of the major earthquake.	99
Figure 7.7. The maps of the TLMB area illustrate the spatial distribution of the Z values of (Puangjaktha and Pailoplee, 2016) with this study.....	101

Figure 7.8. The Graph shows the time of Z-value's seismic quiescence (Q time) to the time of a major earthquake. Black dots show the result from previous work, and red dots show this study's results. (Modified from Puangjaktha and Pailoplee (2016)).... 102

Figure 7.9. The probability percentage of various Z values accords to a random phenomenon calculated at the epicenters of the M_L 5.1 earthquake..... 103

Figure 7.10. Comparative of (a) this study with (b) Puangjaktha and Pailoplee (2018) showing a temporal variation of the RTL score (grey line) of strong-to-major earthquakes (black square). A transparent grey and red strip illustrates the anomalous RTL recognized as the quiescence stage..... 104

Figure 7.11. A comparative of this study with Puangjaktha and Pailoplee (2018) shows that the spatial distribution of RTL values along TLMB during each case study is observed in seismic quiescence. The epicenter of each earthquake defines as a black star..... 105

Figure 7.12. The Graph shows the time of the RTL algorithm's seismic quiescence (Q time) to the time of a major earthquake. Black dots show the result from previous works, and red dots shows the results from this study (Modified from Puangjaktha and Pailoplee (2018))...... 106

Figure 7.13. Temporal variation of the RTL score (grey lines) was evaluated from different characteristic parameters. Black squares denote the origin time of the M_L -5.2 earthquake generated on May 5th, 2014..... 108

Figure 7.14. The photos show (a) a map of Mainland Southeast Asia. (b) The study area focuses on the TLMB overlay with the spatial distribution of the b value. The blue dashed line identifies the prospective area. 113

Figure 7.15. The photos show (a) a map of Mainland Southeast Asia. (b) The study area focuses on the TLMB overlay with the spatial distribution of the Z value. The black dashed identifies the prospective area..... 113

- Figure 7.16. The photos show (a) a map of Mainland Southeast Asia. (b) The study area focuses on the TLMB overlay with the spatial distribution of the RTL score. The red line identifies the prospective area. 114
- Figure 7.17. The photos show (a) a map of Mainland Southeast Asia. (b) The study area focuses on the TLMB overlay with the spatial distribution of the b value. The line identifies the prospective area of three precursors. 114
- Figure 7.18. The study area focuses on the TLMB overlay with the spatial distribution of b value, Z value, and RTL score anomalies. The transparency color area identifies the prospective area of each precursors and describe the details in Table 7.2. 115
- Figure 7.19. The photos show (a) the study area focuses on the TLMB overlay with the spatial distribution of b value, Z value, and RTL score anomalies. The transparency color area identifies the prospective area. (b) A photo of 3-D magnetotelluric imaging at 5.38 km depth slice of the final inverted model. The color bar is the \log_{10} resistivity in Ω m. (Boonchaisuk et al., 2017). 2

CHAPTER 1

INTRODUCTION

1.1 Background

Earthquake forecasting was described by Ahamed and Bolten (2017) as a declaration regarding the occurrence of future earthquakes based on the current information, data, and scientific methodologies. To forecast an earthquake, one must specify the expected magnitude range, the geographical area within which it will occur, and the time interval within which it will happen with sufficient precision so that the ultimate success or failure of the prediction can readily be judged. Therefore, it can only carefully record and analyze failures and successes, evaluate the eventual success of the total effort, and chart future directions. Moreover, scientists should also assign a confidence level to each prediction (Council, 1976).

According to the scientific definition of earthquake forecasting, the length of its time interval and location can identify an earthquake prediction of a specific magnitude range. In earthquake prediction, there are four major stages as shown in Table 1.1, the first long-term stage is based on ten years. On a range of one to several years, the second stage is the intermediate period. The third category is short-term, which is measured in weeks and months. Finally, the stage is immediate, ranging from seconds to hours. We focused on intermediate term using statistical seismology in this thesis. We employ the instrumental record, which is a catalogue of earthquakes, to evaluate statistical seismology. Even if the data in earthquake catalogues, such as longitude, latitude, year, month, day, magnitude, hour, minute, and second, are straightforward, they are nonetheless helpful and provide trustworthy information for statistical seismology.

In the present day, statistical seismology is a fascinating field of research since it is routine to predict earthquakes that will occur within a few months or years. The earthquake catalogue is the data collection used for statistical seismology studies.

Table 1.1. The classification of earthquake predictions.

Temporal	In years	Spatial	In source zone size L
Long term	10-100	Long range	Up to 100
Intermediate term	1	Middle range	5-10
Short term	0.01-0.1	Narrow	2-3
Immediate	0.001	Exact	1

Despite the apparent simplicity of the phrases which are latitude, longitude, magnitude, year, month, day, hour, minute, and second, their measurement is exact. All those mentioned above, the earthquake catalogue is entirely credible and valuable for statistical seismology analysis. Furthermore, the earthquake catalogue is a simple data set that is used in several statistical seismology methods to define earthquake characteristics and earthquake forecasting, including frequency-magnitude distribution: b value (Gutenberg and Richter, 1944), Fractal dimension: D_c (Wyss et al., 2004), the seismicity rate change: Z value (Wiemer and Wyss, 1994) and the seismic quiescence: RTL algorithm (Sobolev and Tyupkin, 1997)

About how interesting the area is to study, according to Pailoplee and Choowong (2014), the area of Thailand-Laos-Myanmar borders (TLMB) is in zone I and J in Figure 1.1, identified as the intraplate seismotectonic setting in Mainland Southeast Asia, which has been acknowledged as one of the most seismically active regions. Furthermore, the study by Pailoplee, Sugiyama, and Charusiri (2009) discovered that the TLMB contains numerous active faults, as shown in Figure 1.2 and Table 1.2. Some faults in this area should focus on, such as no. 19 Mae Chan fault zone, no. 25 Mengxing fault zone, and no. 27 Nam Ma fault zone, all of which are located on the TLMB. No. 4 Dien Bien Fu fault zone and no. 34 Pua fault zone are located on the Thailand-Laos border. The no. 2 Chiang Rai fault zone, no. 22 Mae Tha fault zone, and no. 32 Pha Yao fault zone are located in northern Thailand.

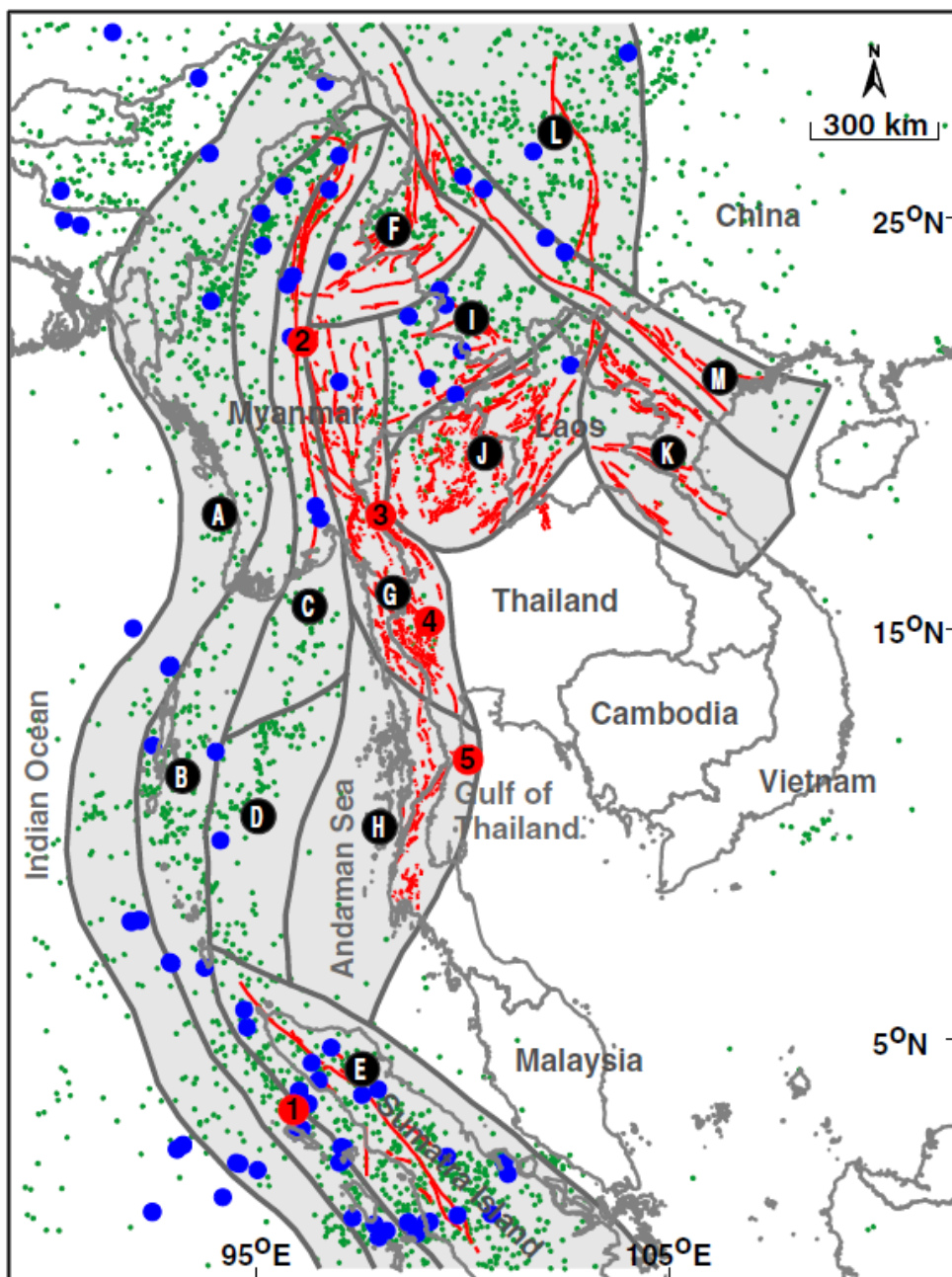


Figure 1.1. A map shows mainland Southeast Asia along with the 13 seismic zones that have been established (A to M). The map shows the locations of the epicenters of completeness earthquakes with $m_b \geq 4.0$ reported from 1974 to 2010 (green circles), completeness earthquakes with $m_b \geq 7.0$ (blue circles), and important earthquakes mentioned in the text (red circles). Red lines denote the fault lines compiled by Pailoplee et al. (2009). Grey polygons represent the geometry of the postulated seismic source zones by Pailoplee and Choowong (2013).

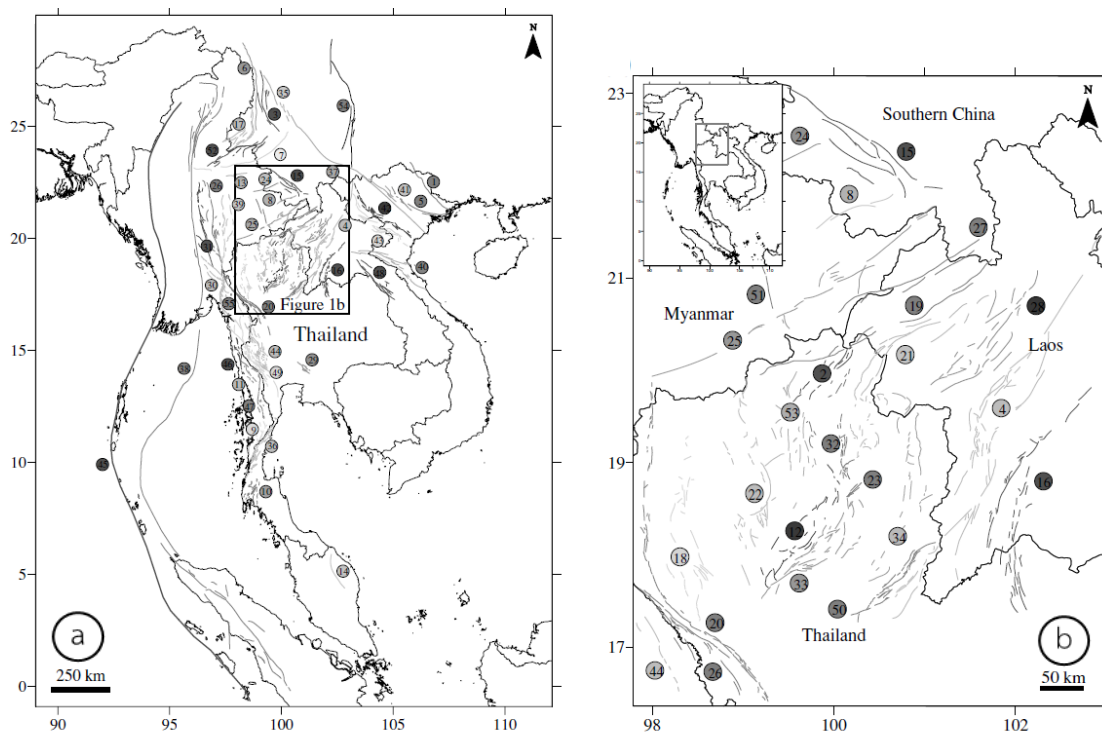


Figure 1.2. Maps of mainland Southeast Asia showing (a) Active faults in Thailand and neighbouring areas interpreted from remote sensing data (IKONOS, LANDSAT, and MODIS) and a previous study (b) an enlarged map was interpreting active faults in northern Thailand and neighbouring areas. The colour and number on both maps distinguish individual fault zones. Therefore, the fault zones can be identified using the numbers in Table 1.2.

Table 1.2. Summary of active fault zone earthquake potential criteria used in seismic hazard assessments in Thailand and neighbouring areas.

Fault no.	Fault zone	Active fault data				Seismicity investigation			Source	
		Fault type ^a	SRL (km)	<i>S</i> (mm/yr)	<i>m</i> _{max}	<i>A</i> _f (km ²)	<i>m</i> _{min}	<i>a</i> value		<i>b</i> value
1	Cao Bang-Tien Yen	S	287	—	7.9	5,000	4.0	1.50	0.34	Cuong <i>et al.</i> (2006)
2	Chiang Rai	S	28	—	6.8	499	4.0	2.25	0.42	This study
3	Chong Shan shear zone	S	298	5.00	8.0	6,166	4.0	7.85	1.34	Akciz <i>et al.</i> (2008)
4	Dein Bein Fu	S	130	2.00	7.5	2,163	4.0	2.68	0.37	Zuchiewicz <i>et al.</i> (2004)
5	Dong Trieu	S, N	187	—	7.7	3,289	4.0	2.71	0.90	Charusiri <i>et al.</i> (2002)
6	Gaoligong Shan shear zone	S	407	5.00	8.1	7,603	4.0	9.67	1.62	Akciz <i>et al.</i> (2008)
7	Hsenwi-Nanting	S	359	1.00	8.0	6,166	4.0	25.80	4.83	Lacassin <i>et al.</i> (1998)
8	Jinghong	S	53	—	7.1	935	4.0	2.33	0.40	Lacassin <i>et al.</i> (1998)
9	Kawthuang	—	36	—	6.9	615	4.0	1.68	0.25	This study
10	Klong Marui	S	29	0.10	6.8	499	4.0	1.68	0.25	Wong <i>et al.</i> (2005)
11	Kungyaungale	S	25	4.00	6.7	405	4.0	1.68	0.25	Wong <i>et al.</i> (2005)
12	Lampang-Thoen	S, N	28	0.83	6.8	499	4.0	2.72	0.55	Charusiri <i>et al.</i> (2004)
13	Lashio	S	50	1.00	7.0	759	4.0	3.15	0.40	Lacassin <i>et al.</i> (1998)
14	Libir	—	170	—	7.7	3,289	4.0	3.44	0.60	Metcalfe (2000)
15	Linchang	S	107	—	7.4	1,754	4.0	2.33	0.29	Lacassin <i>et al.</i> (1998)
16	Loei-Petchabun Suture	S	59	—	7.1	935	4.0	3.01	0.62	Lepvrier <i>et al.</i> (2004)
17	Longling-Ruili	S	70	5.00	7.2	1,153	4.0	6.42	1.01	Bai and Meju (2003)
18	Mae Chaem	—	21	—	6.6	328	4.0	1.89	0.32	This study
19	Mae Chan	S	99	3.00	7.4	1754	4.0	2.64	0.37	Fenton <i>et al.</i> (2003)
20	Mae Hong Sorn-Tak	S	37	—	6.9	615	4.0	2.65	0.38	Charusiri <i>et al.</i> (2004)
21	Mae Ing	S	38	—	6.9	615	4.0	2.56	0.38	Fenton <i>et al.</i> (2003)
22	Mae Tha	S	47	0.80	7.0	759	4.0	2.36	0.38	Rhodes <i>et al.</i> (2004)
23	Mae Yom	S	22	0.80	6.6	328	4.0	1.92	0.60	RID (2006)
24	Menglian	S	117	0.50	7.5	2,163	4.0	2.13	0.28	Lacassin <i>et al.</i> (1998)
25	Mengxing	S	75	4.80	7.3	1,422	4.0	2.95	0.40	Lacassin <i>et al.</i> (1998)
26	Moei-Tongyi	S	259	0.73	7.9	5,000	4.0	3.46	0.54	This study
27	Nam Ma	S	177	2.40	7.7	3,289	4.0	3.18	0.58	Morley (2007)
28	Nam Peng	S	51	—	7.1	935	4.0	3.08	0.59	Charusiri <i>et al.</i> (1999)
29	Ongkalak	S, N	47	0.17	7.0	759	4.0	2.52	0.40	Charusiri (2005)
30	Pa Pun	S	143	—	7.6	2,667	4.0	2.58	0.37	Nutalaya <i>et al.</i> (1985)
31	Pan Luang	S	219	—	7.8	4,055	4.0	2.98	0.51	Nutalaya <i>et al.</i> (1985)
32	Pha Yao	S, N	20	0.10	6.6	328	4.0	2.95	0.40	Fenton <i>et al.</i> (2003)
33	Phrae	S	28	0.10	6.8	499	4.0	2.68	0.53	Fenton <i>et al.</i> (2003)
34	Pua	N	29	0.60	6.8	499	4.0	2.44	0.55	Fenton <i>et al.</i> (2003)
35	Qiaohou	—	145	—	7.6	2,667	4.0	2.35	0.25	Lacassin <i>et al.</i> (1998)
36	Ranong	S	46	1.00	7.0	759	4.0	1.68	0.25	Wong <i>et al.</i> (2005)
37	Red River	S	812	4.00	8.5	17,579	4.0	17.60	3.16	Duong and Feigl (1999)
38	Sagiang-Sumatra	S	958	23.00	8.5	17,579	4.0	6.92	0.86	Bertrand and Rangin (2003)
39	Shan	S	66	—	7.2	1,153	4.0	2.93	0.39	This study
40	Song Ca	S	225	—	7.8	4,055	4.0	2.58	0.48	Takemoto <i>et al.</i> (2005)
41	Song Chay	S, N	55	2.00	7.1	935	4.0	3.05	0.58	Cuong and Zuchiewicz (2001)
42	Song Da	S	46	—	7.0	759	4.0	2.73	0.45	Phoung (1991)
43	Song Ma	S	72	—	7.2	1,153	4.0	6.52	1.06	Phoung (1991)
44	Sri Sawat	S	43	2.00	7.0	759	4.0	2.50	0.40	Songmuang <i>et al.</i> (2007)
45	Andaman subduction	R	3,388	47.00	9.2	76,208	4.0	6.08	0.69	Paul <i>et al.</i> (2001)
46	Tavoy	S	32	—	6.8	499	4.0	2.80	0.79	Wong <i>et al.</i> (2005)
47	Tenasserim	S	50	4.00	7.0	759	4.0	1.68	0.25	Wong <i>et al.</i> (2005)
48	Tha Khaek	S	250	—	7.9	5,000	4.0	3.15	0.67	DMR (2006)
49	Three Pagoda	S	141	2.00	7.6	2,667	4.0	2.62	0.51	Fenton <i>et al.</i> (2003)
50	Uttaladith	S	27	0.10	6.7	405	4.0	1.63	0.46	Fenton <i>et al.</i> (2003)
51	Wan Na-awn	—	69	—	7.2	1,153	4.0	2.28	0.35	This study
52	Wanding	S	199	1.90	7.7	3,289	4.0	5.34	0.93	Morley (2007)
53	Wang Nua	—	31	—	6.8	499	4.0	2.27	0.40	This study
54	Xianshuihe	S	505	15.00	8.2	9,376	4.0	6.74	1.05	Eleftheria <i>et al.</i> (2004)
55	Hutgyi	S, R	5	0.03	5.9	76	4.0	1.67	0.34	EGAT (2006)

SRL is surface rupture length (km), *m*_{max} is maximum possible earthquake magnitude calculated from empirical relationship between SRL and *M*_w (Wells and Coppersmith, 1994), *A*_f is rupture area (km²) calculated from the empirical relationship between *A*_f (Wells and Coppersmith, 1994), *S* is slip rate (mm/yr), *m*_{min} is the minimum magnitude. ^aFault type: S = strike-slip fault, N = normal fault, R = reverse fault.

While Pailoplee, Channarong, and Chutakositkanon (2013) examined the earthquake activity in this area from 1984 to 2010, the Thailand Meteorological Department (TMD) earthquake catalogue shows that large earthquakes occurred in this area, for example, the M_w -6.8 earthquake that struck the Tarlay city, Myanmar, on March 24th, 2011 (Wang et al., 2014b) in Figure 1.3, and the M_w -6.3 earthquake that struck the Prayao fault zone on May 5th, 2014, in Figure 1.4, and the M_w -6.4 earthquake that struck northwest Laos near the Thai border on November 21st, 2019, could all be felt in Bangkok, Thailand. As a result, the TLMB is now designated as a zone of high seismic activity that warrants further investigation. The research results show that the spatial distribution of the b value indicates that the earthquake's epicenter did not occur at the lowest b value in the blue area in Figure 1.5. In contrast, unlike other studies, Pailoplee (2014b) analyzes the b value from the earthquake catalogue in the Indonesian island chain from 1980 to 2005. The result indicates that the earthquake's epicenter has the lowest b value in the blue area of Figure 1.6.

There are numerous methods for earthquake prediction. According to Sobolev (1995), laboratory rock experiments revealed two distinct phases of seismicity rates prior to a significant earthquake rupturing process, which are the quiescence (seismicity decrease) and activation (seismicity increase) stages. The best of these stages for predicting earthquakes is seismic quiescence, which has been successful for the past 40 years. Several ideas have been proposed recently to identify earthquake precursors. Moreover, some significant investigations have reinforced the theory that seismic quiescence precedes large earthquakes (Katsumata, 2011).

Thus, a variety of statistical methods for earthquake forecasting were demonstrated to determine the earthquake precursor, including the seismicity rate change (Z value) (Wiemer and Wyss, 1994) and the seismic quiescence (RTL algorithm) (Sobolev and Tyupkin, 1997). The Z value is one of the additional techniques for detecting the precursory seismic quiescence that occurs before strong-to-major earthquakes. For examples, the M_w -5.8 Coyote lake earthquake, USA and the M_w -6.2 Morgan Hill earthquake (Bachman, 2001), the 2008 M_w -6.4 SW-Achaia, Western Greece (Chouliaras, 2009), the 2003 M_w -7.6 Colima earthquake (Rudolf-Navarro, Diosdado, and Angulo-Brown, 2010), the 2003 M_w -8.3 Tokachi-Oki, Japan (Katsumata, 2011), the M_w -

6.4 Turkey earthquake (Öztürk and Bayrak, 2011), and the 2006 M_w -6.1 Silakhour, Iran (Sorbi, Nilfouroushan, and Zamani, 2012) in Figure 1.7.

Another successful forecasting tool for quantifying relative seismic quiescence is the RTL algorithm. Several RTL investigations have revealed the successful correlation between the quiescent and activation stages and subsequent moderate-to-major earthquakes in various seismogenic settings. For example, the M_w -7.2 Kobe earthquake, Japan (Huang, Sobolev, and Nagao, 2001), the M_w -7.3 Izmit earthquake, Turkey (Huang, Öncel, and Sobolev, 2002), the M_w -6.8 Nemuro earthquake, Japan (Huang and Sobolev, 2002), , the M_s -7.3 Tottori earthquake, Japan (Huang and Nagao, 2002), the M_w -7.3 Chi-Chi earthquake, Taiwan (Chen and Wu, 2006), M_s -8.0 Wenchuan earthquake, China (Huang, Li, and WL, 2009), the M_w -9.0 Tohoku earthquake, Japan (Huang and Ding, 2012), and the events in the Sumatra-Andaman (Sukrungsri and Pailoplee, 2017) in Figure 1.8.

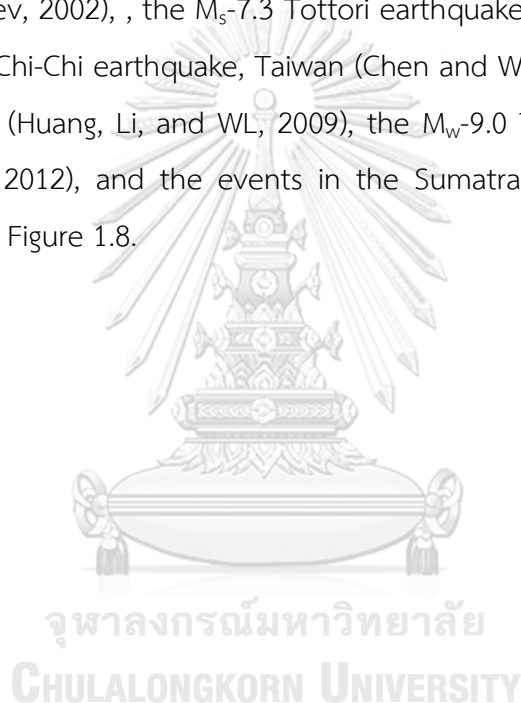




Figure 1.3. The photo shows the damage established by The M_w -6.8 Tarlay earthquake on March 24th, 2011, in Myanmar. (<https://upload.wikimedia.org>)



Figure 1.4. The photo shows the damage establishment by The M_w -6.3 Mae Lao earthquake on May 5th, 2014, in Chiang Rai, Thailand (<https://www.asiaone.com/>)

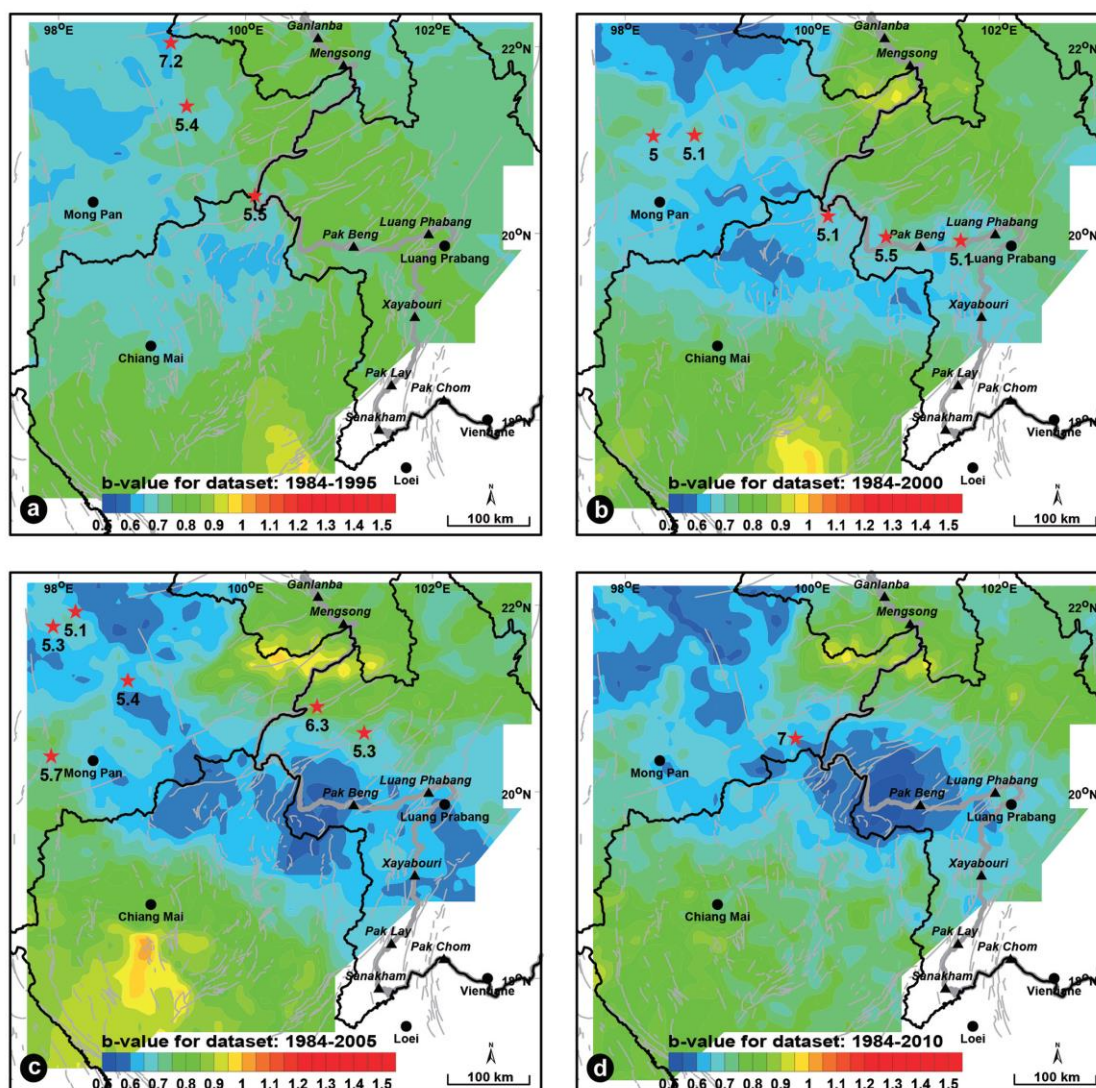
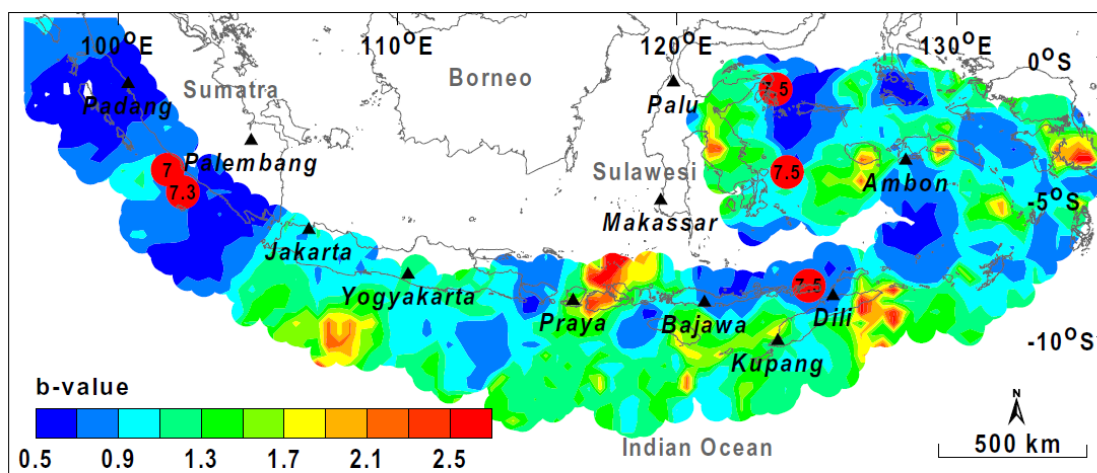
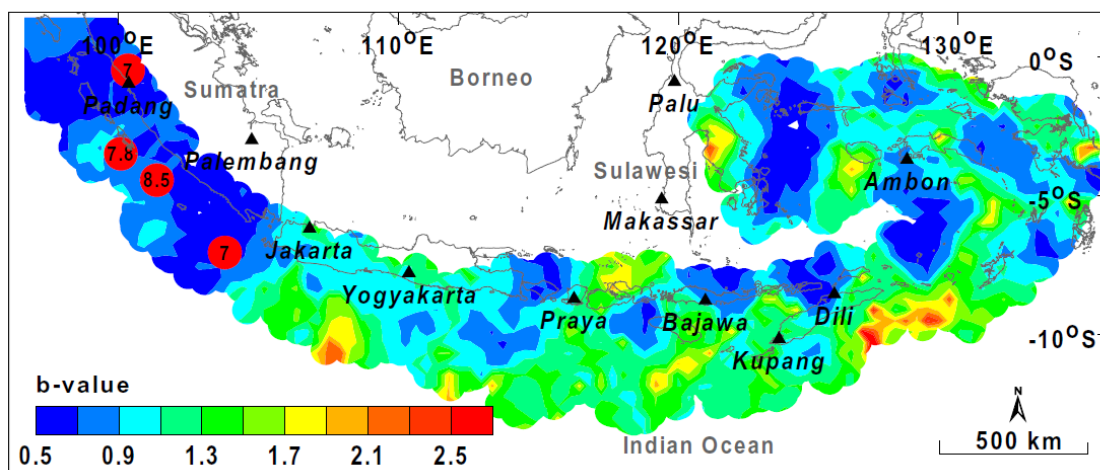


Figure 1.5. Distribution of b value along the TLMB in (a) 1984-1995, (b) 1984-2000, (c) 1984-2005, and (d) 1984-2010. The red star indicates earthquakes greater than 5.0 that occurred after the data collection. (Pailoplee et al., 2013).



(a)



(b)

Figure 1.6. Distribution of b value along the Indonesian island chain between (a) 1980-2000 and (b) 1980-2005. The red star indicates earthquakes greater than 7.0 that occurred five years after the earthquake data collection (Pailoplee, 2014b).

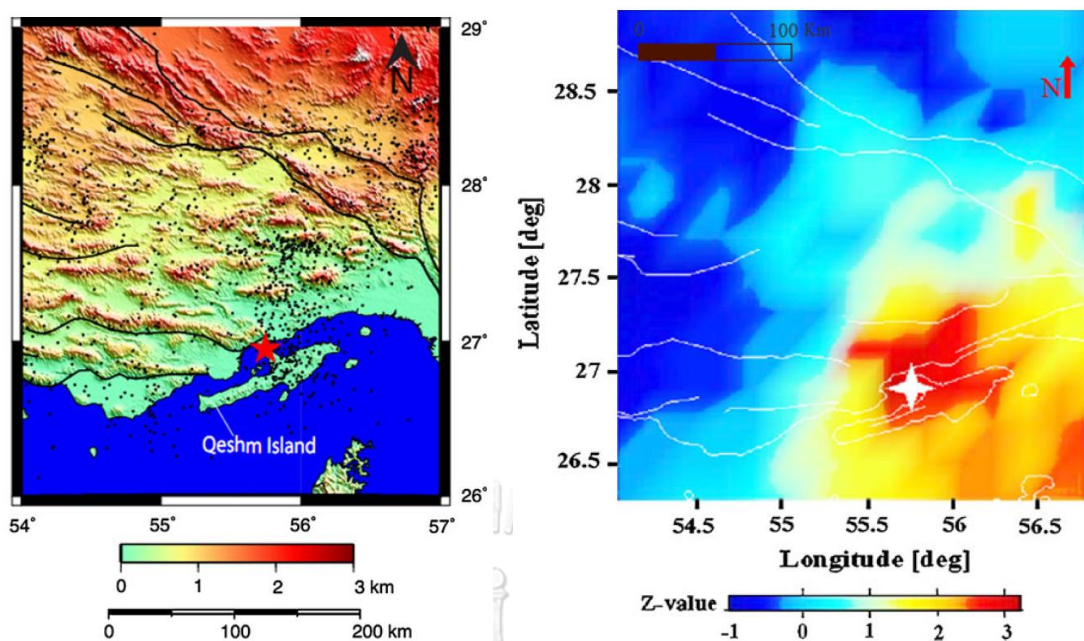


Figure 1.7. (a) Topographic map of the study area with significant faults and earthquakes (b) Map of the spatial distribution of Z statistic before the 6.1 M_w earthquake in 2008 in South Iran. The white star indicates the epicenter of the 2008 Qeshm main shock. The red colour indicates a positive Z value, which corresponds to a drop in seismicity rate, whereas the blue colour indicates an increase in seismicity rate. (Sorbi et al., 2012)

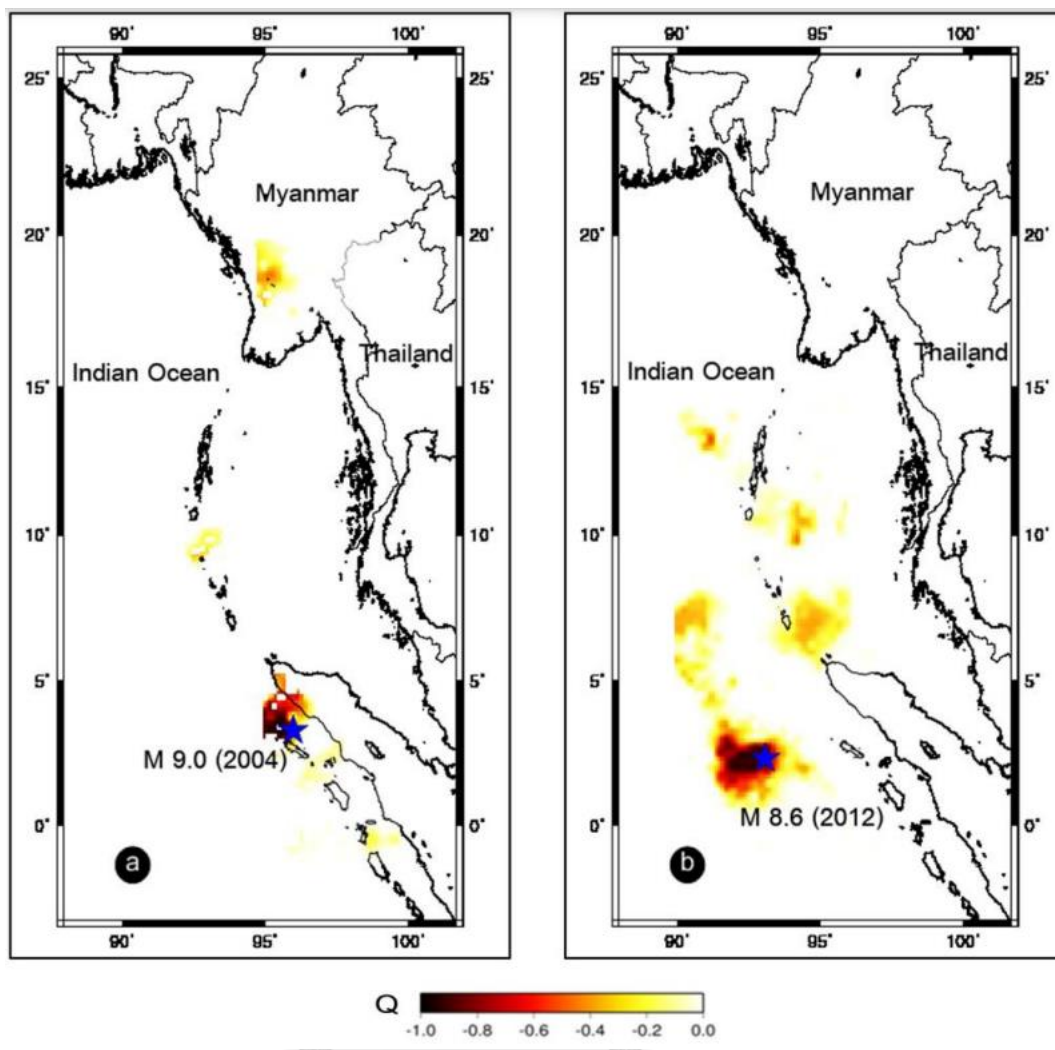


Figure 1.8. The spatial distribution in the RTL algorithm at the Sumatra-Andaman. (a) from November 2002 to August 2004. (b) from April 1996 to October 1998. The star represents the epicenters of the Sumatra earthquake of 2004 and the Indian Ocean earthquake of 2012. (Sukrungsri and Pailoplee, 2017).

As mentioned above, the purpose of this study was to investigate the statistical seismology of the TLMB region and use the occurrence of nineteen earthquakes ($M_L \geq 5.0$) as a case study by using the methods mentioned earlier and then to determine the prospective areas of upcoming earthquakes along the TLMB using the most recent seismicity data. The findings should help constrain the potential locations of future earthquakes.

1.2 Study Area

The study effort focuses mainly on applying the statistical seismology mentioned in the preceding topic along the TLMB region ($16.77^{\circ} - 22.35^{\circ}\text{E}$ and $97.48^{\circ} - 103.17^{\circ}\text{N}$) in Figure 1.9 since it is one of the locations that have important cities, hydropower dams, and historical architecture. Moreover, Pailoplee and Choowong (2014) defined the TLMB as the intraplate seismotectonic setting in Mainland Southeast Asia, one of the most seismically active zones. An examination of the earthquake catalogue accessible from the Thailand Meteorological Department reveals that 19 significant earthquakes ($M_L \geq 5.0$) had occurred in this area, as illustrated in Table 5.1

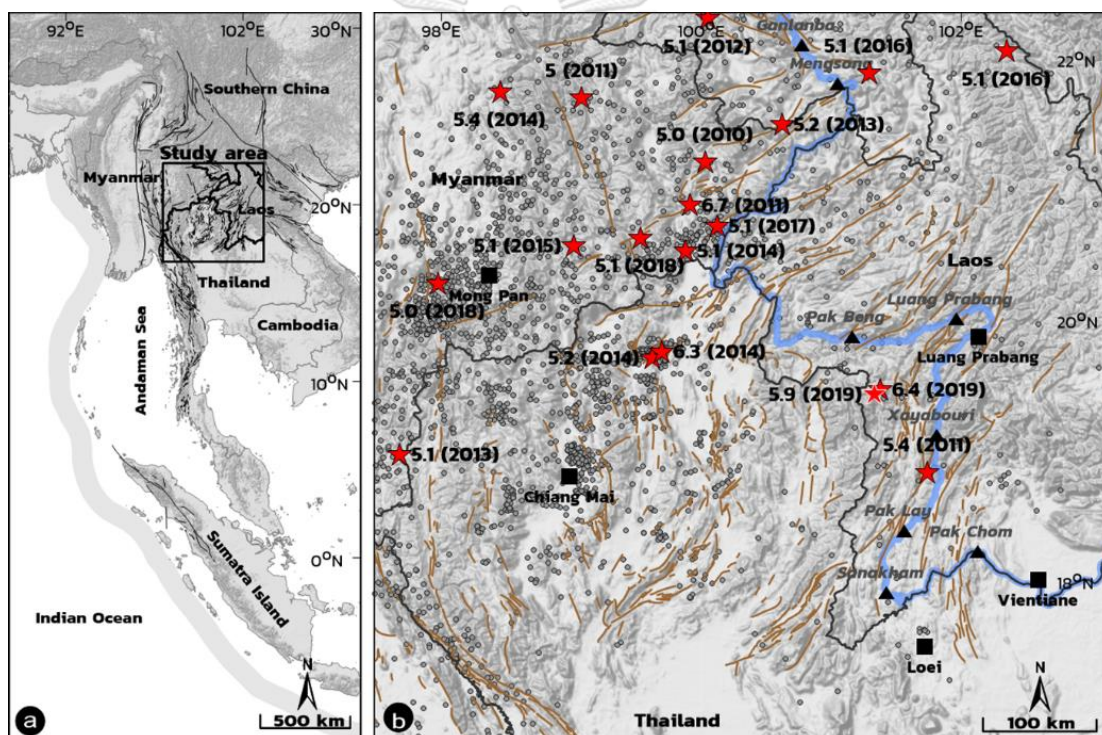


Figure 1.9. (a) Map of Thailand and neighbouring countries indicating the study area.

(b) Map displays the complete seismicity catalogue epicenters distribution along TLMB from 2010 and 2020. (grey dots are all earthquake epicenters, and the black star is $M_w \geq 5.0$. A grey line, a thick blue line, black triangles, and black squares represented fault lines, the Mae Kong River, hydropower dams, and major cities, respectively)

1.3 Objective

This thesis has three main goals that it hopes to achieve using its findings following;

i) To determine the nature of the seismic patterns by categorizing them into line source, area source, and volume source.

ii) To analyze the seismic activity by determining the maximum magnitude, return period, and probability of earthquake occurrence.

iii) To identify prospective areas by employing three different methods: seismotectonic stress (b value), seismicity rate change (Z value), and seismic quiescence (RTL algorithm).



CHAPTER 2

THEORY AND METHODOLOGY

2.1 Theory

This section explains the concept of statistical seismology and the method of analyzing earthquake characteristics and prospective area in TLMB. According to the literature review, the theory employed in this analysis discovered the following topics: i) seismotectonic stress: b value, ii) seismic pattern: fractal dimension), iii) seismicity rate change: Z value, and iv) seismic quiescence: RTL Algorithm. Each of these concepts are presented in details following.

2.1.1 Seismotectonic Stress (b value)

Small earthquakes have occurred more frequently than major earthquakes throughout the history of the earth. This idea was demonstrated by developing the frequency–magnitude distribution (FMD) or the Gutenberg-Richter magnitude-frequency relationship (G-R relationship) of earthquakes (Gutenberg and Richter, 1944; Ishimoto, 1939) was developed to prove that theory. It is one of the most essential laws for investigating seismicity. The equation utilized in this study is denoted by the symbol Equation (2.1).

$$\log(N) = a - bM \quad \text{Eq. (2.1)}$$

where N is the cumulative number of earthquakes with a magnitude equal to or greater than M, a and b are empirical constants that vary with time and window. The a constants describe seismic activity, whereas the b constant is a tectonic parameter that denotes tectonic stress and the frequency ratio of minor to major earthquakes. Increased b levels are associated with reduced stress (Scholz, 1968; Wyss, 1973).

Regarding the frequency-magnitude distribution, Equation (2.1) expresses the empirical relationship between the annual average number of earthquakes (N) of each year with a magnitude equal to or greater than M.

$$\log(N) = \alpha - \beta M \quad \text{Eq. (2.2)}$$

For Equation (2.1), the constants a and b are positive. The a value represents the overall seismicity rate or the annual number of earthquakes with a Richter magnitude greater than 0. In contrast, the b value determines the ratio of minor to major earthquakes. Similarly, Equations (2.3) and (2.4) demonstrate that the parameters α and β are associated with a and b .

$$\alpha = \exp[a \ln(10)] \quad \text{Eq. (2.3)}$$

or

$$\beta = b \ln(10) \quad \text{Eq. (2.4)}$$

2.1.2 Seismic Pattern (D_c value)

The correlation dimension developed by Grassberger and Procaccia (1983) in Equation (2.5) utilized to estimate the fractal dimension or D_c value. It calculates the distance between a set of points. In this example, the earthquake epicenters. The spatial fractal dimension is used in this study.

$$C(r) = \frac{2}{N(N-1)} N(R < r), \quad \text{Eq. (2.5)}$$

where $N(R < r)$ is the number of pairs of (X_i, X_j) pairings with a smaller distance than r . The correlation integral is related to the standard correlation function in the same method as Kagan and Knopoff (1980):

$$C(r) \sim r^{D_2} \quad \text{Eq. (2.6)}$$

where D_2 is a fractal dimension or the correlation dimension (Grassberger and Procaccia, 1983), in this study, D_c is used instead of D_2 for representing the fractal dimension. The fractal dimension describes how much of the surrounding space the

fractal takes up. Knowing the value of D allows us to forecast the fracture characteristic. For example, a D_c value around 3 indicates that earthquake fractures are filling up a volume of the crust, a value near 2 indicates that a plane is being filled up, and a value near 1 indicates that line sources are the most common. Moreover, Tosi (1998) demonstrated that the range of possible fractal dimension values is between 0 and 2, depending on the dimension of the embedding space. The interpretation of such limit values is that a set with D_c near to 0 suggests that all events are concentrated at a single place, whereas D_c close to 2 indicates that events are randomly or homogeneously dispersed over a two-dimensional embedding space.

2.1.3 Seismicity Rate Change (Z value)

The change in the rate of seismicity comes from the idea of the seismic gap. In it, McCann et al. (1979) explain that the significant drop in seismicity from the background rate is due to seismic quiescence, which is limited to the main shock and its area in the intermediate term, which is measured in months to years. This is shown in Figures 2.1 and 2.2.

Figure 2.1a depicts a straight line for the cumulative number curve during the uniform seismicity rate. Figure 2.1b depicts a straight line for the cumulative number curve during the uniform seismicity rate. While the seismicity rate in Figure 2.2a did not occur between 40 and 60, the cumulative number curve in Figure 2.2b indicates a flat portion between 40 and 60. The lack of seismic activity in Figure 2.2a and the flattening of the cumulative number curve in Figure 2.2b indicate the seismic quiescence stage. (Bachmann, 2001)

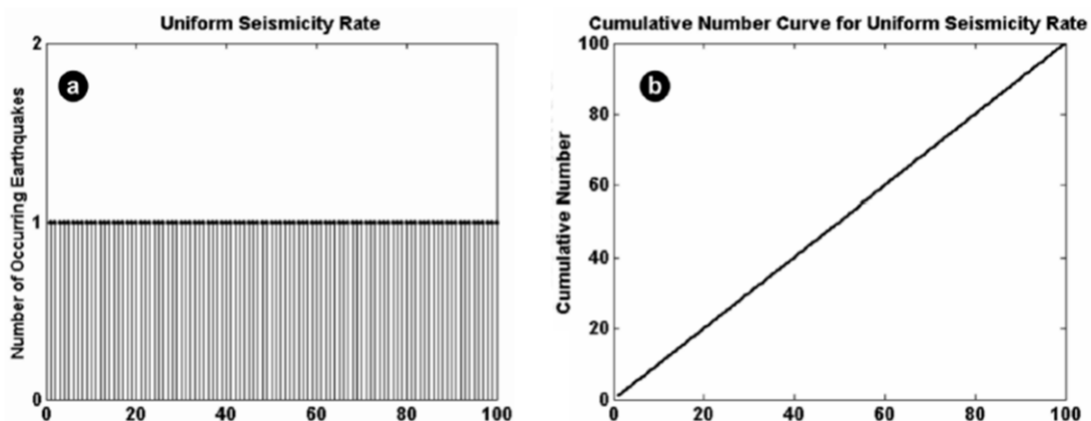


Figure 2.1. illustrates (a) a uniform seismicity rate and (b) a cumulative number of earthquakes plot against time. (Bachmann, 2001)

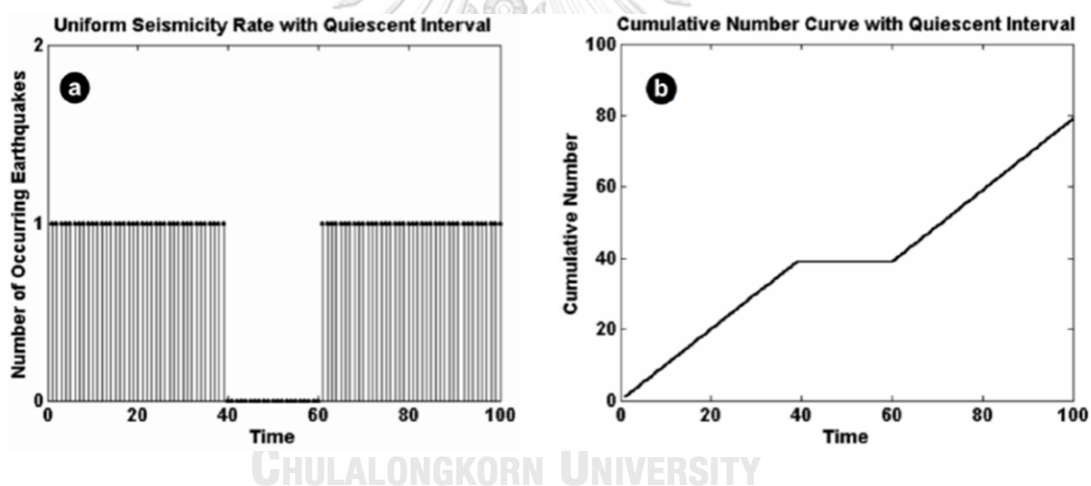


Figure 2.2 illustrates (a) a uniform seismicity rate with quiescence interval and (b) a cumulative number of earthquakes with quiescence interval plot against time. (Bachmann, 2001)

In this study, the Z value, as indicated by Equation (2.7), was employed to assess the precursory seismic quiescence, which is a decrease in seismicity generated before to dangerous earthquakes. (Wiemer and Wyss, 1994)

$$Z = \frac{R_{bg} - R_w}{\sqrt{\frac{S_{bg}^2}{N_{bg}} + \frac{S_w^2}{N_w}}} \quad \text{Eq. (2.7)}$$

where Z is the seismic quiescence rate, given as the difference between the average seismicity rate inside a specified time window (R_w) and the general period prior to the studied time window (R_{bg}). In this equation, the parameters S_w and S_{bg} are defined as the standard deviations of R_w and R_{bg} , respectively. The parameters N_w and N_{bg} are specified as the number of earthquakes.

Positive and negative Z values, according to seismology, describe the quiescence and activation stages, respectively, during which the seismicity rate is lower or higher than the background rate.

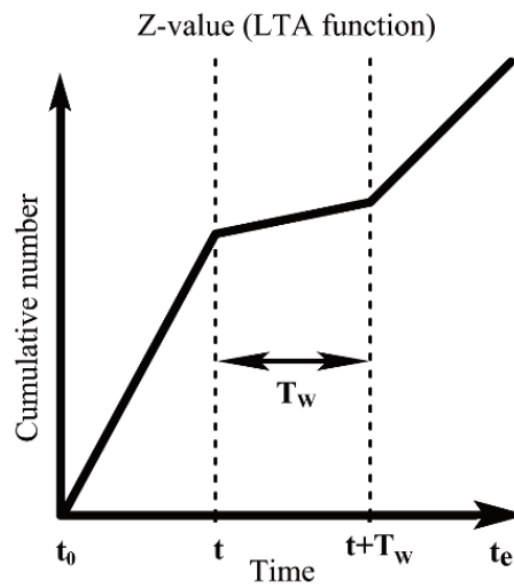


Figure 2.3. Schematic explanation of how to calculate the Z value (Öztürk and Bayrak, 2011)

2.1.4 Seismic Quiescence (RTL Algorithm)

The RTL algorithm (Sobolev, 1999; Sobolev and Tyupkin, 1997) is a statistical seismology method designed to detect the presence of precursory seismicity variations. Moreover, it is associated with the occurrence of the main shock (Sobolev, 1995), which weight three parameters called R (interested region), T (time), and L (rupture length but in the study we consider it as magnitude), which can be expressed as the following Equations (2.8)-(2.10):

$$R(x, y, z, t) = \left[\sum_{i=1}^n \exp\left(-\frac{r_i}{r_0}\right) \right] - R_{bg}(x, y, z, t), \quad \text{Eq. (2.8)}$$

$$T(x, y, z, t) = \left[\sum_{i=1}^n \exp\left(-\frac{t-t_i}{t_0}\right) \right] - T_{bg}(x, y, z, t), \quad \text{Eq. (2.9)}$$

$$L(x, y, z, t) = \left[\sum_{i=1}^n \exp\left(-\frac{l_i}{l_0}\right) \right] - L_{bg}(x, y, z, t), \quad \text{Eq. (2.10)}$$

where (x, y, z, t) indicates the investigation location and time, and r_i indicates the distance between (x, y, z) and the epicenter of the i_{th} earthquake. Meanwhile, t_i and l_i are the origin time and length of the earthquake's surface fault rupture, respectively, which are proportional to the earthquake's magnitude (M_i) (Wells and Coppersmith 1994). $R(x, y, z, t)$, $T(x, y, z, t)$, and $L(x, y, z, t)$ which $R_{bg}(x, y, z, t)$, $T_{bg}(x, y, z, t)$, and $L_{bg}(x, y, z, t)$ determine the background values, respectively, whereas t_0 and r_0 define the characteristic time and distance, respectively. The parameter n represents the total amount of earthquakes more significant than the magnitude of completeness (M_c) (Woessner, 2005). Meanwhile, $2r_0$ equals T_{max} , t , and t_i equals to R_{max} , r_i , and $2t_0$. The RTL score or $V_{RTL}(x, y, z, t)$ may be calculated using the R, T, and L functions in Equation (2.11).

$$V_{RTL}(x, y, z, t) = \frac{R(x, y, z, t)}{R(x, y, z, t)_{max}} \bullet \frac{T(x, y, z, t)}{T(x, y, z, t)_{max}} \bullet \frac{L(x, y, z, t)}{L(x, y, z, t)_{max}} \quad \text{Eq. (2.11)}$$

After all, the RTL score is a numeric number ranging from -1 to 1. $V_{RTL} = 0$ implies the normal activity of the seismicity. Meanwhile, $V_{RTL} < 0$ and > 0 represent a seismic quiescence and activation, respectively. Moreover, in the spatial distribution for the RTL algorithm, Huang and Nagao (2002) developed the $Q(x, y, z, t_1, t_2)$ function as Equation (2.12) to measure the average of RTL values during the time window (t_1, t_2)

$$Q(x, y, z, t_1, t_2) = \frac{1}{m} \sum_{i=1}^m RTL(x, y, z, t_i) \quad \text{Eq. (2.12)}$$

Where m is the number of RTL data points in the window (t_1, t_2) , the RTL parameter is obtained using Equation (2.11), which is contained in (t_1, t_2) .

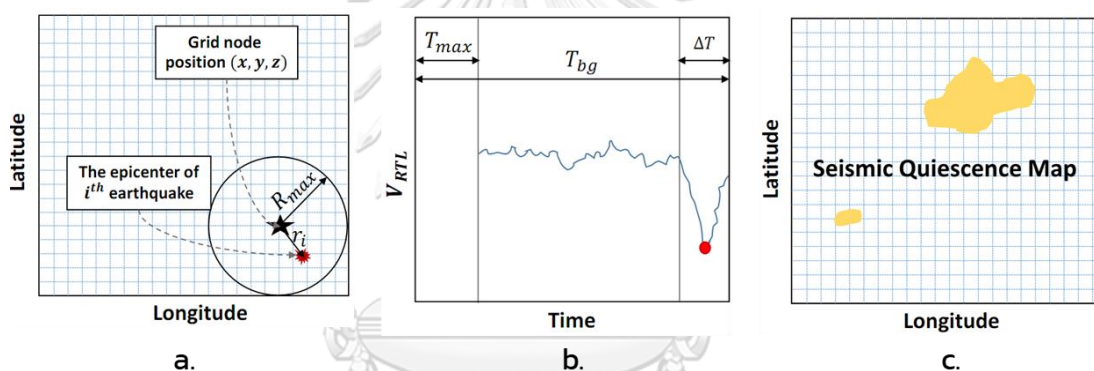


Figure 2.4. The diagrams illustrating the spatial distribution of seismic quiescence at the position (x, y, z) show (a) the R_{max} , (b) The V_{RTL} curve, and (c) the seismic quiescence map in the shaded region (Puangjaktha and Pailoplee, 2016)

2.2 Literature Review

2.2.1 Earthquake Activities in the Thailand-Laos-Myanmar Border

Pailoplee et al. (2013) research aims to examine earthquake activity in the TLMB region. Thus, this earthquake hazard assessment focuses on statistical seismic data analysis. They used the IRIS NEIC and TMD earthquake catalogues for 1984–2010. Following the completeness of the data, the catalogue was divided into three period: 1984-1995, 1984-2000, and 1984-2005. Using the complete earthquake catalogue, they explored the spatial distributions of the a and b values in Figure 1.5 from the

frequency-magnitude distribution relationship. Analyses of the probable maximum magnitude earthquakes based on the a and b values suggest that the northern part of Mong Pan and the Pak Beng-Luang Prabang regions can generate an earthquake with a magnitude of 4.0 to 5.0 in a year and a magnitude of 7.0 within the next 50 years.

Additionally, for earthquakes with m_b values from 4.0 to 7.0, the calculated short return periods are in the northern area of Mong Pan, around 1 to 500 years. However, the eastern section of Chiang Mai has a very long return period of up to 5000 years. In terms of earthquake prediction, the three sub-datasets examined demonstrated a strong correlation between a location with a low b value and the occurrence of a major earthquake in that region. Thus, based on this adequate condition and current data, an earthquake in the northern region of Mong Pan and the Pak Beng-Luang Prabang dams is a possible earthquake source.

2.2.2 Spatial and Temporal of b value Anomalies

Nuannin (2005) focuses on the spatial and temporal variations of b values. They were investigated using data from 624 earthquakes in the Andaman-Nicobar Islands region over five years prior to the giant earthquake on December 26th, 2004. The 50 events are contained in sliding time and space windows. The occurrence of two large shocks ($M_s \geq 7.0$) at the end of 2002 and the M_w -9.0 event in 2004 correspond with two significant declines in the b value. The stress buildup (low b value) near the epicenters of the 2002 and 2004 events and an event in North Andaman is seen in the spatial distribution in Figure 2.5. Around the 2004 epicenter, a 450 km long area of elevated stress spreads in an NNW-SSE direction.

2.2.3 Regional Variations and Correlations of Gutenberg–Richter Parameters and Fractal Dimension

Bayrak and Bayrak (2012) examined the regional variations in Gutenberg–Richter (G–R) parameters (a and b) and fractal (correlation) dimension (D_c) for different locations in Western Anatolia. The studied area is classified into 15 separate seismogenic zones based on their tectonic and seismotectonic regimes. For the instrumental record period from 1900 to 2011, they utilized a database with 69,182 earthquakes. The b value, which is the slope of the frequency–magnitude Gutenberg–Richter relationship, was computed using the maximum likelihood (ML) approach, and

the D_c value, which is the slope of $\log_{10}C(r)$ vs $\log_{10}r$, was obtained using the least-squares (LS) method. For each range of b and D_c values, computed values for 15 distinct. Seismogenic locations are mapped using a separate colour scale. Regional distributions of these parameters provide insight into regional differences in stress levels and geological complexity. Aegean arc and Aegean islands, Aliag a fault, and the Büyük Menderes Graben are the most likely places in WA to have big earthquakes because these areas have the lowest b values the highest D_c -values, which make them more likely to have big earthquakes. Because D_c/b values are highest in these areas, this ratio may determine the earthquake danger levels of various seismogenic zones in a given area.

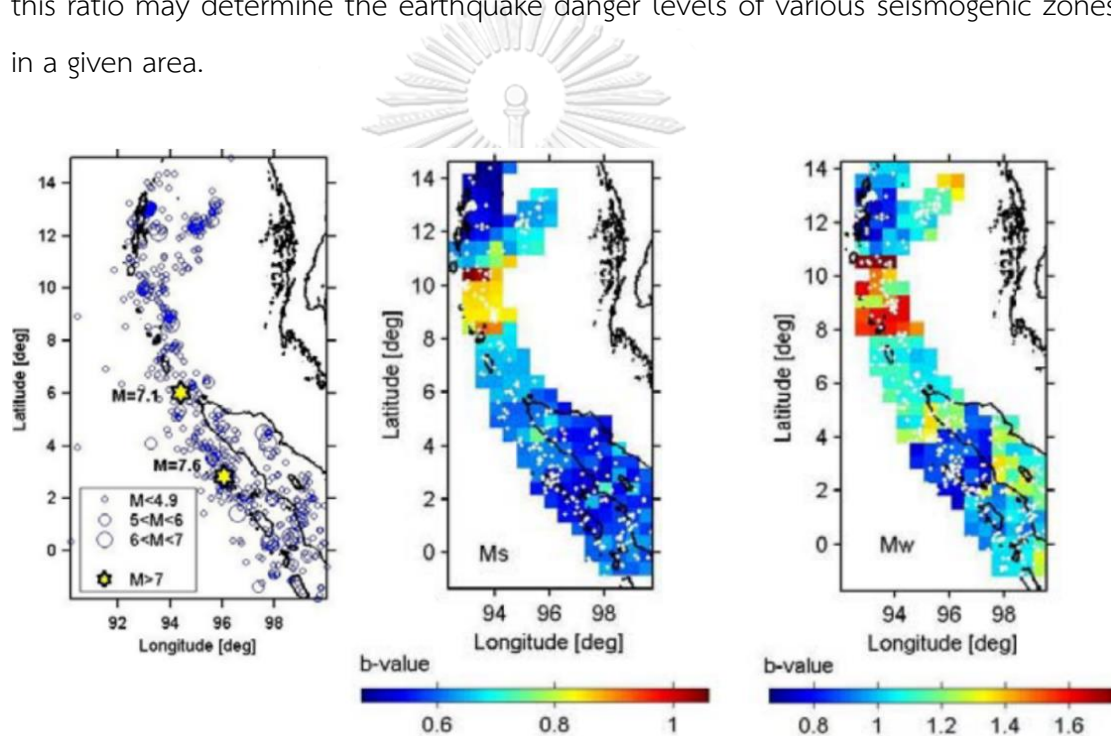


Figure 2.5. The spatial distribution of b value and epicenters of earthquakes was reported by the USGS between January 1st, 2000, and December 25th, 2004. The stars indicate the positions of the two most significant shocks (before the December 26th, 2004, earthquake) on October 24th, 2002, the M_s -7.1 (upper star), and November 2nd, 2002, the M_s -7.6 (lower star). b) Spatial distribution of b value. The magnitudes M_s (left) and M_w (right) were employed. Low b is represented by blue, whereas high b is represented by red. White dots show the epicentral sites. (Nuannin, 2005) A search for

correlations between the G–R parameters and fractal dimension is conducted. For different locations of Western Anatolia, we found a negative relation between D_c and b values and a positive association between D_c and a/b values. Because of the computed high correlation coefficient and less dispersion of these parameters, they found that the link between a/b and D_c may be employed for seismicity, earthquake risk, and hazard research.

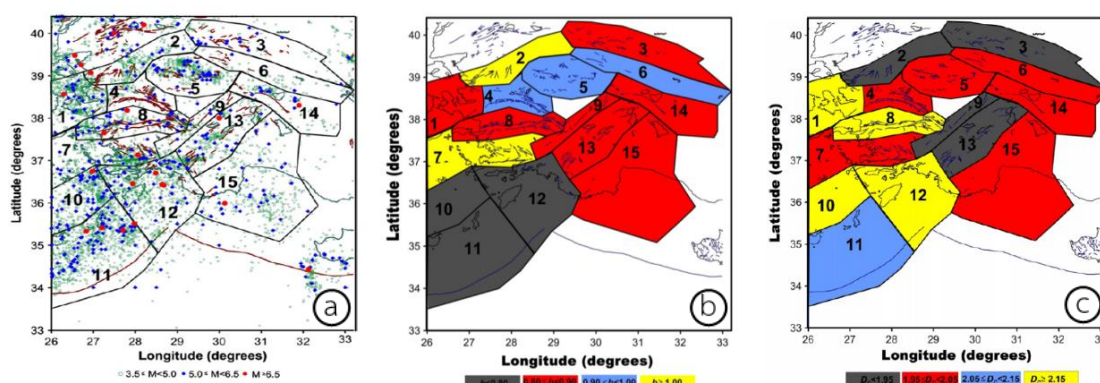


Figure 2.6. (a) The epicenters of earthquakes with a magnitude more than 3.5 for the last 50 years and 15 different seismicogenic zones in Western Anatolia. (b) b values, and (c) D_c values (Bayrak and Bayrak, 2012).

2.2.4 Precursory Seismic Quiescence before the earthquake

Katsumata (2011) research examined the activation and quiescence stages before the 2003 Tokachioki earthquake ($M_w = 8.3$), which struck off the coast of Hokkaido, Japan, on September 26th, 2003. A detailed analysis of the predetermined earthquake catalogue between 1994 and 2003 using a gridding technique (ZMAP) reveals that the 2003 Tokachioki earthquake was preceded by two neighbouring seismic quiescence anomalies that began in early 1999 and lasted approximately five years until the main shock occurred (Figure 2.7). These quiescence anomalies are situated near the asperity ruptured by the main shock, with Z values of 3.9 and 4.0 for a time frame of $T_w = 4$ years and a sample size of $N = 100$ earthquakes after five years till the main shock occurs.

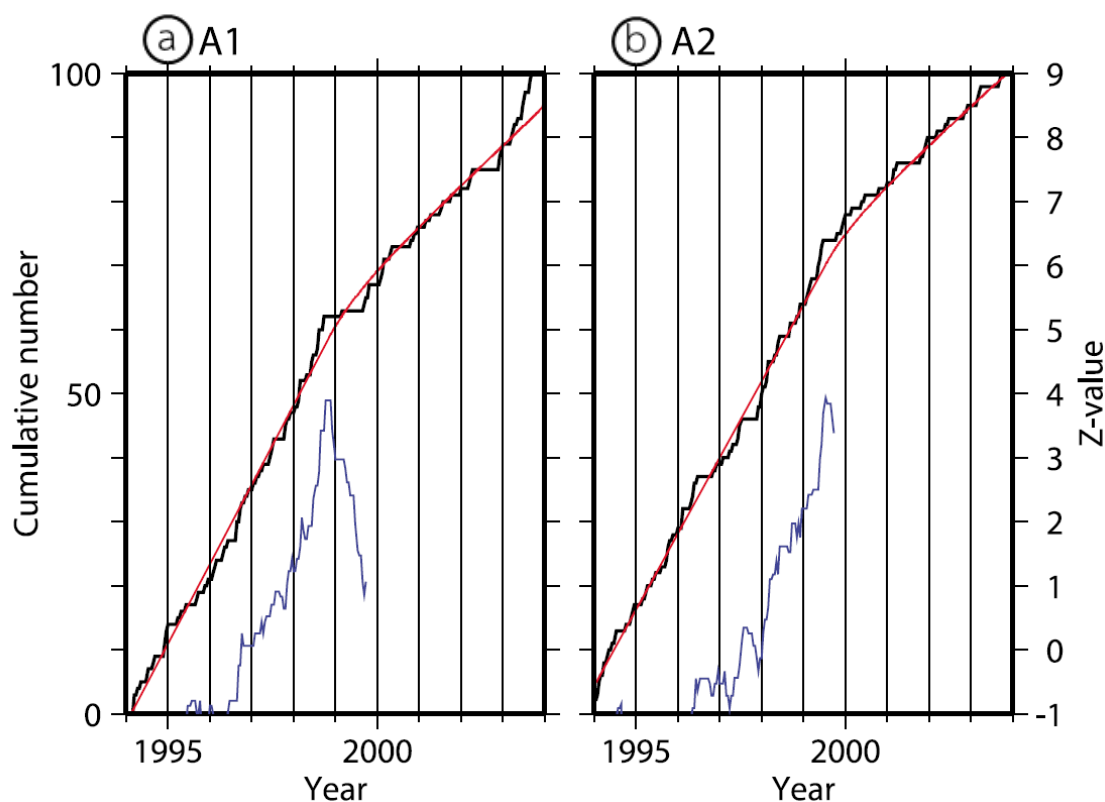


Figure 2.7. Cumulative number (black line) and Z value (blue line) plots for anomalous areas at Tokachioki, Japan. (Katsumata, 2011)**2.2.5 Applied region–time–length algorithm**

Chen and Wu (2006) studied the region–time–length (RTL) algorithm, which is used to examine changes in seismic activity before earthquakes in China, Italy, Japan, Russia, and Turkey, is used to look at changes in seismic activity around the epicenter of 1999, M_w -7.6, Chi-Chi earthquake. According to this analysis of the RTL values as seen in Figure 2.8, the epicenter area has a significant signal of anomalous activity, which is connected with and seismic activation seismic quiescence before the significant shock. As a result, temporal variation of RTL algorithm at the epicenter of the 1999 Chi-Chi earthquake shows that seismic activation began in 1993, while seismic quiescence began in 1997, and the incidence of earthquakes greater than 5.5 occurred within a typical distance of $2r_0$ from the epicenter of the Chi-Chi main shock.

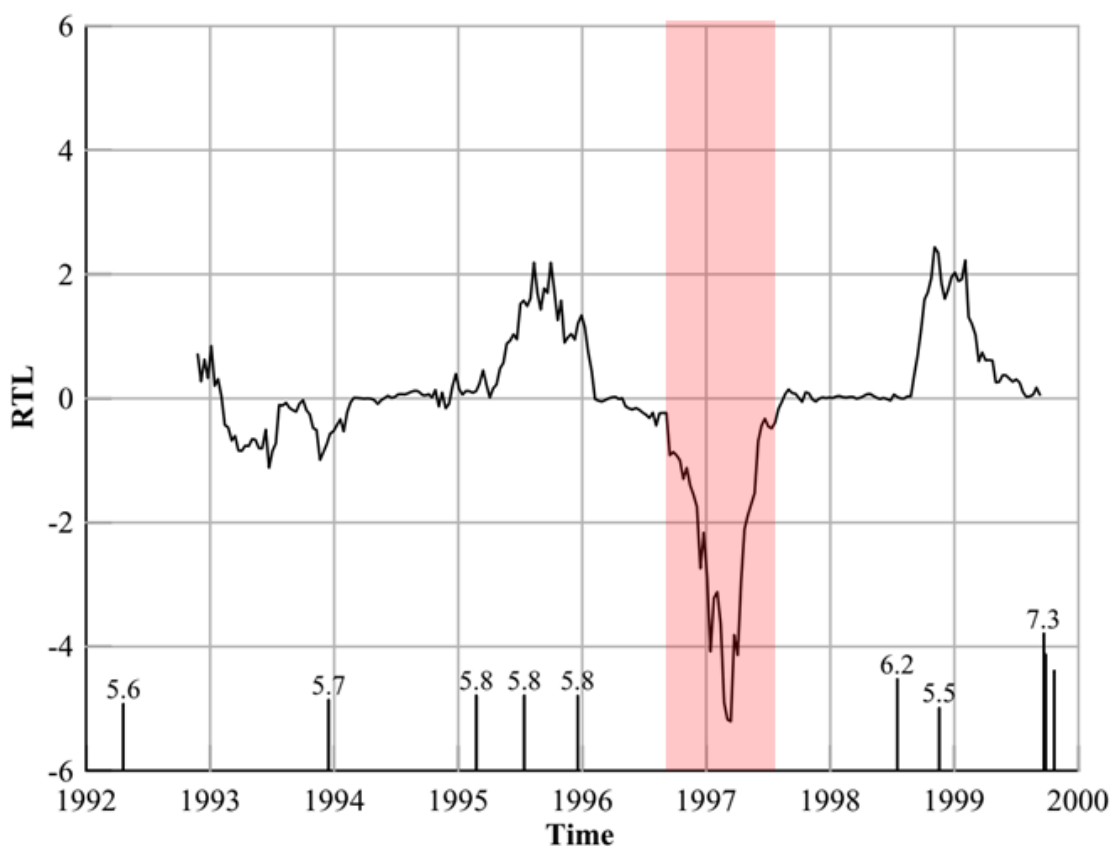


Figure 2.8. Temporal variation in the RTL function at the epicenter of the 1999 Chi-Chi earthquake. The bar chart depicts the incidence of earthquakes greater than 5.5 that occurred within a typical distance of $2r_0$ from the epicenter of the Chi-Chi main shock; the number next to each bar indicates the magnitude. Seismic activity began in 1993, while seismic quiescence began in 1997 (Chen and Wu, 2006).

2.3 Methodology

The methodology used in this work to investigate the statistical seismology in TLMB is split into eight steps, which are present in the sequence below (Figure 2.8).

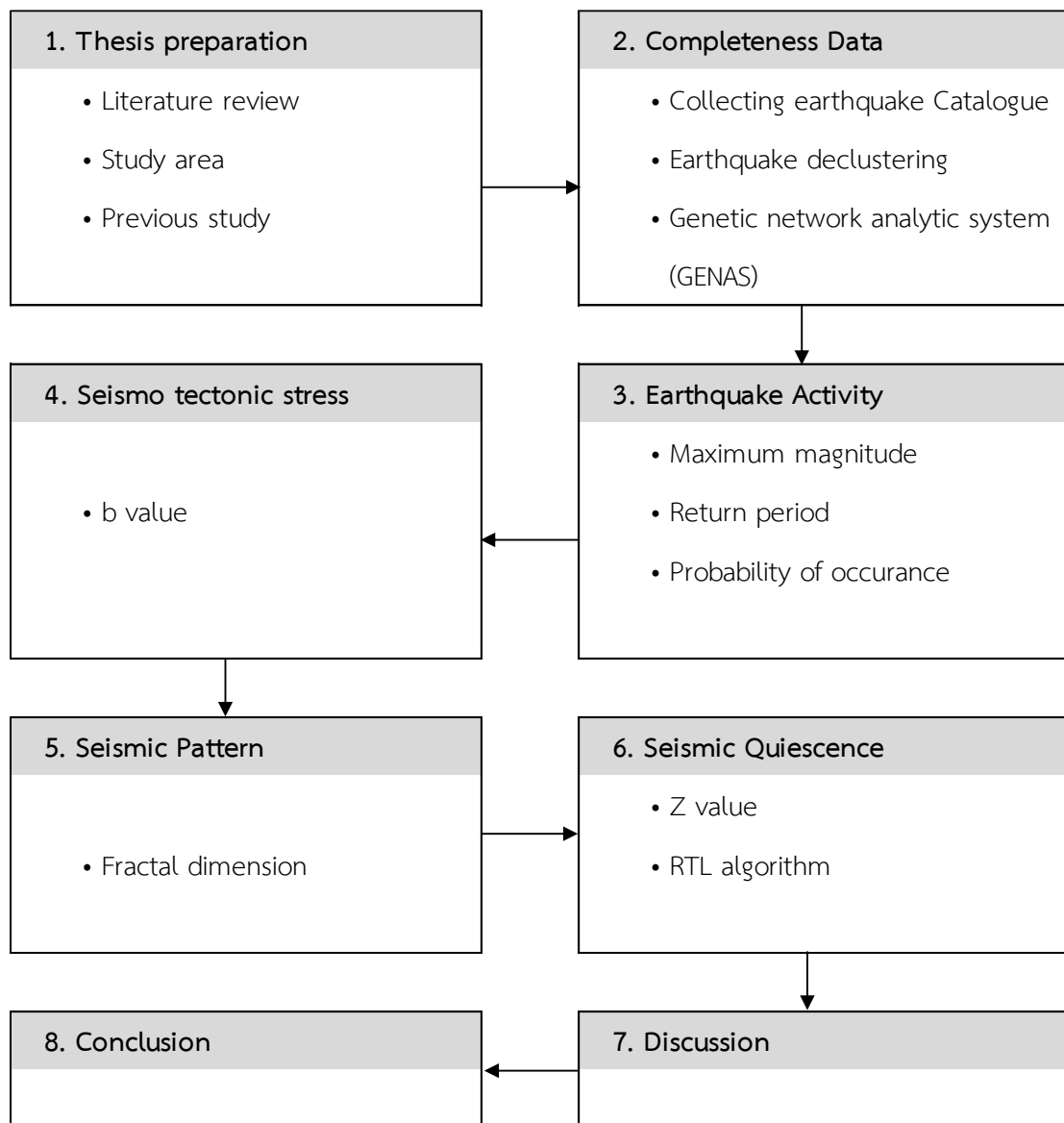


Figure 2.9. A simplified flow chart illustrating the eight steps of the methodology used in this study.

2.3.1 Thesis Preparation

This section is divided into three sections: a review of the literature, previous works on statistical seismology methodologies, and a discussion of the geology of the study area. This procedure aims to understand the methodology and conceptual information, specifically the various methods used to analyze the characteristics of the earthquake and prospective area, especially frequency-magnitude distribution, seismic pattern, seismotectonic stress, seismicity rate change, and seismic quiescence.

2.3.2 Completeness Data

The second stage is collected in the seismicity catalogue from the TMD. The raw data of the earthquake catalogue has been recorded non-systematically and non-clearly depending on the measurement capability. As a result, the data obtained is unreliable and cannot be analyzed statistically. It can be concluded that the earthquake catalogue must be modified and improved before being analyzed by statistical seismology to produce the most accurate earthquake catalogue. In this study, the improved parts such as earthquake declustering and genetic network analytic systems are described in further details in Chapter 3.

2.3.3 Earthquake Activity

The third section is to identify earthquake activity by finding the maximum magnitude, the return period, and the probability of occurrence using the adaptive frequency-magnitude distribution. Chapter 4 will go into further depth about it.

2.3.4 Seismotectonic Stress

This section concentrated on the b value in the frequency-magnitude distribution to identify a potential prospective area associated with seismotectonic stress. Chapter 5 will go deeper into the topic.

2.3.5 Seismic Pattern

This section focused on the fractal dimension or D_c value to indicate the seismic pattern and categorized it into line source, area source, volume source. Chapter 5 will go much further into the topic.

2.3.6 Seismic Quiescence

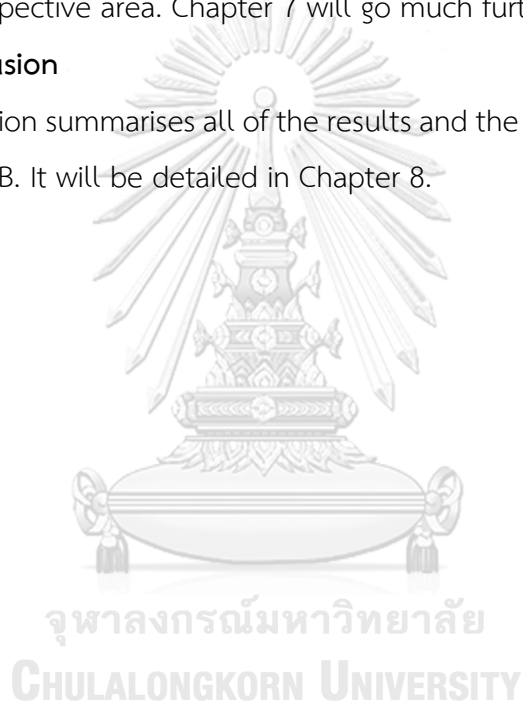
This part uses the data to analyze the seismic quiescence in TLMB by applying the seismicity rate change: Z value and seismic quiescence: RTL algorithm. It will be discussed in further depth in Chapter 6.

2.3.7 Discussion

The section will discuss statistical seismology results and compare them with the previous work on several topics such as earthquake activity, seismic stress, present-day activity and stress, the quiescence time span, the quiescence map, and the forecasting of prospective area. Chapter 7 will go much further into the topic.

2.3.8 Conclusion

The last section summarises all of the results and the discussion of the statistical seismology in TLMB. It will be detailed in Chapter 8.



CHAPTER 3

DATA COMPLETENESS

3.1 Collecting the Earthquake Catalogue

In this study, we used the earthquake from Thailand Meteorological Department (TMD) in this investigation. The earthquakes that occurred between January 4th, 2007, and September 22nd, 2020, near the TLMB (16.77° – 22.35°E and 97.48° – 103.17°N) will be investigated. There were 4,782 earthquakes with magnitudes ranging from 1.1 to 6.7 reported. The depth of the earthquake catalogue is from 0 to 230 km. The example of the earthquake catalogue is shown in Table 3.1.

Table 3.1. Example of Earthquake catalogue in TLMB.

Longitude	Latitude	Year	Month	Day	Magnitude	Depth	Hour	Minute	Second
97.58	19.54	2010	1	6	3.7	0	16	55	59
97.93	20.08	2010	1	15	2.9	0	23	1	38
98.14	20.45	2010	1	26	2.7	0	16	31	2
97.68	17.70	2010	1	29	2.9	0	20	18	18
97.90	19.50	2010	1	31	1.4	0	13	59	15
98.79	18.66	2010	2	1	1.1	0	10	44	23
99.04	19.00	2010	2	7	2.5	0	2	36	24
98.90	18.64	2010	2	7	1.1	0	10	47	55
98.98	18.20	2010	2	8	1.2	0	15	40	1
99.15	18.84	2010	2	8	1.2	0	21	21	12
98.86	20.93	2010	2	9	4.0	0	16	23	38
99.13	18.88	2010	2	12	1.0	0	15	0	40
99.07	19.79	2010	2	14	2.2	0	9	49	21

According to Pailoplee (2014a), the Thailand–Laos–Myanmar boundaries, where the BKK agency or TMD reports earthquakes most frequently with local magnitude (M_L) scales. In this work, we have used just the TMD catalog with local magnitude, which is homogeneity, and have therefore omitted magnitude conversion.

Figure 3.1 shows basic statistical detail of the catalogue and the histogram graph of the earthquake catalogue from TMD during the period 2007-2020 with magnitude histogram in Figure 3.1a, depth histogram in Figure 3.1b, date histogram in Figure 3.1c and hour histogram in Figure 3.1d.

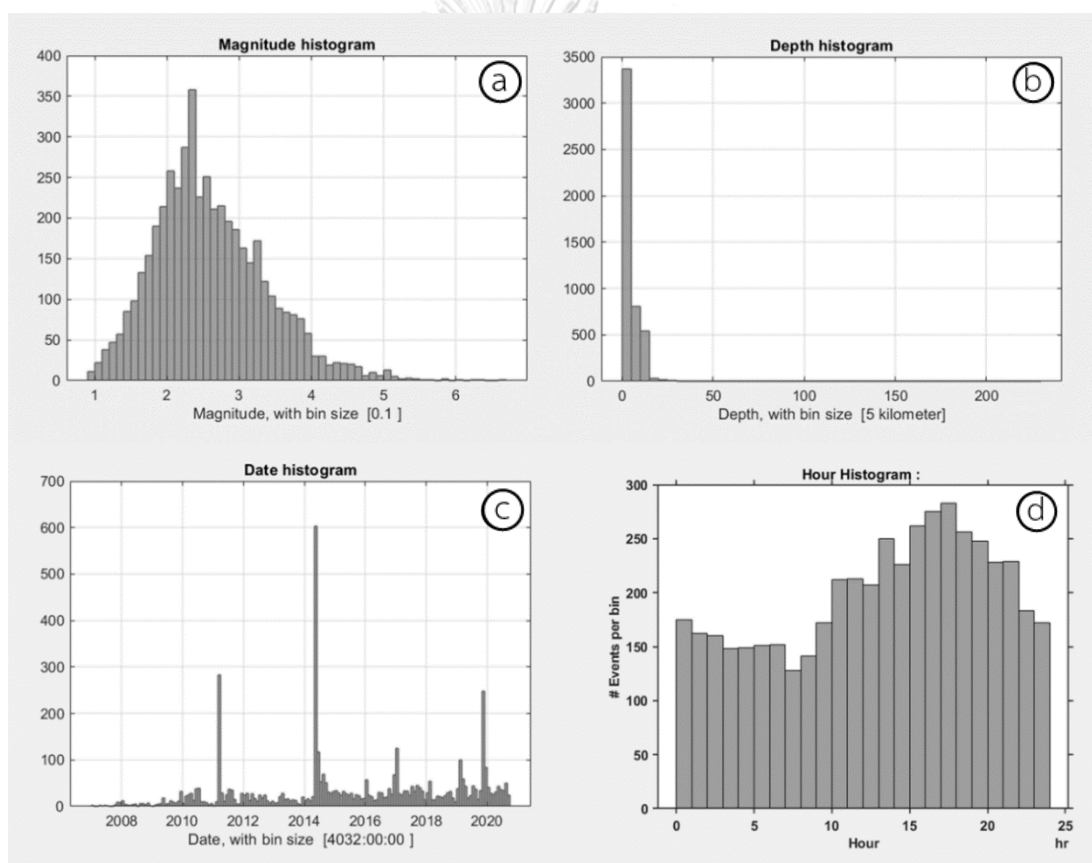


Figure 3.1. The photos from the ZMAP program (Wiemer, 2001) show the histogram graph of the earthquake catalogue from TMD during 2007-2020 (a) magnitude histogram, (b) depth histogram, (c) date histogram, and d) hour histogram.

3.2 Earthquake Declustering

Earthquake declustering is used to improve the earthquake catalogue by removing foreshocks and aftershocks to establish completeness. The foreshock and aftershock, and if not removed, it would bring bias into investigations of failure stress-related seismotectonic activities. Theoretically, the earthquake's main shock immediately corresponds to the released tectonic stress. In the meanwhile, the foreshock and aftershock are a byproduct of the pre- and co-seismic stress change of the main shock (Felzer, Abercrombie, and Ekstrom, 2004). Therefore, prior to any seismotectonic investigation, the foreshock and aftershock events must be declustered from the earthquake database. The declustering earthquakes in Mainland Southeast Asia, including the TLMB, Petersen et al. (2004) used the Gardner and Knopoff (1974) assumption. Consequently, Gardner and Knopoff (1974) categorization were used to classify the earthquake data in this study. After earthquake declustering 2,378 earthquakes with magnitudes ranging from 1.1 to 6.7 were reported. The depth of the earthquake catalogue is from 0 to 230 km.

3.3 Genetic Network Analytic System

Then, using the GENAS algorithm (Habermann, 1983; Habermann, 1987), eliminate the magnitude completeness's harmonic main shock. As seen in Figure 3.2, there is no evidence of apparent manufactured activity in the bulk seismicity rate, as noted by Wyss (1991) and Zúñiga and Wiemer (1999). On the other hand, there have been some rate changes in the seismicity rate in 2008, 2010, and 2016 (Figure 3.2). We must pick the catalogue without regard for rate change, but for the profits of this research, we must limit ourselves to the catalogue from 2008 to 2010 (Figure 3.3). Otherwise, there is a shortage of catalogues to examine. Thus, the remaining GENAS database is the 2010-2020 catalogue. As a result, we chose to include all 2,202 remaining main shocks with a magnitude of 1.0 reported between 2010 and 2020 in this analysis. Finally, the cumulative number of $M_L \geq 1.0$ main shocks produced a nearly straight line for the entire timeframe (Figure 3.4c), establishing the completeness of seismic data appropriate for statistical seismicity analysis.

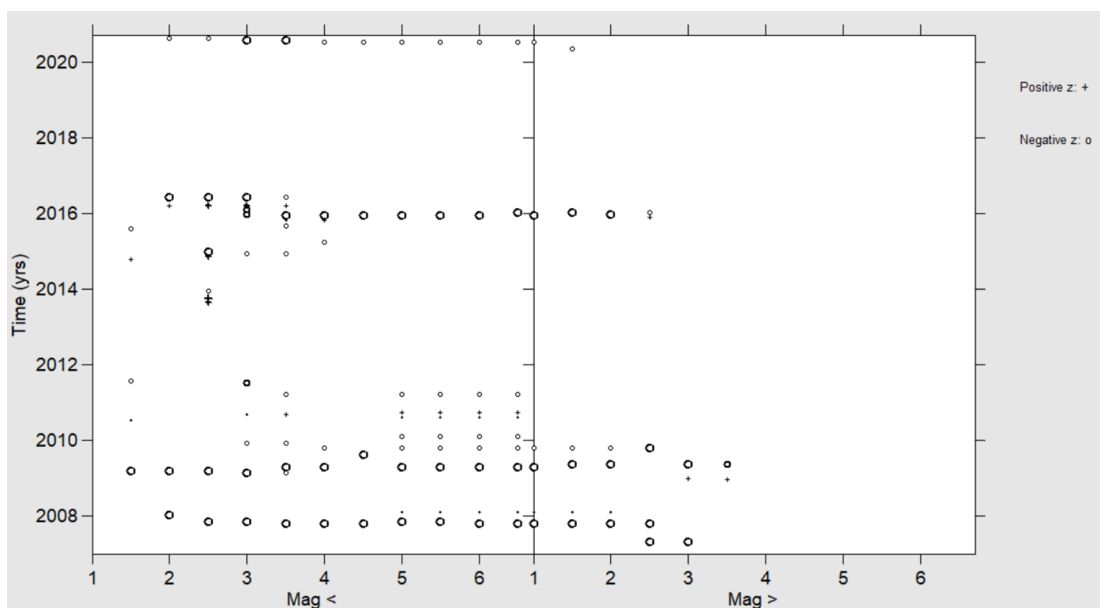


Figure 3.2. The photos from the ZMAP program (Wiemer, 2001) show the details of the earthquake catalogue from TMD from 2007 to 2020 after declustering.

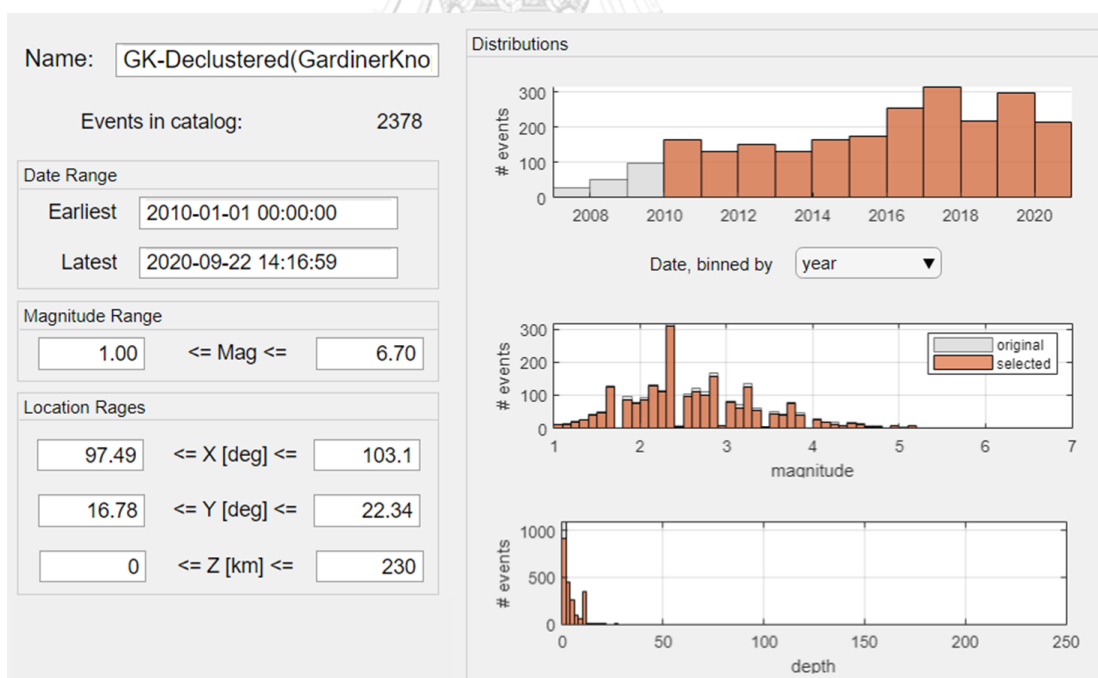


Figure 3.3. The photos from the ZMAP program Wiemer (2001) show the details of the earthquake catalogue from TMD during the period 2007-2020 after declustering and GENAS.

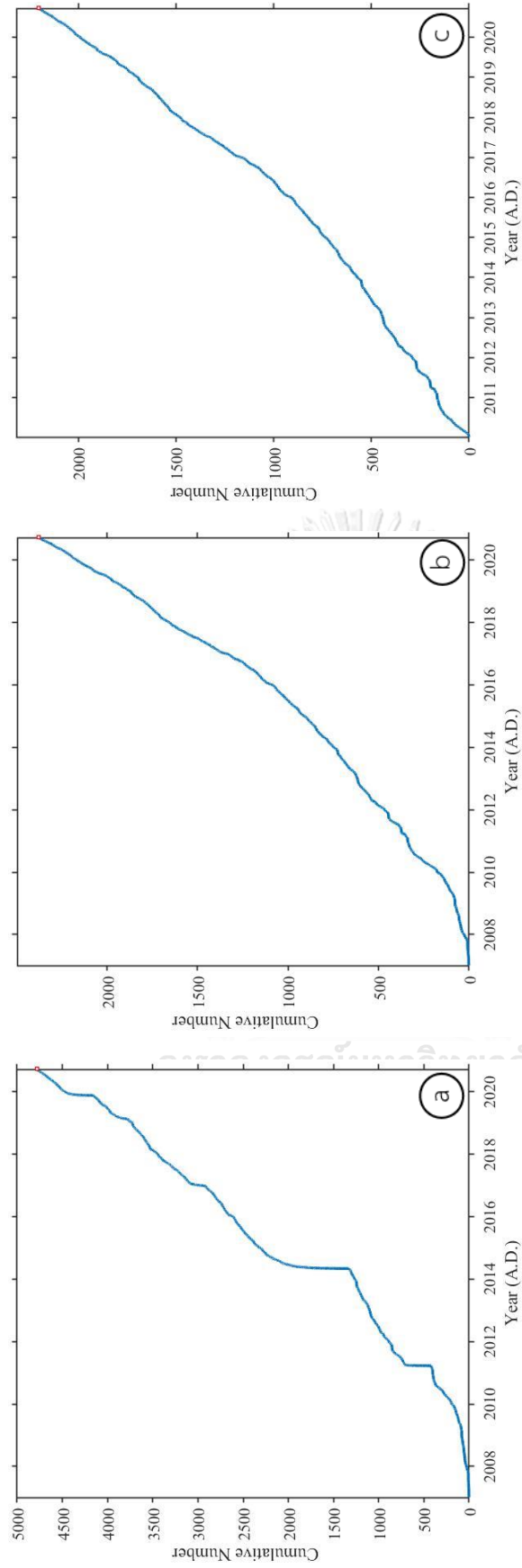


Figure 3.4. Cumulative number graph showing the (a) seismicity detected from TMD during period 2007-2020 (b) the earthquake catalogue after declustering and GENAS. after declustering and (c) the earthquake catalogue after declustering and GENAS.

CHAPTER 4

EARTHQUAKE ACTIVITY

4.1 Earthquake Frequency-Magnitude Distribution

To investigate earthquake activity, we first investigated the FMD of all chosen earthquake data (i.e., $M_L \geq 1.0$ reported between 2010 and 2020) and calculated the magnitude of completeness (M_c), which represents the magnitude level of the whole report. The FMD in Figure 4.1 estimates the a and b values, which are 4.85 and 0.68, respectively. The M_c is approximately $3.0 M_L$ using the maximum likelihood method.

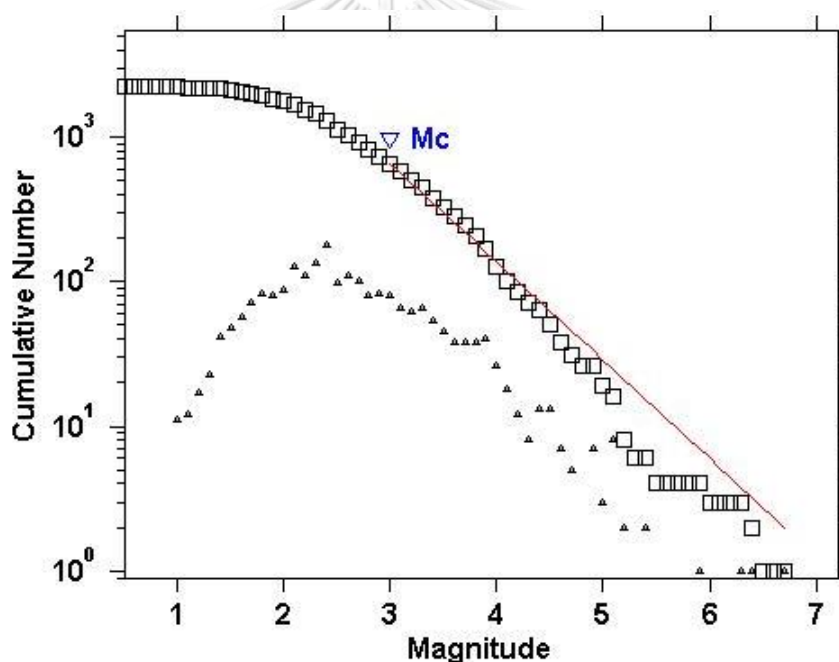


Figure 4.1. FMD plot of the earthquake catalogue from TMD from 2007 to 2020. White squares show the cumulative number of earthquakes equal to or larger than each magnitude, Grey squares shows the number of earthquakes of each magnitude and solid lines are the lines of best fit, following Woessner and Wiemer (2005). M_c defined as the magnitude of completeness.

The research area was gridded at $0.25^\circ \times 0.25^\circ$ spacing to analyze seismic activity spatially. Following iterative tests, all earthquake occurrences from the specified catalogue (the 2,022 mainshock events mentioned above) occurred within a 100 km radius of each chosen grid node. The a and b values and other statistically significant values were then computed and spatially mapped using the ZMAP tool (Wiemer, 2001). Finally, The FMD was plotted spatially for selected locations, as seen in Figure 4.2. Moreover, we covered the area in Figure 4.2a and b where the FMD goodness of fit was less than 60 percent with a white mask in order to avoid unreliable data.

Figure 4.2a the a -value map shows the obvious zone of low a value at the boundary of Thai-Laos on southwest of Luang Prabang, Laos. On the other hand, the zone of high a value at the north of Mong Pan, Myanmar.

Figure 4.2b the b -value map, the southwestern part of Luang Prabang, Laos and the boundary of Thai-Laos-Myanmar shows low b value indicating high activity area. On the other hand, Chiang Mai, Thailand, and north of Mong Pan, Myanmar, show the area of high b values that indicate low activity area.

Figures 4.2c and 4.2d show that the FMD standard deviation and goodness of fit that derived a and b values are likely to be reliable with low variation.

Based on Figure 4.2a and 4.2b, the spatial distribution of a and b values was nearly identical. Low a and b values indicate high earthquake activity. Seismotectonically, comparatively low a and b values indicates a low ratio of minor to major earthquakes and low earthquake activity.

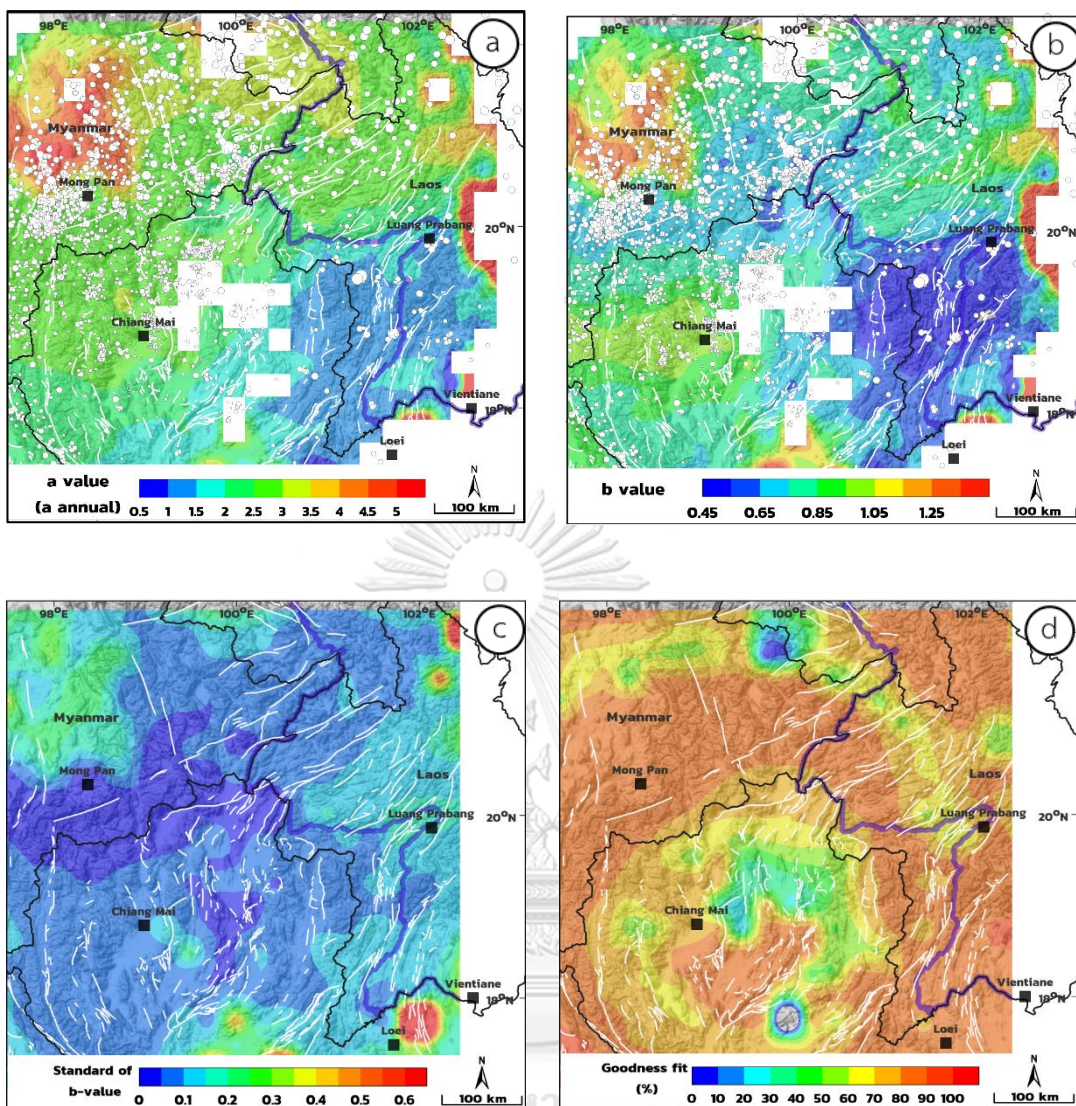


Figure 4.2. Spatial distributions of the (a) a value, (b) value, (c) standard deviation of b value, and (d) Percent of the goodness fit of the FMD (white dots are earthquake epicenters).

4.2 Maximum Magnitude

According to Yadav et al. (2011), the a and b values from the FMD may be used to derive a variety of values that describe the earthquake activity in term of the possible maximum magnitude in 1, 5, 30 and 50 years was then calculated and mapped in Figure 4.3.

In figure 4.3a, the results indicate that the small portions at east of Mong Pan, Myanmar is the high activity area, generating a maximum magnitude of around 5.1 M_L in 5 years. On the other hand, the lowest activity area is in the south of the study area, generating a maximum magnitude of 2.0-3.0 in 5 years.

In Figure 4.3b, the results indicate the area of Mong Pan, Myanmar, the boundary of Thai-Laos-Myanmar, generating a maximum magnitude of around 5.6 M_L in 10 years. In contrast, the lowest activity is in the south of the study area, generating a maximum magnitude of 3.0-4.0 in 10 years.

In Figure 4.3c, the results indicate that from Mong Pan, Myanmar to the northeast of Myanmar, and the small portions of the south of Luang Prabang, Laos, can generate a maximum magnitude of around 6.3 M_L in 30 years. On the other hand, the lowest activity is located in the south of the study area around the lower northern of Thailand, generating a maximum magnitude of 3.0-4.0 in 30 years.

Figure 4.3d indicate that from Mong Pan, Myanmar, to the northeast of Myanmar, and southwest of Luang Prabang, Laos, can generate a maximum magnitude of around 6.7 M_L 50 years. On the other hand, the lowest activity is in the south of the study area around the lower northern of Thailand, generating a maximum magnitude of 3.5-4.5 in 5 years.

It may be concluded that the high-activity zone spans to the northwest and southeast of the study area. In contrast, the high-activity region located in the south of the research area.

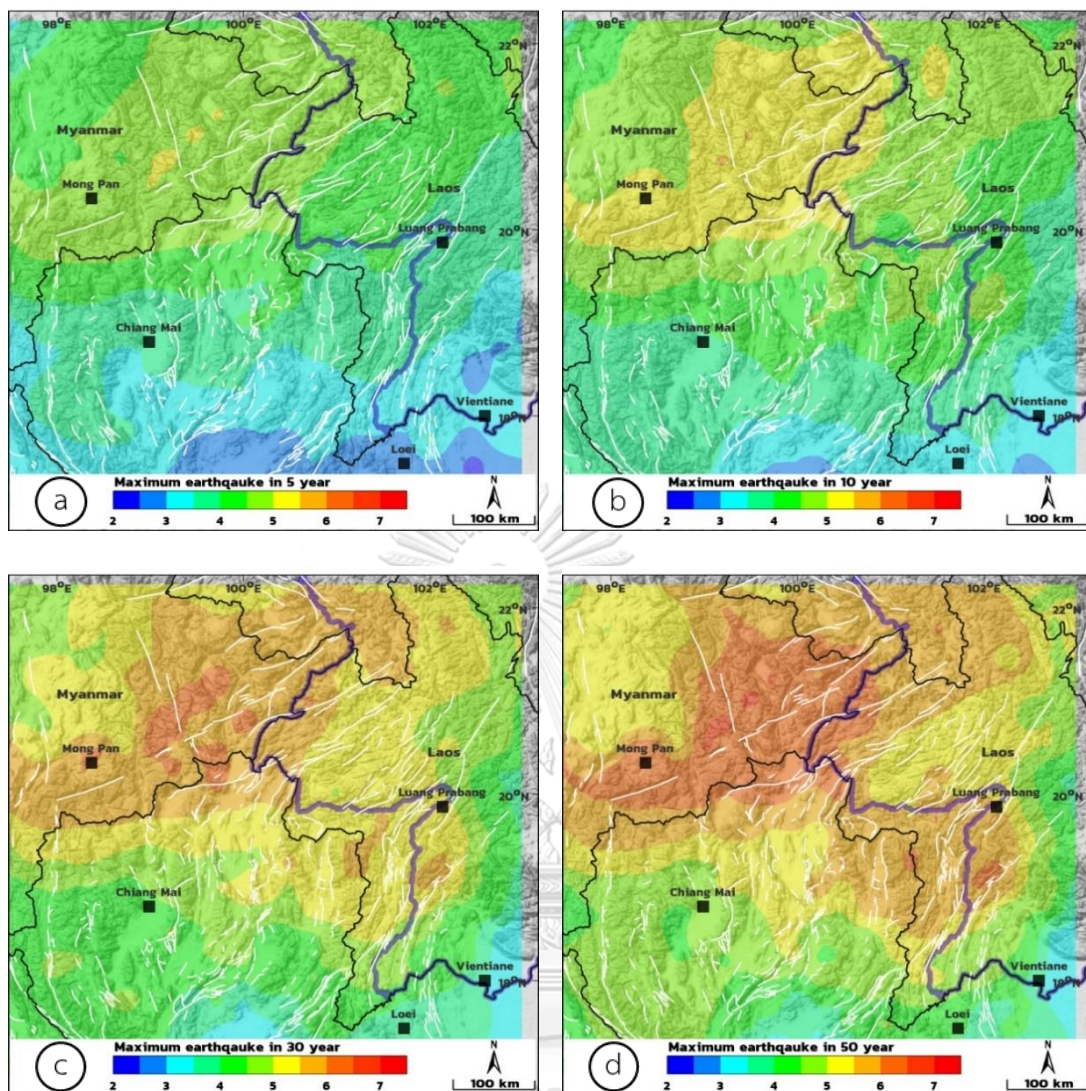


Figure 4.3. Map of TLMB showing the maximum earthquake magnitude generated in the particular period of the next (a) 5, (b) 10, (c) 30, and (d) 50 years.

4.3 Return Period

Figure 4.4a is the map showing the return period of the M_L -4.0 earthquake. The results reveal that the east of Mong Pan, Myanmar, to east of Myanmar have a return period of 4.0 M_L in 1 year. The area of Chiang Mai, Thailand, to Luang Prabang, Laos, has a five-year return period of 4.0 M_L .

Figure 4.4b is the map showing the return period of the M_L -5.0 earthquake. The results reveal that the east of Mong Pan, Myanmar to east of Myanmar, and south of Luang Prabang, Laos have a return period of 5.0 M_L in 10 years. On the other hand, the area of Chiang Mai, Thailand, and north of Luang Prabang, Laos, has a return period of 5.0 M_L around 25 years.

Figure 4.4c is the map showing the return period of the M_L -6.0 earthquake. The results reveal that the border of three countries covering the east of Mong Pan, Myanmar, east of Myanmar, and south of Luang Prabang, Laos, have a return period of 6.0 M_L around 25 years.

Figure 4.4d is the map showing the return period of the M_L -7.0 earthquake, and the results reveal that the border of three countries covering east of Mong Pan, Myanmar to east of Myanmar, and south of Luang Prabang, Laos, has a return period of 7.0 M_L around 75 years.

The results of the return period reveal that the results indicate that around the border of three countries covering the northeastern part of Mong Pan, Myanmar, and the southwestern part of Luang Prabang, Laos, has the potential to generate an earthquake within a short period. In contrast, the average time intervals of the earthquake occurrences were longer for the western part of Chiang Mai.

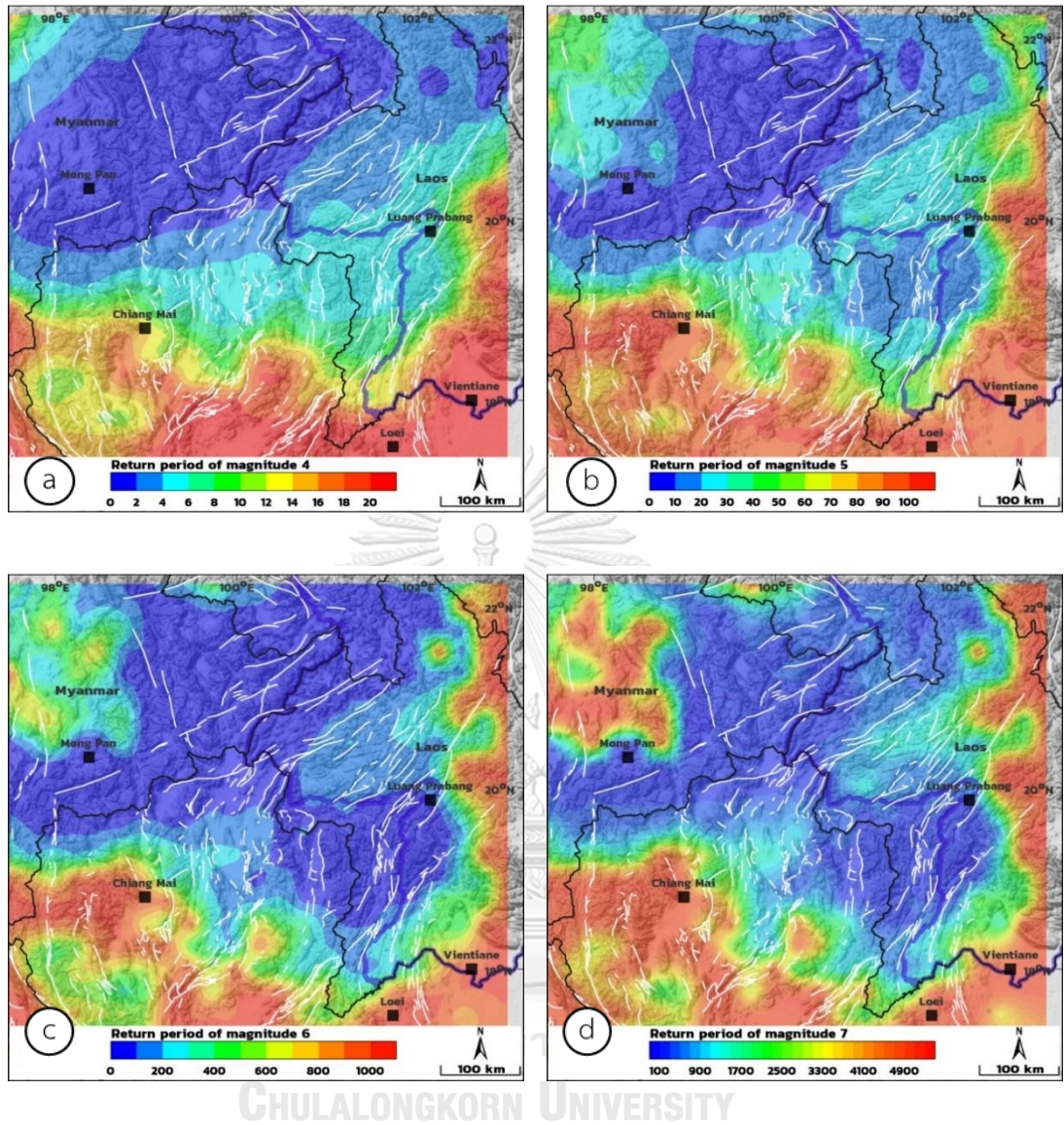


Figure 4.4. Map of the TLMB showing the recurrence interval of earthquakes with an individual M_L of (a) 4.0, (b) 5.0, (c) 6.0, and (d) 7.0

4.4 Probability of Occurrence

Figure 4.5a is the map showing the probability of occurrence of the M_L -4.0 earthquake. The results reveal that the probability of occurrence of the earthquake with M_L of 4.0 is almost 100% covering the study area.

Figure 4.5b is the map showing the probability of occurrence of the M_L -5.0 earthquake. The results reveal that the probability of occurrence of the earthquake with M_L of 5.0 in the Mong Pan, Myanmar Luang Prabang, Laos is 100%, and in Chiang Mai, Thailand is 30-70%.

Figure 4.5c is the map showing the probability of occurrence of the M_L -6.0 earthquake. The results reveal that the probability of occurrence of the earthquake with M_L of 6.0 on the border of three countries covering east of Mong Pan, Myanmar to east of Myanmar, and south of Luang Prabang, Laos is 60-90%, and in Chiang Mai to Loei, Thailand is 0-30%.

Figure 4.5d, the results reveal the probability of occurrence of the earthquake with M_L of 7.0 on the border of three countries covering east of Mong Pan, Myanmar to east of Myanmar, and south of Luang Prabang, Laos is 30-60%.

The results reveal that the results indicate that around the border of three countries covering the eastern part of Mong Pan, Myanmar, the southwestern part of Luang Prabang, Laos covering the east of Chiangmai, Thailand is the high activity zone with a high probability of generating an earthquake. In contrast, the eastern part of Chiang Mai is a low activity zone with a low probability of earthquake occurrence.

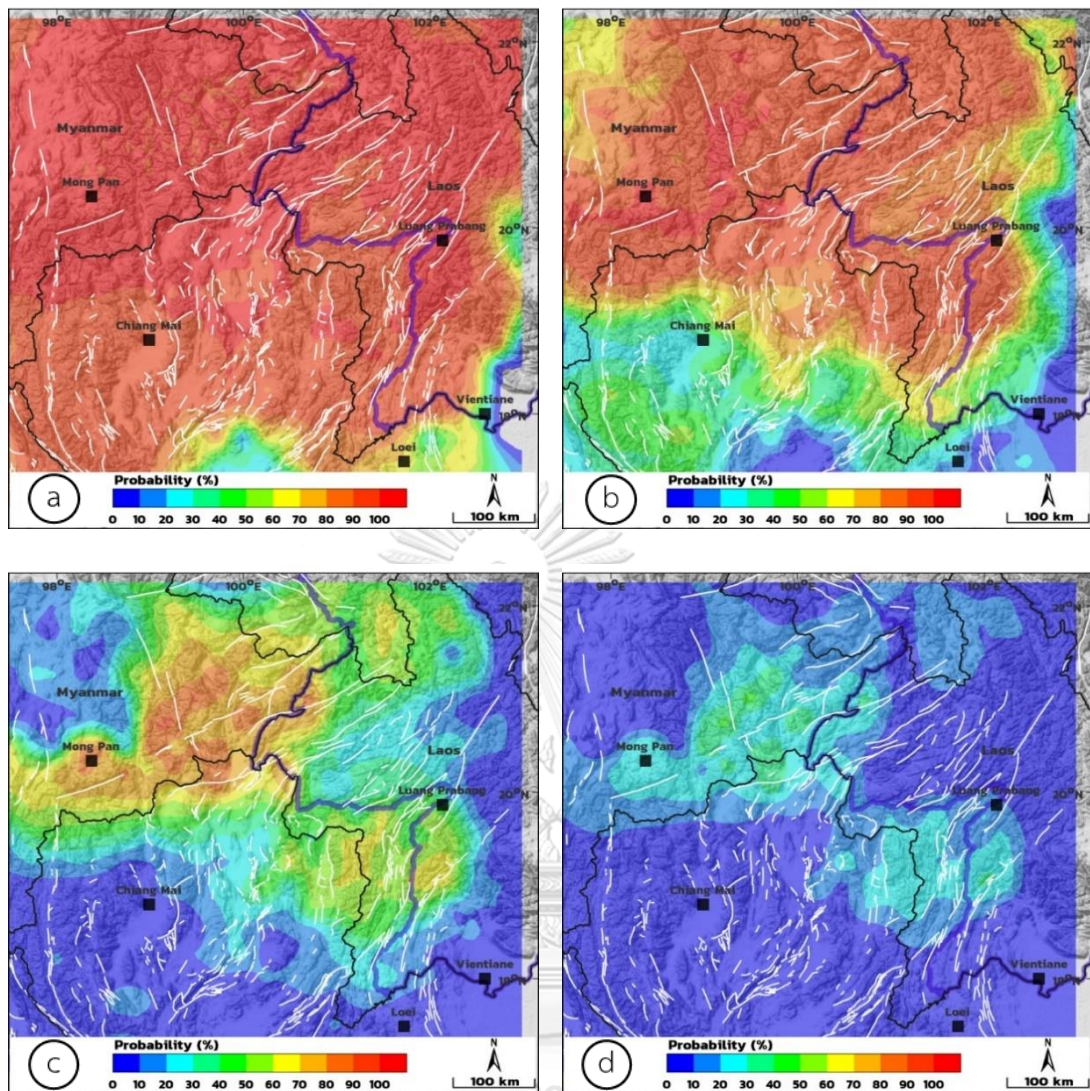


Figure 4.5. Map of the TLMB showing probabilities of an earthquake with a magnitude of (a) 4.0, (b) 5.0, (c) 6.0, and (d) 7.0 M_L that could be generated in the next 50 years.

CHAPTER 5

SEISMOTECTONIC STRESS AND SEISMIC PATTERN

5.1 Seismotectonic Stress

In this study, we evaluate large earthquakes with a magnitude more than 5.0 M_L to conduct a retrospective test, which looks back on past occurrences and examines the factors that contributed to the results defined at the start of the study. Although this term is used in the scope of b-value analysis, it all began with determining the circumstances surrounding seismic incidents, which led to the investigation of case studies in Table 5.1 detailing 19 occurrences.

Once we obtain the earthquake catalogue, we can compute the b value using the ZMAP program in the MATLAB script by Wiemer (2001). It requires the gridding of the study area at each node. First, the M_c and b values were calculated using the N events that occurred nearest the node, where N is a fixed number. Then it uses the greatest likelihood method to compute b values. Finally, calculate the standard deviation of the b value and the goodness of fit of the spatial map in addition to the standard deviation to verify that the outcome is accurate.

To compute b values representing temporal changes, we needed to establish a suitable condition for computing b values in the TLMB zone, where the number of events was fixed at any radius. The sample size of events varied between 20, 25, 30, 35, and 40 to obtain a suitable number for detecting more stable findings, plotting the FMD, and determining the b value. Additionally, the earthquake catalogue is separated into four categories based on year, namely 2010-2012, 2010-2014, 2010-2016, and 2010-2018. The radius of this approach varies with the earthquake density while the number of events remains constant. Then, using the Surfer v.16 software, the estimated b value in each node was converted to a color code to identify anomalies and map the spatial distribution of b values, standard deviation, and percent of goodness fit. The parameters of 40 events are the most appropriate. The high consistency between locations with a low b value and the subsequent occurrence of an earthquake with a magnitude ≥ 5.0 in each area was identified.

Table 5.1. List earthquakes with a magnitude (M_L) greater than 5.0 that occurred along the TLMB between 2010 and 2020.

No	Longitude (°N)	Latitude (°E)	Date	Time (UTC)	Depth (km)	M_L
1	100.03	21.2	19-03-2010	23:23	0	5.0
2	101.74	18.82	23-02-2011	16:10	0	5.4
3	99.91	20.87	24-03-2011	14:17	0	6.7
4	99.08	21.69	12-07-2011	21:46	0	5.0
5	100.05	22.3	17-09-2012	07:23	0	5.1
6	97.68	18.96	10-04-2013	02:35	0	5.1
7	100.62	21.49	22-09-2013	23:44	10	5.2
8	99.62	19.7	05-05-2014	00:50	7	5.2
9	99.692	19.748	05-05-2014	11:19	7	6.3
10	99.88	20.52	09-06-2014	14:10	5	5.1
11	98.45	21.74	26-12-2014	17:31	10	5.4
12	99.02	20.56	24-05-2015	10:55	16	5.1
13	101.29	21.88	05-03-2016	12:20	10	5.1
14	102.35	22.05	22-04-2016	01:38	20	5.1
15	100.12	20.71	18-04-2017	19:42	2	5.1
16	99.53	20.62	03-02-2018	15:31	5	5.1
17	97.97	20.27	01-07-2018	20:42	2	5.0
18	101.376	19.456	20-11-2019	00:02	3	6.4
19	101.333	19.421	20-11-2019	21:19	5	5.9

The result is shown in Figure 5.1. First, in Figure 5.1a, the spatial distribution of b values in 2010-2012 indicates that two regions with low b values were discovered: i) in the east of Mong Pan, Myanmar, along TLMB, ii) surrounding Chiangmai to Loei, Thailand. The fourteen earthquakes (no. 6-19 in Table 5.1) occur after this period. Five earthquakes were located in a low b -value area (no. 7, 10, 15, 16, 17, and 18). The 5.1 M_L in 2014, 5.1 M_L in 2017, and 5.1 M_L in 2018 (no. 10, 15, and 16 in Table 5.1) are in the east of Mong Pan, Myanmar. The 5.0 M_L in 2018 (no.17 in Table 5.1) in East of Mong Pan and the Last one of 5.2 M_L in 2013 (no. 7 in Table 2) is in south Yunnan. The other nine earthquakes (no. 6, 8, 9, 11, 12, 13, 14, 18, and 19) are not located in a low b -value area.

Figure 5.1b, the spatial distribution of b value in 2010-2014. Three regions with low b values were discovered: i) east of Mong Pan, Myanmar, ii) NW to SE trend from NE Chiangmai to Vientiane, Laos, and iii) south of Chiangmai. Eight earthquakes (No. 12-19 in Table 5.1) with an $M_L \geq 5.0$, which recorded after this period. Five earthquakes were located in a low b value area (No. 12-17 in Table 2).

Figure 5.1c, the spatial distribution of b value in 2010-2016. The area with a low b value was discovered: i) west of Mong Pan, Myanmar, ii) from the east of Mong Pan, Myanmar, southward to Vientiane, Laos, iii) south of Chiangmai, and iv) Luang Prabang, Laos. Five earthquakes with an M_L greater than 5.0, which recorded after this period. All the earthquakes are in the low b -value area except 5.1 M_L in 2021 in the northwest of Mong Pan

Figure 5.1d, the spatial distribution of b value in 2000-2018; Low b -value areas were found to be in the northwest-southeast trend from i) the eastern part of Mong Pan, Myanmar, ii) the southern part of Chiangmai, and iii) the northeastern-eastern part of Chiangmai, Thailand. Two earthquakes with an M_L greater than 5.0 were recorded after this period. All the earthquakes are in a low b -value area except 5.1 M_L in 2021 in the northwest of Mong Pan, Myanmar, which shows a high SD of b value and low goodness fit

Abnormally high b value also showed a high standard deviation of b value and low percent of goodness. The remark in the east of Chiang Mai, Thailand, in the area with low b values, but no earthquake with $M_L > 5.0$ occurred.

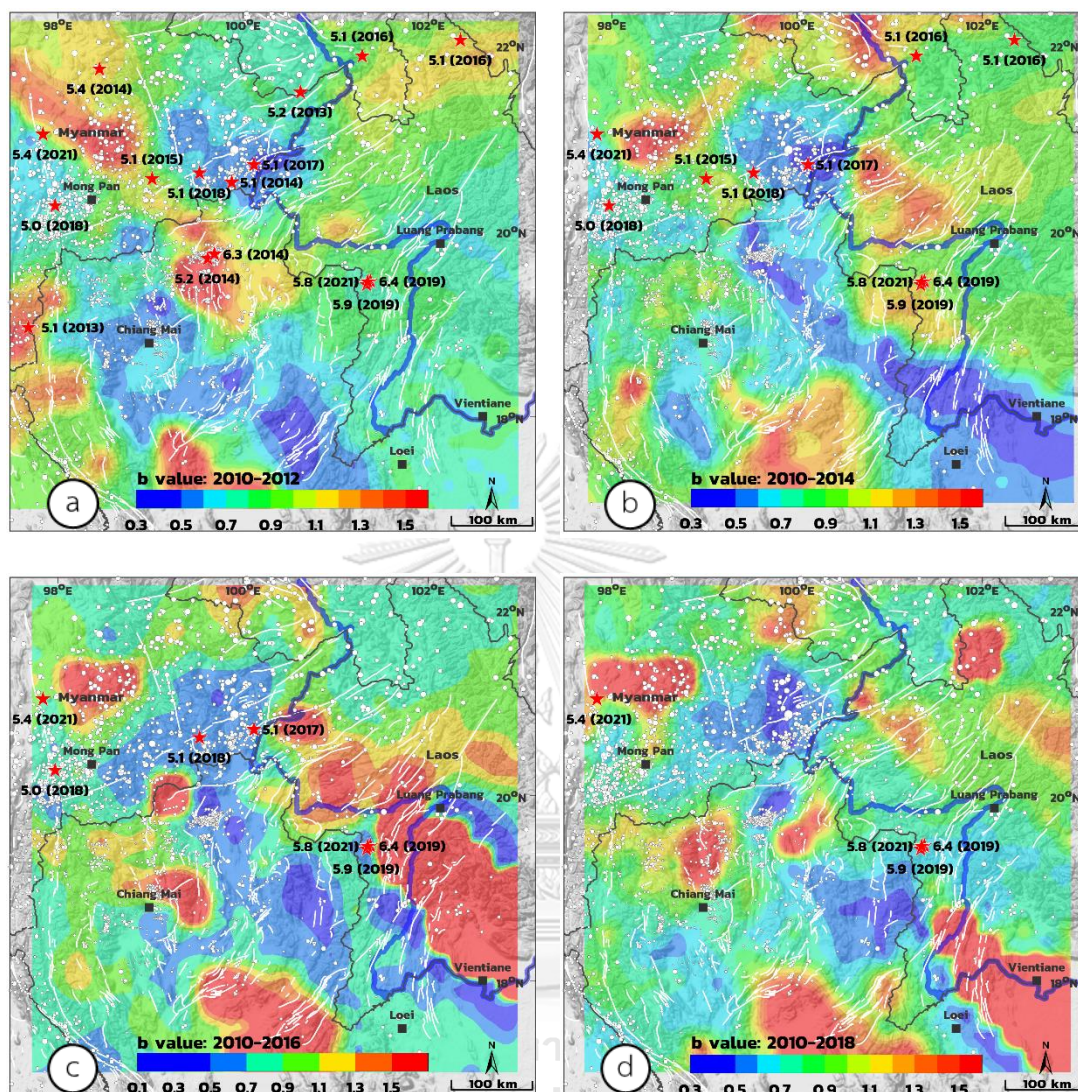


Figure 5.1. Distribution of b value along the TLMB between (a) 2000-2012, (b) 2000-2014, (c) 2000-2016, and (d) 2000-2018. The red stars indicate earthquakes greater than 5.0 that occurred after the data collection and the white dots are the epicenters.

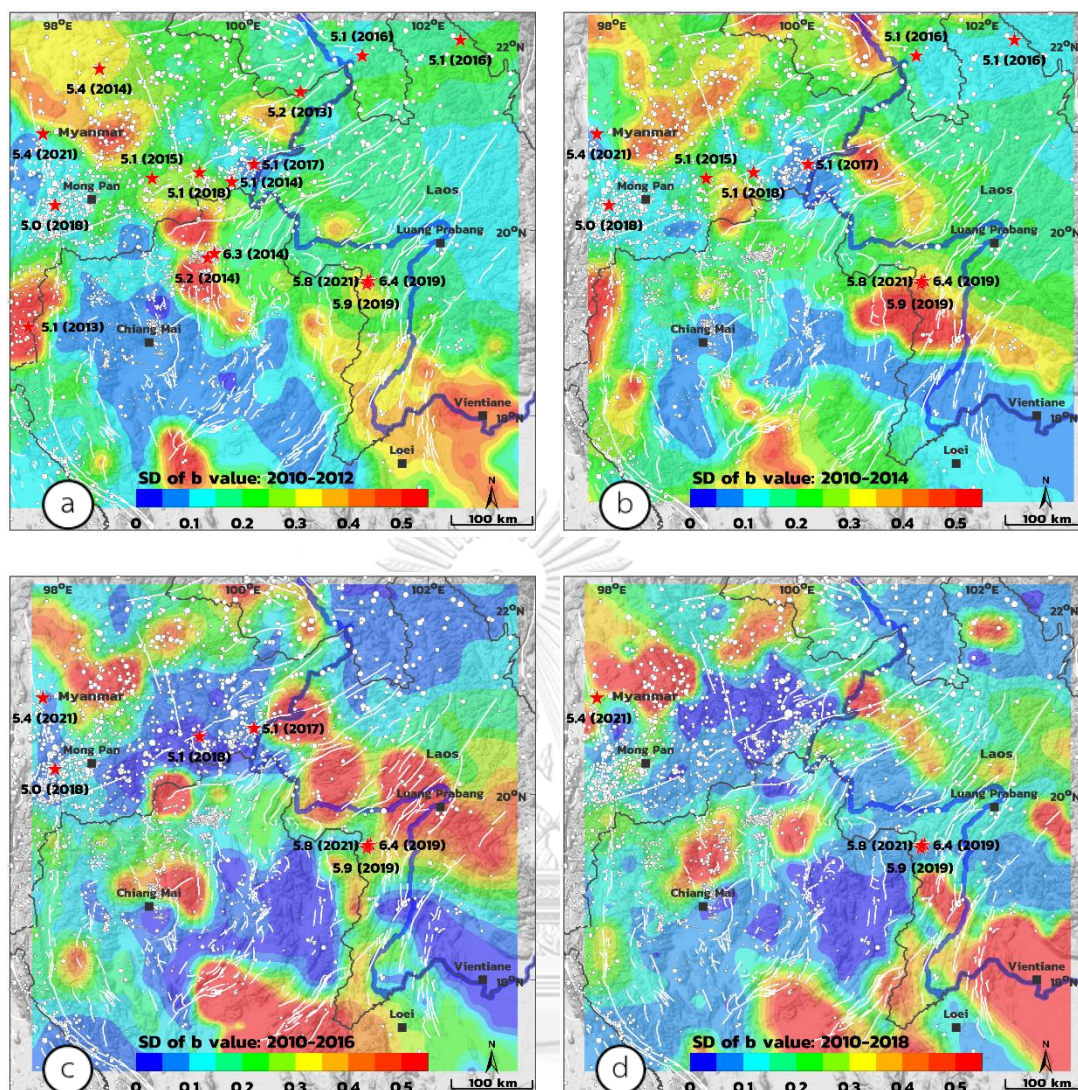


Figure 5.2. Distribution of Standard deviation of b value along the TLMB between (a) 2000-2012, (b) 2000-2014, (c) 2000-2016, and (d) 2000-2018. The black star indicates earthquakes with a magnitude greater than 5.0 that occurred after the period for gathering earthquake data and the white dots are the epicenters.

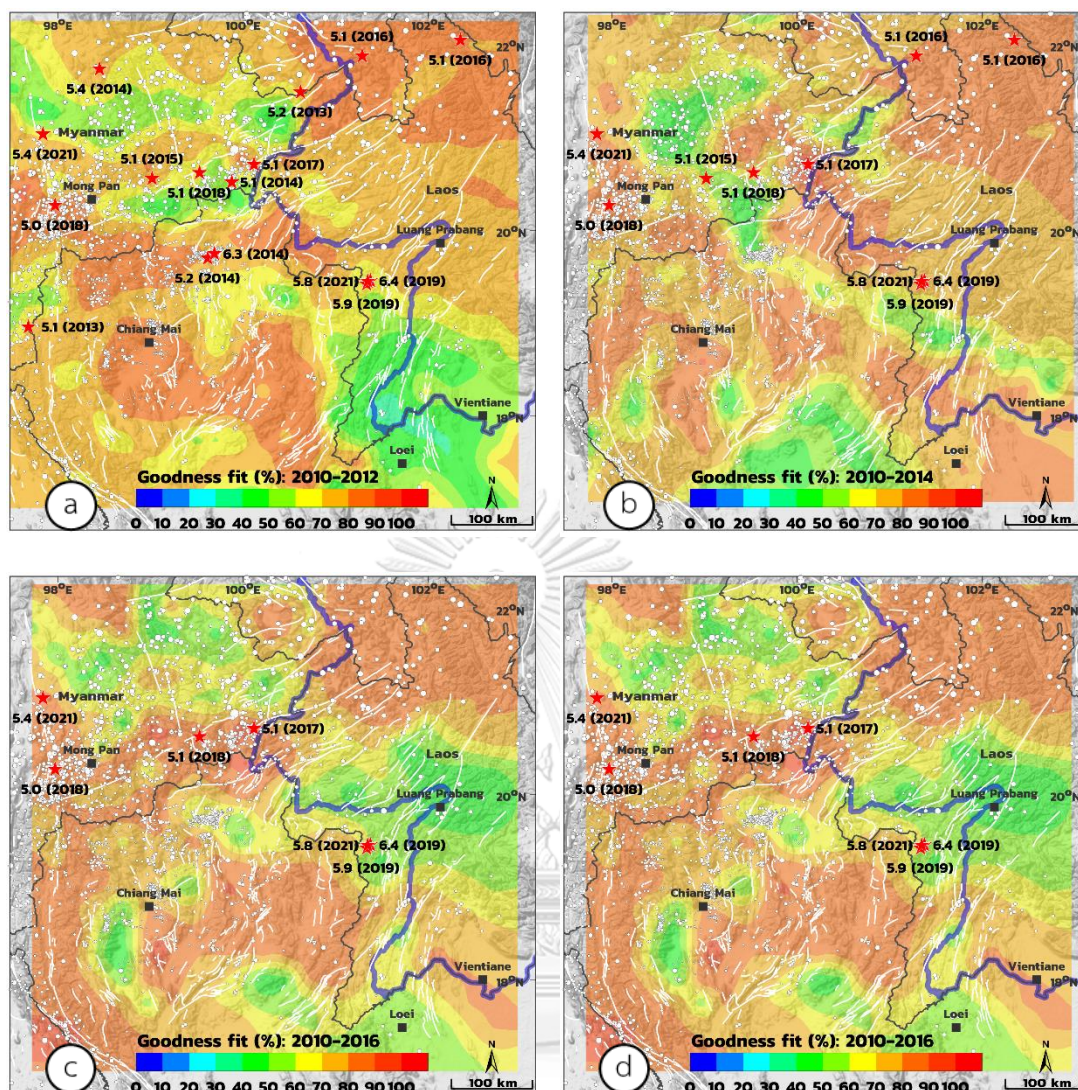


Figure 5.3. Distribution of percent of goodness fit of b value along the TLMB between (a) 2000-2012, (b) 2000-2014, (c) 2000-2016, and (d) 2000-2018. The red star indicates earthquakes greater than 5.0 that occurred after the data collection and the white dots are the epicenters.

5.2 Seismic Pattern

The fractal dimension (D_c value) is a natural phenomenon that analyses seismicity's spatial distribution. It explains the earthquake's seismic pattern. The integral correlation approach for fractals analysis is employed in this work to explore the spatial distribution of the earthquake in TLMB (Grassberger and Procaccia, 1983). First, the fractal dimension was calculated by fitting the data to the log-log plot of $C(r)$ versus r and finding the slope in a straight line.

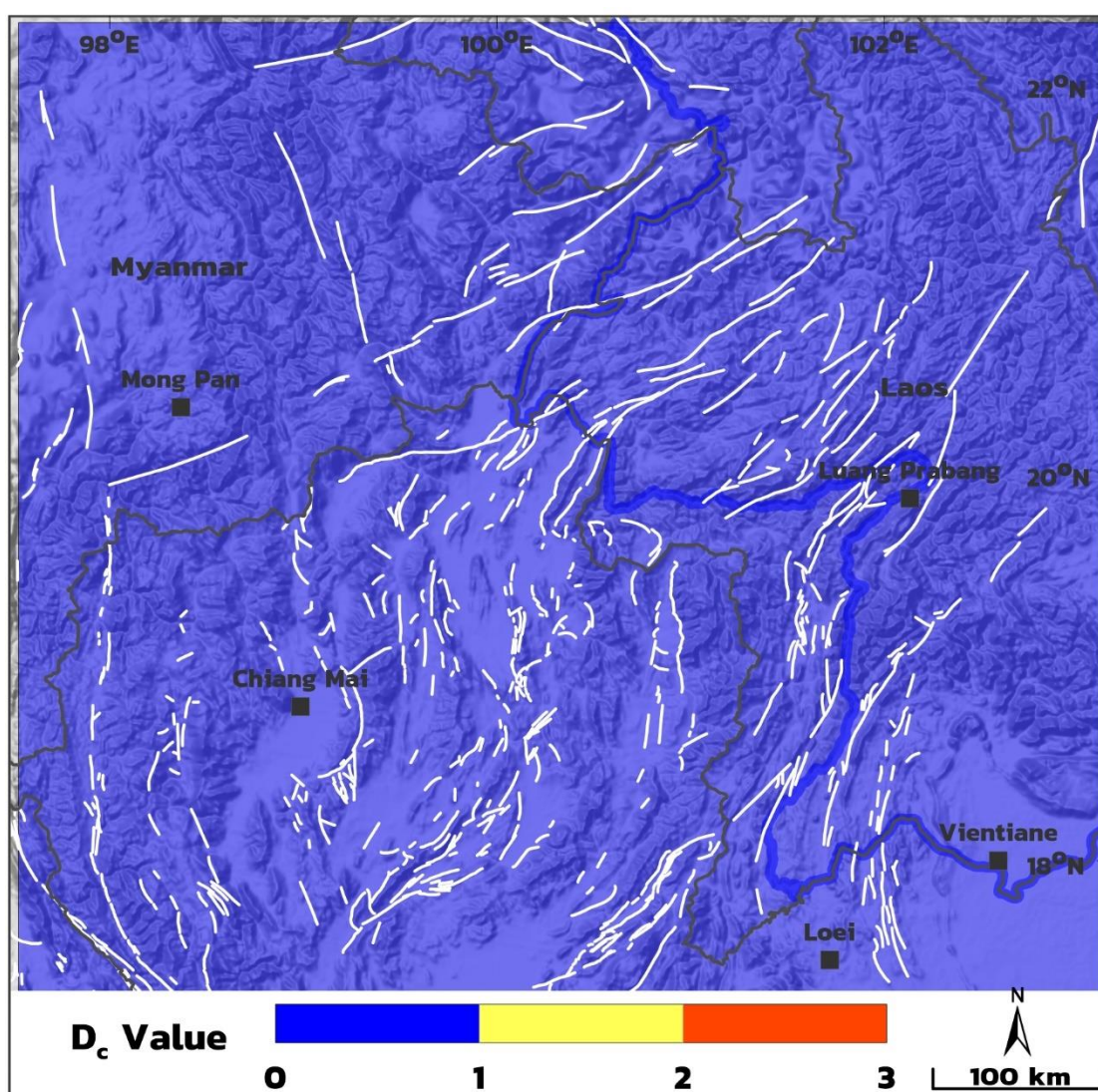


Figure 5.4. The spatial distribution of D_c value with the radius 150 km from fractal dimension.

Next, the study area was gridded at 5 km intervals from 5 to 200 km to determine the best possible study radius. Figure 5.4 depicts the plotting and mapping of the research findings.

As mentioned in Chapter 2, the fractal dimension describes how much of the surrounding space the fractal takes up. Knowing the value of D_c allows us to forecast the fracture characteristic. For example, a D_c value around 3 indicates that earthquake fractures are filling up a volume of the crust, a value near 2 indicates that a plane is being filled up, and a value near 1 indicates that line sources are the most common. Additionally, Tosi (1998) showed that, depending on the dimension of the embedding space, the range of possible fractal dimension values is between 0 and 2. The meaning of these limit values is that a set with D_c close to 0 means that all events are happening in one place, while a set with D_c close to 2 means that events are spread out randomly or evenly over a two-dimensional embedding space.

As a result, in Figure 5.4, the D_c value varied from 0.1 to 0.3, a D_c value close to 1 means that line sources are predominant (Aki, 1981) and with D_c near to 0 suggests that all events are concentrated at a single place. In addition, because of the geological setting in this location, the faults are geographically dispersed throughout the region, and the seismic pattern in the research area may be interpreted as a fault line based on the D_c value.

The result show that the best possible radius is 125 and 150 km and the D_c value from both radiuses are nearly identical and varied from 0.1 to 0.3, indicating into line source of the earthquake.

CHAPTER 6

SEISMIC QUIESCENCE

6.1 Seismicity Rate Change

In order to investigate the Z value in terms of temporal investigation, the free characteristic parameters, including i) the number of earthquakes (N; 25-150 with 25 event intervals) and ii) the time window (T_w ; 0.5-15 year with 0.5-year intervals), were adjusted. Therefore, the N and T_w variables are valid, depending on the time and location of interest. The repeated test of 180 (6×30) characteristic variables found that $N = 25$ events and $T_w = 1.5$ years were the most appropriate characteristic parameters. In this work, we discovered thirteen seismicity precursors during the retrospective temporal investigation of the nineteen strong-to-major earthquake occurrences shown in Table 6.1. However, due to a lack of seismicity data, the M_L -5.0, M_L -5.4, M_L -6.7, M_L -5.0, M_L -5.1, and M_L -5.1 earthquakes of 2010-2013, and M_L -5.1 of 2016 could not discover any anomalous Z values prior to the earthquakes' occurrences.

6.1.1 Temporal investigation

The cumulative number of earthquakes shown versus time for each case study. Following that, the Z value was calculated using the long-term average function developed by Wiemer and Wyss (1994), as shown in Equation (2.7). The following paragraph contains the findings of the retrospective temporal research shown in Figure 6.1.

Figure 6.1a shows two peaks of the highest z values, at 2010.40 and 2011.70. However, the peak at 2011.70 is designated as the precursory seismic quiescence of the M_L -5.1 earthquakes created on April 4th, 2013 (no. 6 in Table 6.1), around 100 km east of Chiang Mai, Thailand.

In Figure 6.1b, the greatest Z value is 2.3 in 2011.70; approximately two years later, on September 22nd, 2013, in Northwestern Laos, a 5.2 M_L earthquake occurred (no. 7 in Table 6.1).

Table 6.1. The lists of strong-to-major earthquakes ($M_L \geq 5.0$) that occurred within the TLMB from 2010 to 2020, as well as the results from the Z value investigation using $N = 25$ events and $T_w = 1.5$ years.

No.	Longitude (°N)	Latitude (°E)	Date	Time (UTC)	Depth (km)	M_L	Z	Qs (A.D.)	Q-time (years)
1	100.03	21.20	19-03-2010	23:23	0	5.0	-	-	-
2	101.74	18.82	23-02-2011	16:10	0	5.4	-	-	-
3	99.91	20.87	24-03-2011	14:17	0	6.7	-	-	-
4	99.08	21.69	12-07-2011	21:46	0	5.0	-	-	-
5	100.05	22.30	17-09-2012	07:23	0	5.1	-	-	-
6	97.68	18.96	10-04-2013	02:35	0	5.1	0.5	2011.70	2.9
7	100.62	21.49	22-09-2013	23:44	10	5.2	2.3	2011.70	2.0
8	99.62	19.70	05-05-2014	00:50	7	5.2	1.7	2012.70	1.6
9	99.69	19.75	05-05-2014	11:19	7	6.3	2.2	2012.70	1.6
10	99.88	20.52	09-06-2014	14:10	5	5.1	3.0	2011.44	3.2
11	98.45	21.74	26-12-2014	17:31	10	5.4	1.1	2010.48	4.5
12	99.02	20.56	24-05-2015	10:55	16	5.1	2.2	2010.98	4.4
13	101.29	21.88	05-03-2016	12:20	10	5.1	2.0	2014.12	2.1
14	102.35	22.05	22-04-2016	01:38	20	5.1	-	-	-
15	100.12	20.71	18-04-2017	19:42	2	5.1	4.7	2011.24	6.7
16	99.53	20.62	03-02-2018	15:31	5	5.1	4.3	2010.67	7.4
17	97.97	20.27	01-07-2018	20:42	2	5.1	2.9	2011.59	6.9
18	101.38	19.46	20-11-2019	00:02	3	6.4	4.4	2012.01	7.9
19	101.33	19.42	20-11-2019	21:19	5	5.9	4.7	2012.01	7.9

The parameters Z, Qs, and Q-time indicate the maximum Z value, starting time of the defined seismic quiescence, and the period between the quiescence and the occurrence time of the earthquake, respectively.

Figure 6.1c shows a maximum Z value of 1.7 in 2012.70, followed by a 5.2 M_L earthquake on May 5th, 2014, northeast of Chiang Mai, Thailand (no. 8 in Table 6.1).

In Figure 6.1d, the greatest Z value is 2.2 in 2012.70, and then 1.6 years later, on May 5th, 2014, a 5.2 M_L earthquake struck northeast of Chiang Mai, Thailand (no. 9 in Table 6.1).

Figure 6.1e shows a maximum Z value of 3.0 at 2011.24, and then three years later, an M_L 5.1 earthquake occurred on June 9th, 2014, east of Mong Pan, Myanmar (no. 10 in Table 6.1).

There are two peaks of maximum Z values in Figure 6.1f; however, the peak at 2012.35 is defined as the precursory seismic quiescence of the M_L -5.4 earthquake, and the estimated Z value depicts the peak ($Z = 1.1$) at 2010.48. Following that, approximately 4.5 years later, on December 26th, 2014, an M_L -5.4 earthquake occurred north of Mong Pan, Myanmar. (no. 11 in Table 6.1).

Figure 6.1g shows a maximum Z value of 2.2 in 2010.98, and 4.4 years later, on May 24th, 2015, an M_L -5.1 earthquake struck northern Laos (No. 12 in Table 6.1).

Figure 6.1h shows a maximum Z value of 2.0 in 2014.12, and 2.1 years later, on March 5th, 2015, an M_L -5.1 earthquake struck northern Laos (No. 13 in Table 6.1).

For Figure 6.1i, the highest Z value of 4.7 occurred in 2011.24, and then, around 6.7 years later, the M_L -5.1 earthquake struck eastern Mong Pan, Myanmar, on April 18th, 2017. (no. 15 in Table 6.1).

The determined Z value in Figure 6.1j depicts the peak ($Z = 4.3$) at 2010.67. Following that, approximately 7.4 years later, on Feb 3rd, 2018, the M_L -5.1 earthquake struck eastern Mong Pan, Myanmar. (no. 16 in Table 6.1).

The computed Z value in Figure 6.1k depicts the 2011.59 peaks ($Z = 2.9$). Following that, approximately 6.9 years later, on July 1st, 2018, the M_L -5.0 earthquake occurred east of Mong Pan, Myanmar (no. 17 in Table 6.1).

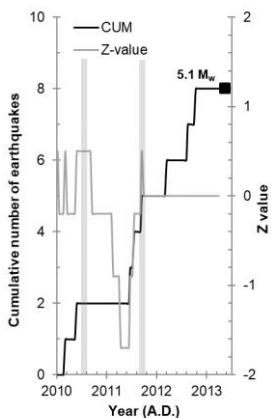
For Figure 6.1l, the maximum Z value is 4.4, which occurred in 2012.01, and then, around 7.9 years later, the M_L -6.4 earthquake occurred on November 20, 2019, west of the Xyabouri dam in Laos (no. 18 in Table 6.1).

Finally, for Figure 6.1m, the maximum Z value of 4.7 occurred in 2012.01, and then, around 7.9 years later, the M_L -5.9 earthquake occurred west of Xyabouri dam in Laos on November 20th, 2019. (no. 19 in Table 6.1)



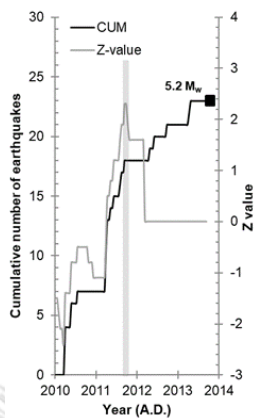
(a) 5.1 M_L , 10/04/2013

$Q_s = 2011.70$



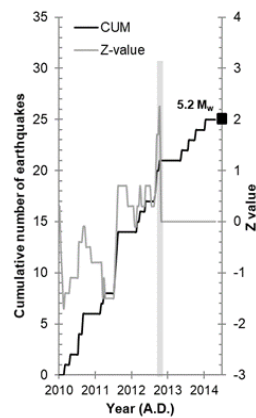
(b) 5.2 M_L , 22/09/2013

$Q_s = 2011.70$



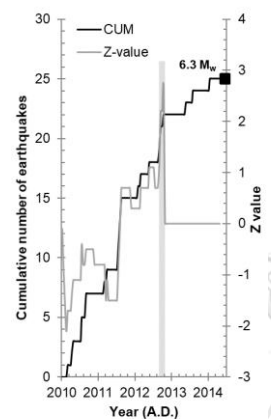
(c) 5.2 M_L , 05/05/2014

$Q_s = 2012.70$



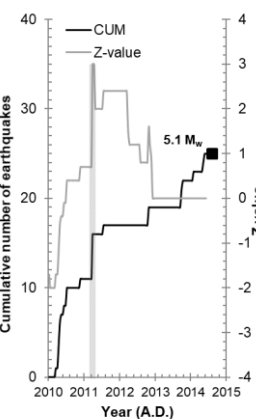
(d) 6.3 M_L , 05/05/2014

$Q_s = 2012.70$



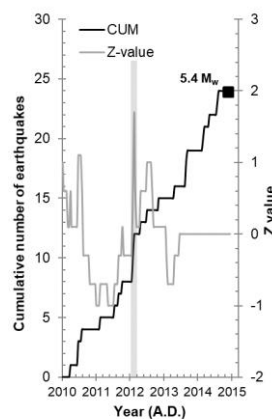
(e) 5.1 M_L , 09/06/2014

$Q_s = 2011.24$



(f) 5.4 M_L , 26/12/2014

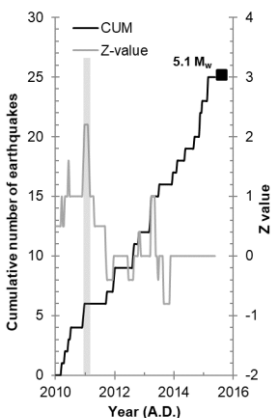
$Q_s = 2010.48$



CHULALONGKORN UNIVERSITY

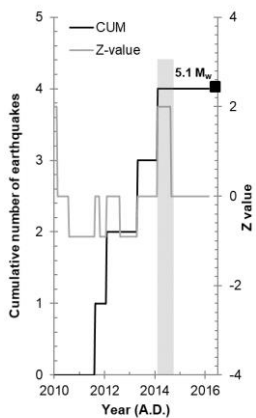
(g) 5.1 M_L , 24/05/2015

$Q_s = 2010.98$



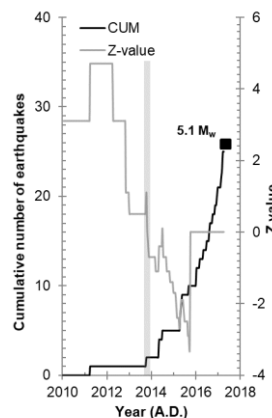
(h) 5.1 M_L , 05/03/2016

$Q_s = 2014.12$



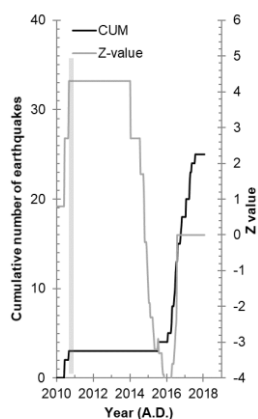
(i) 5.1 M_L , 18/04/2017

$Q_s = 2011.24$

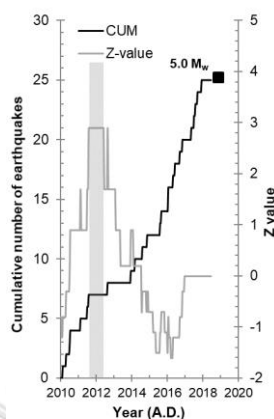


(j) 5.1 M_L , 03/02/2018

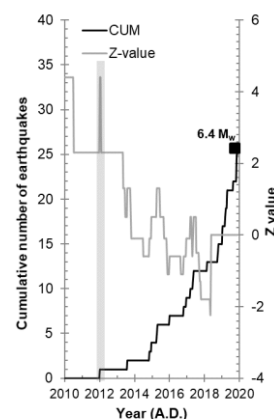
$$Q_s = 2010.67$$

(k) 5.0 M_L , 01/07/2018

$$Q_s = 2011.59$$

(l) 6.4 M_L , 20/11/2019

$$Q_s = 2012.01$$

(m) 5.9 M_L , 20/11/2019

$$Q_s = 2012.01$$

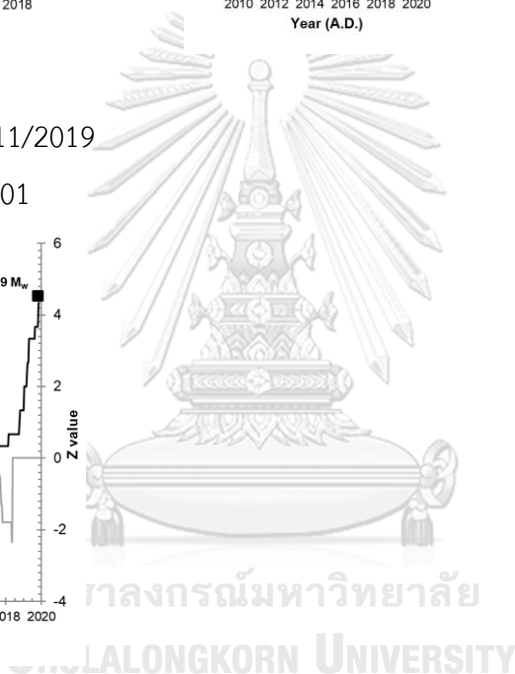
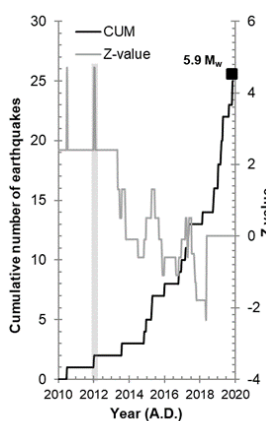


Figure 6.1. (a-m) the graph plot between the cumulative number of earthquakes (grey line) and Z value (black line) plotted against time. The black stars indicate the time of each earthquake occurrence. The transparent grey strip illustrates the Z value anomaly, which is recognized as the quiescence stage.

6.1.2 Spatial investigation

The potential Z value for identifying earthquake precursors in the TLMB region was spatially explored and mapped. In order to restrict the potential Z value for detecting earthquake precursors in the region. The TLMB region was gridded using cells with a dimension of $0.25^\circ \times 0.25^\circ$, the nearest 50 events from the earthquake data found in each grid node and the Z value derived temporally in the same method as in the prior temporal investigation. Then, the Z value of each grid node was picked, contoured, and mapped following the previously stated quiescence time (Figure 6.1 and column Q_s in Table 6.1). The resulting maps of thirteen samples are given in Figure 6.2 and discussed below.

The spatial distribution results were classified into excellent, good, and fair precursors. The first group is the excellent precursor, including Figures 6.2c, 6.2d, and 6.2e. The second group is the good precursor in Figures 6.2b, 6.2f, 6.2g, 6.2j, 6.2k, and 6.2i. Finally, the fair precursor's last group includes Figures 6.2a, 6.2h, 6.2l, and 6.2m.

When the Z values were spatially mapped in 2011.59 (Figure 6.2a), a relatively high Z value was located in the NW–SE direction across northeastern Thailand and northern Laos, and 6.9 years later, the M_L 5.1 earthquake (no. 17 in Table 1) occurred southwest of Mong Pan, Myanmar on April 10th, 2013.

For the Z map in 2011.70 (Figure 6.2b), an anomalous Z value was dispersed over the TLMB boundary and a small portion surrounding Chiangmai, Thailand. Following that, about two years later, the epicenter of the M_L -5.2 earthquake that occurred on September 22nd, 2013 (see no.7 in Table 6.1) was located in the south of Yunnan, China, close to the China-Myanmar border in the northernmost portion of the Z anomalies with a positive Z value of 2.3 (Figure 6.2b).

The spatial distribution of the Z value investigated in 2012.70 and 2012.70 (Figures 6.2c and 6.2d) indicated a more significant Z anomaly scattered in three areas: western Mong Pan, Myanmar; northern Chiangmai, Thailand; and western Luang Prabang, Laos. Then, on May 5th, 2014, 1.6 and 1.6 years later, respectively. The M_L -5.2 and M_L -6.3 earthquake struck northeast of Chiangmai, Thailand, inside the highest Z anomaly area mentioned before (no. 8-9 in Table 6.1).

In 2011.24 (Figure 6.2e), the spatial distribution of the Z value indicated a more apparent Z anomaly scattered in two parts: along the TLMB and surrounding Chiangmai, Thailand. Then, on June 9th, 2014, an earthquake struck northeast of Chiangmai, Thailand, near the noticeable Z anomaly region displayed above (Figure 10e). It was a 5.1 magnitude earthquake. (no.10 in Table 6.1).

In 2010.48, the Z values show on a map. In the NW–SE direction, there was a high Z value over eastern Myanmar and northwestern Laos. 4.5 years later, the M_L -5.4 earthquake happened on December 26th, north of Mong Pan, Myanmar, on the edge of the high Z value anomalies. (Figure. 6.2f)

In 2010.98 (Figure 6.2g), an anomalous Z value was distributed west of the TLMB boundary and around Chiangmai, Thailand. About 4.4 years later, the epicenter of the M_L -5.1 earthquake that occurred on May 24, 2015 (no. 12 in Table 6.1) was located east of Mong Pan, Myanmar, along the rim of the positive Z anomalies with a Z value of 2.2.

When the Z values were spatially mapped in 2014.12 (Figure 6.2h), a comparatively high Z value was found northeast of Chiangmai, Thailand, and 2.1 years later, an earthquake of the M_L -5.1 (no. 13 in Table 6.1) was generated on March 5th, 2016 in Yunnan, China, close to the China-Laos border but outside of the Z value anomalies.

Figure 6.2i shows the Z map for 2011.24. It shows that an anomalous Z value spread from NW to SE over northern Thailand and Laos. After around 6.7 years, the epicenter of the M_L -5.1 earthquake that occurred on April 18th, 2017 (No. 15 in Table 6.1) was discovered east of Mong Pan, Myanmar, on the rim of the Z anomalies with a positive Z value of 4.7.

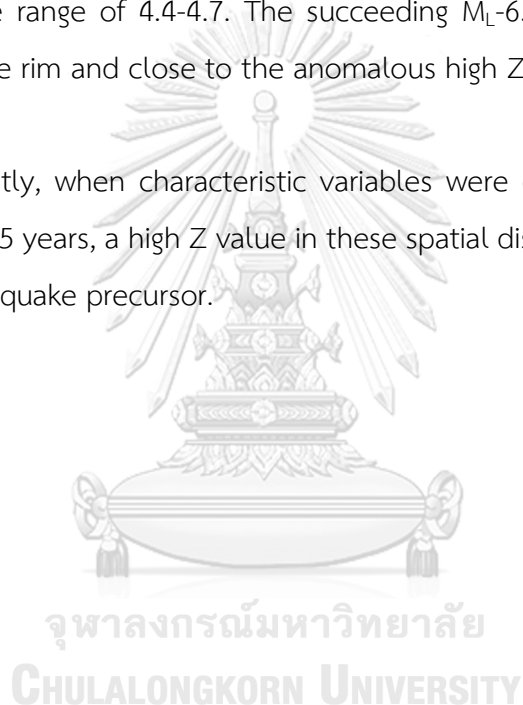
An anomalous Z value was spread in an NW–SE direction throughout northern Thailand and northern Laos for the Z map in 2012.01 (Figure 6.2j). The epicenter of the M_L 5.1 earthquake that occurred on February 3rd, 2018 (no. 16 in Table 6.1) was situated around 7.9 years later to the east of Mong Pan, Myanmar, on the rim of the Z anomalies with a positive Z value of 4.3. (Figure 6.2j).

According to the Z map from 2011.59 (Figure 6.2k), an anomalous Z value was dispersed along the NW–SE axis over northern Thailand and Laos. After that, the

epicenter of the M_L -6.4 earthquake that occurred in Myanmar on July 1st, 2018 (no. 17 in Table 6.1) was located on the rim of the Z anomalies with a positive Z value of 2.9, some 6.9 years later (Figure 6.2k).

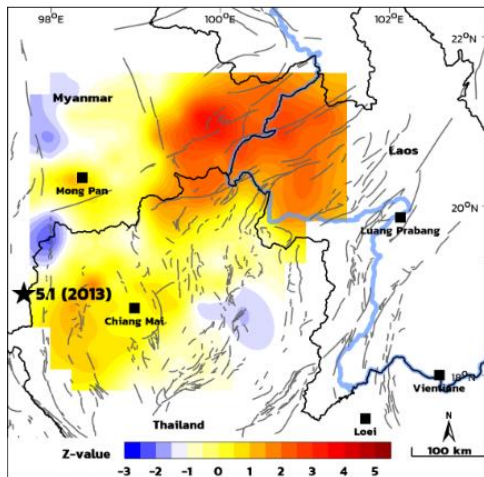
The M_L 6.4 and 5.9 earthquakes occurred on November 20th, 2019 (No. 18 and 19 in Table 6.1). The spatial distribution of the Z value mapped in 2015.42 (Figures 6.2l and 6.2m) revealed that the positive Z value was consistent throughout the study area. A relatively high Z value is defined reasonably well in the western part of Laos and the surrounding areas of Mong Pan, Myanmar, and Chiang Mai, Thailand, with a maximum Z value range of 4.4-4.7. The succeeding M_L -6.2 and M_L -5.9 earthquakes occurred within the rim and close to the anomalous high Z, respectively. (Illustrations 6.2l and 6.2m).

Consequently, when characteristic variables were determined to be $N = 25$ events and $T_w = 1.5$ years, a high Z value in these spatial distributions was revealed to represent an earthquake precursor.



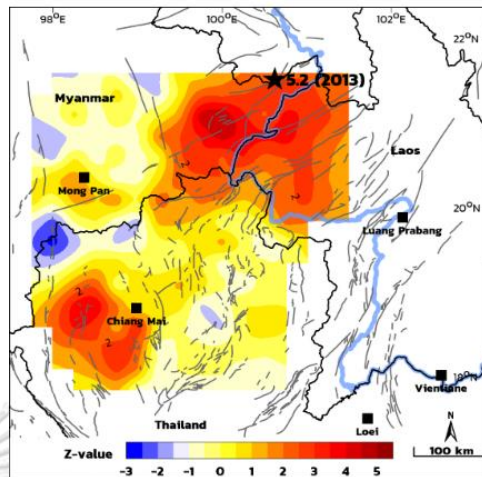
a) 5.1 M_L , 10/14/2013

$Q_s = 2011.70$



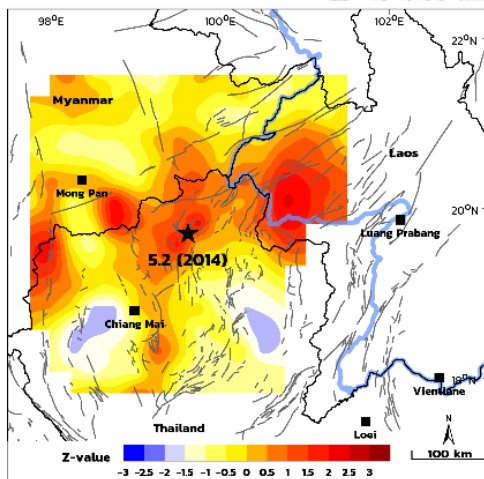
b) 5.2 M_L , 22/09/2013

$Q_s = 2011.70$



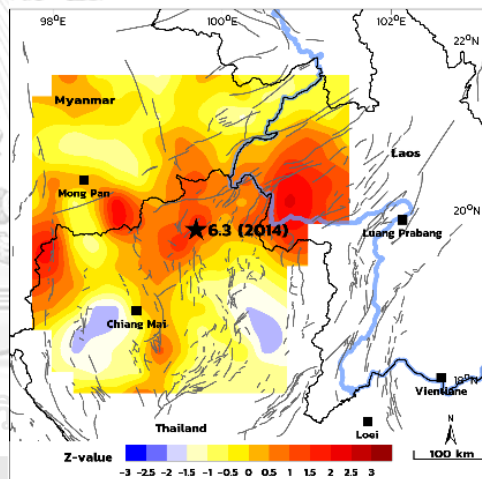
c) 5.2 M_L , 05/05/2014

$Q_s = 2012.70$



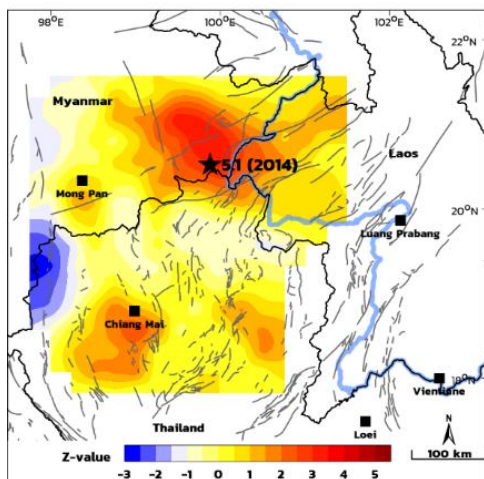
d) 6.3 M_L , 05/05/2014

$Q_s = 2012.70$



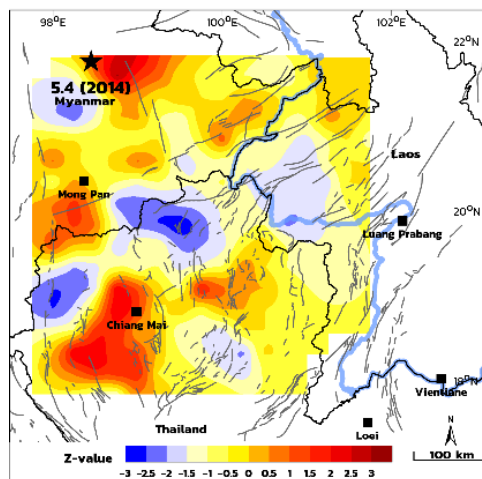
e) 5.1 M_L , 09/06/2014

$Q_s = 2011.24$



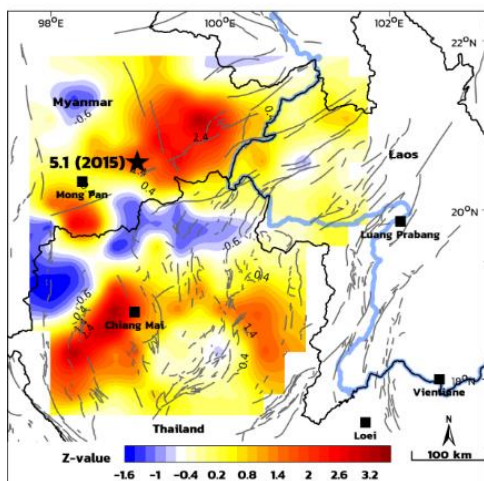
f) 5.4 M_L , 26/12/2014

$Q_s = 2010.48$



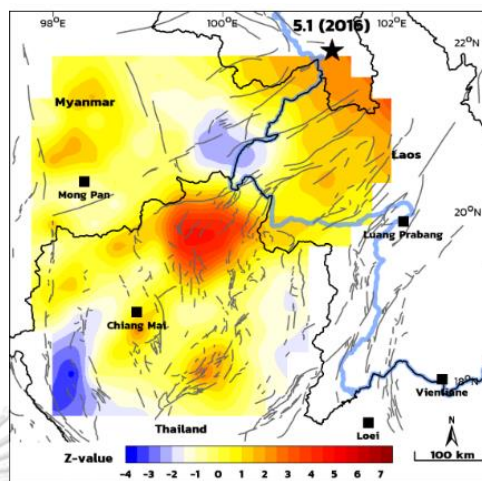
g) 5.1 M_L , 24/05/2015

$Q_s = 2010.98$



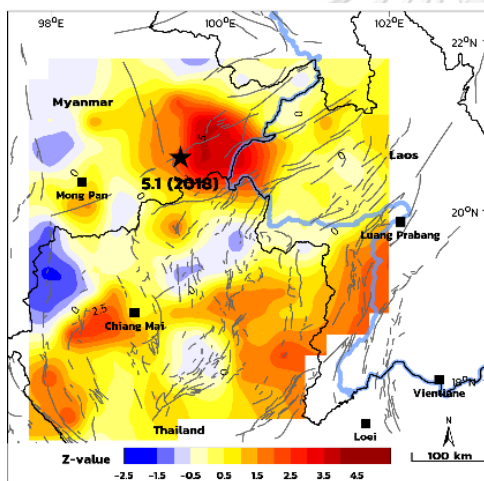
h) 5.1 M_L , 05/03/2016

$Q_s = 2014.12$



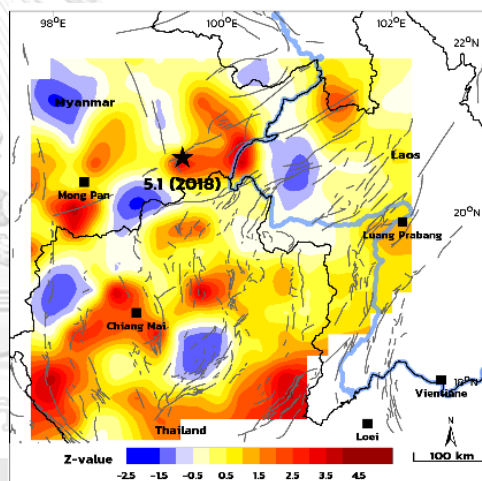
i) 5.1 M_L , 18/04/2017

$Q_s = 2011.24$



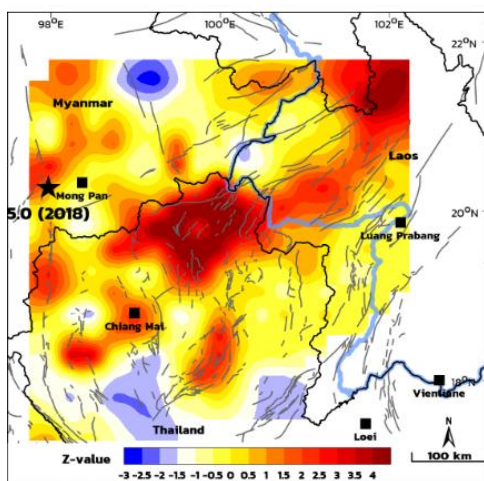
j) 5.1 M_L , 03/02/2018

$Q_s = 2010.67$



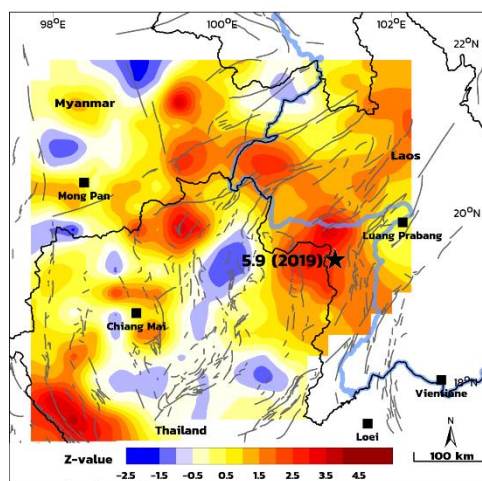
k) 5.1 M_L , 01/07/2018

$Q_s = 2011.59$



l) 5.9 M_L , 20/11/2019

$Q_s = 2012.01$



m) 6.4 M_L , 20/11/2019

$Q_s = 2012.01$

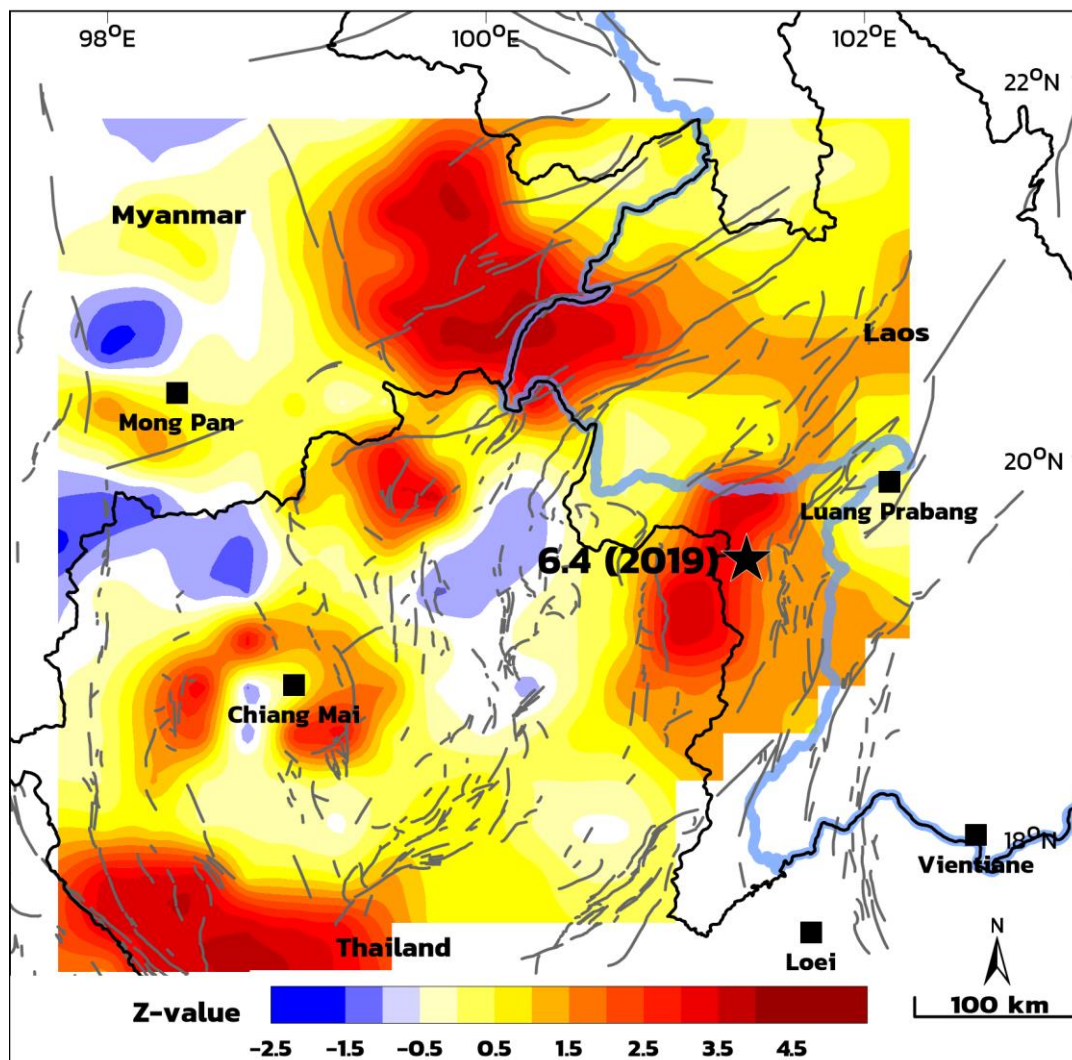


Figure 6.2. The spatial distribution of a-m the Z values for thirteen of nineteen large earthquakes (nos. 6-13 and 15-19 in Table 6.1) during the time slice of seismic quiescence determined from the temporal investigation are depicted on a map of the TLMB. The colors red and blue represent a decrease (+Z) and an increase (-Z) in seismicity rate, respectively. Black stars show the epicenter of the earthquake case study.

6.2 Region-Time-Length Algorithm

6.2.1 Temporal investigation

The RTL algorithm was investigated retrospectively in both temporal and spatial aspects at the epicenters of nineteen strong-to-major earthquakes ($M_L \geq 5$) previously recorded within the TLMB in order to define the relationship between the RTL score and the subsequent occurrence of a hazardous earthquake at a given locality (Table 1.1). The result is a set of distinctive characteristics (r_0 and t_0 , which are connected to R_{\max} and T_{\max} , respectively) that are used to detect the precursory RTL score generated before the dangerous earthquake in the TLMB. To do this, r_0 was altered from 50 to 200 km. Furthermore, at 5 km intervals, t_0 varied from 1 to 5 years at 0.5-year intervals. Thus, for each case study of an earthquake, 144 (16×9) situations of the distinctive parameters were examined repeatedly. The results showed that the characteristic distance r_0 of 90 km ($R_{\max} = 180$ km) and time t_0 of 2 years ($T_{\max} = 4$ years) were the most effective conditions for finding the anomalous RTL score connected to nine of the nineteen detected earthquakes after repeated tests (Table 6.2).

The RTL score was analyzed every ten days at the beginning of accessible seismicity data in 2010 until the occurrence time of each earthquake examined in the retrospective temporal investigation. The temporal variations of the RTL score for the nine of nineteen successful case studies are shown in Figure 6.3.

Figure 6.3a shows the temporal variations in the RTL score at the location of the M_L -5.2 earthquake, revealing the activation stage in 2012.13. Following that, the RTL score dropped sharply, and the RTL curve had a slight variant for one year before reaching the quiescence stage in 2013.70, with the lowest RTL score of -0.90.

Table 6.2. The lists of strong-to-major earthquakes ($M_L \geq 5.0$) that occurred within the TLMB from 2010 to 2020 and the RTL algorithm investigation results using $r_0 = 90$ km and $t_0 = 2$ years.

No.	Longitude (°N)	Latitude (°E)	Date	Time (UTC)	Depth (km)	M_L	RTL score	Q_s (A.D.)	Q-time (years)
1	100.03	21.20	19-03-2010	23:23	0	5.0	-	-	-
2	101.74	18.82	23-02-2011	16:10	0	5.4	-	-	-
3	99.91	20.87	24-03-2011	14:17	0	6.7	-	-	-
4	99.08	21.69	12-07-2011	21:46	0	5.0	-	-	-
5	100.05	22.30	17-09-2012	07:23	0	5.1	-	-	-
6	97.68	18.96	10-04-2013	02:35	0	5.1	-	-	-
7	100.62	21.49	22-09-2013	23:44	10	5.2	-0.90	2013.70	0.0
8	99.62	19.70	05-05-2014	00:50	7	5.2	-0.80	2014.24	0.1
9	99.69	19.75	05-05-2014	11:19	7	6.3	-0.66	2014.31	0.0
10	99.88	20.52	09-06-2014	14:10	5	5.1	-0.21	2013.70	0.7
11	98.45	21.74	26-12-2014	17:31	10	5.4	-	-	-
12	99.02	20.56	24-05-2015	10:55	16	5.1	-0.18	2013.01	2.4
13	101.29	21.88	05-03-2016	12:20	10	5.1	-	-	-
14	102.35	22.05	22-04-2016	01:38	20	5.1	-	-	-
15	100.12	20.71	18-04-2017	19:42	2	5.1	-0.17	2013.70	3.6
16	99.53	20.62	03-02-2018	15:31	5	5.1	-0.25	2013.70	4.4
17	97.97	20.27	01-07-2018	20:42	2	5.1	-	-	-
18	101.38	19.46	20-11-2019	00:02	3	6.4	-0.20	2014.81	5.1
19	101.33	19.42	20-11-2019	21:19	5	5.9	-0.20	2014.81	5.1

The parameters RTL score, Q_s , and Q-time indicate the minimum RTL score, starting time of the defined seismic quiescence, and the time between the quiescence and the occurrence time of the earthquake, respectively

Figure 6.3b shows the temporal variations in the RTL score at the location of the M_L -5.2 earthquake, revealing that the activation stage began in 2012.01. Following that, the RTL score dropped sharply, and the RTL curve had a minor variant for 1.5 years before reaching the quiescence stage in 2014.24, with the lowest RTL score of -0.80. The similarity in Figures 6.3b and 6.3c might be because the earthquake in the case study happens at a similar time and location.

Figure 6.3c shows the temporal variations in the RTL score at the location of the M_L -6.3 earthquake, revealing the activation stage in 2012.01. Following that, the RTL score dropped sharply, and the RTL curve had a slight variant for 1.5 year before reaching the quiescence stage in 2014.31, with the lowest RTL score of -0.90.

Figure 6.3d shows the temporal variations in the RTL score at the location of the M_L -5.1 earthquake, revealing the activation stage in 2012.16. Following that, the RTL score dropped sharply, and the RTL curve had a slight variant for one year before reaching the quiescence stage in 2013.70, with the lowest RTL score of -0.21.

Figure 6.3e, by the beginning of the activation stage in 2012.01. The RTL score then dropped sharply, reaching the first stage of quiescence in 2013.01, with the lowest RTL score of -0.18

The RTL score at the location of the M_L -5.1 earthquake on April 18th, 2017 (Figure 6.3f) was stable between 2010.09 and 2012.51, revealing the quiescence stage in 2013.70 with the lowest RTL score of -0.17. On the other hand, the 5.1 M_L earthquake happened during the activation stage.

According to Figure 6.3g, seismic quiescence began to decline in 2012.43 and peaked in 2013.70 (RTL score = -0.25). Additionally, the RTL score suggested an activation stage between 2017.42 and 2017.96, with a maximum RTL score of 0.85, although on February 3rd, 2018, a 5.1 M_L earthquake occurred during an activation stage.

According to Figure 6.3i, seismic quiescence began to decline in 2012.93 and peaked in 2014.81 (RTL score = -0.20). Additionally, the RTL score suggested an

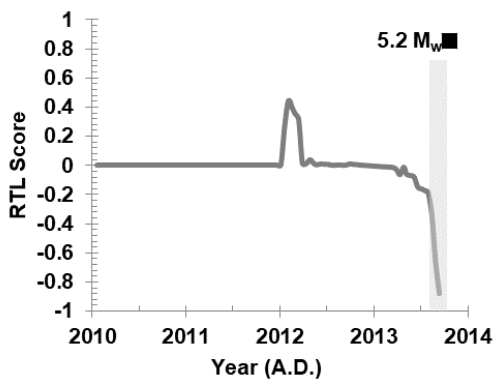
activation stage between 2016.88 and 2019.87, with a maximum RTL score of 0.94, although the November 20th, 2019, 6.4 M_L earthquake occurred during an activation stage.

Finally, the variation in the RTL score demonstrated the seismic quiescence in Figure 6.3j. The RTL began dropping in 2013.85 and peaked at - 0.20 in 2014.81. Following that, the RTL score indicated an activation stage between 2016.88 and 2019.87, with a maximum RTL score of 0.64; nevertheless, the November 20th, 2019, 5.9 M_L earthquake happened during this time.



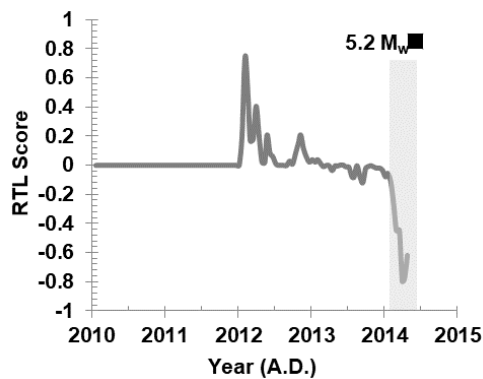
(a) 5.2 M_L , 22/09/2013

$RTL_{min} = -0.90$



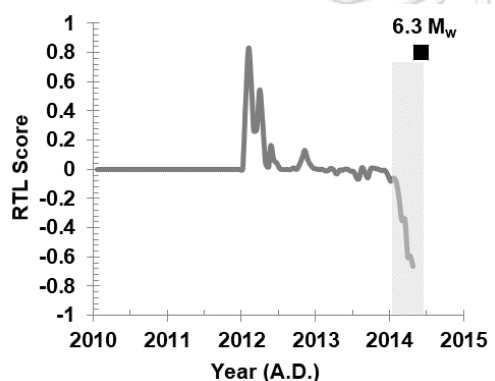
(b) 5.2 M_L , 05/05/2014

$RTL_{min} = -0.80$



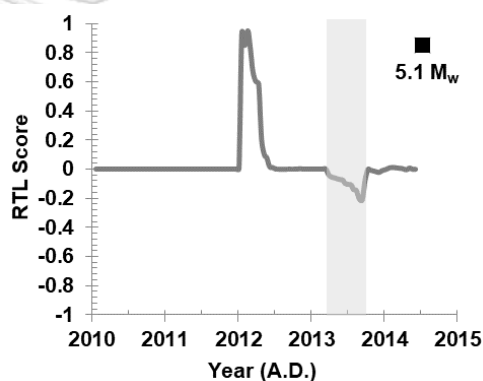
(c) 6.3 M_L , 05/05/2014

$RTL_{min} = -0.66$



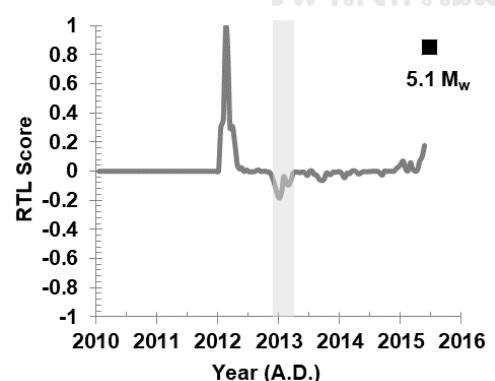
(d) 5.1 M_L , 09/06/2014

$RTL_{min} = -0.21$



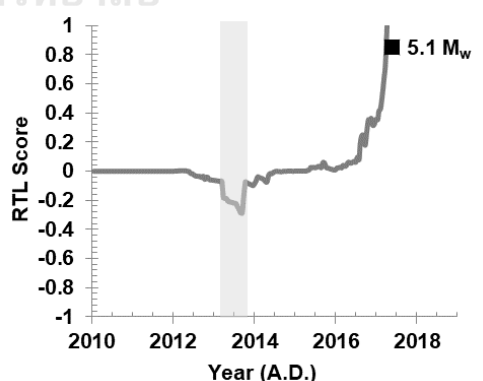
(e) 5.1 M_L , 24/05/2015

$RTL_{min} = -0.18$



(f) 5.1 M_L , 18/04/2017

$RTL_{min} = -0.17$



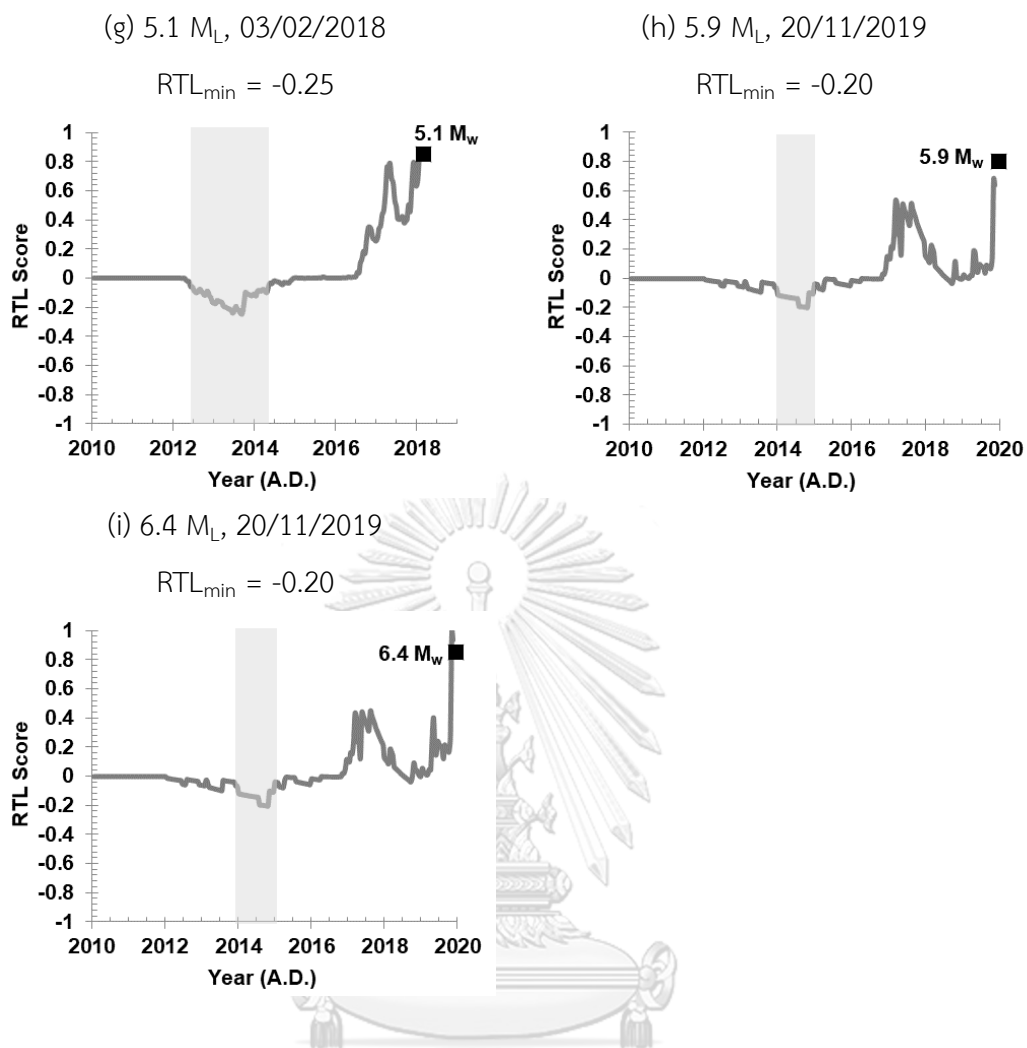


Figure 6.3. (a-i) Temporal variation of the RTL score (grey line) of nine strong-to-major earthquakes recognized in the retrospective test. The black square indicates the origin time of each strong-to-major earthquake.

6.2.2 Spatial investigation

This method aims to evaluate the suitability parameters for the RTL algorithm for earthquake forecasting. The RTL score was evaluated spatially. The study area (Figure 1.9) was gridded using a grid interval spacing of $0.25^\circ \times 0.25^\circ$. The temporal variation of the RTL score was determined at each grid node using Equations (2.8)-(2.11). The Q_s parameter (Huang 2004) which used to spatially map the RTL score, as described in Equation (2.12); for each grid node, the Q_s parameter was computed, contoured, and mapped, as shown in Figure 6.4

To begin with, Figure 6.4a displays the Q_s parameters for 2013.47-2013.70, during which an anomaly was formed in a 200 km^2 region along Thailand and Myanmar borders. The M_L -5.2 earthquake that struck on September 22nd, 2013, occurred at the boundary between South Yunnan and Myanmar. It occurred around 50 km far from the minimal RTL area is located.

In Figure 6.4b, the distribution of the Q_s parameter averaged for 2014.08-2014.31 reveals seismic quiescence in an area covering approximately 200 km^2 north of Chiang Mai, Thailand. The epicenter of the M_L -5.2 earthquake that struck on May 5th, 2014, occurred within the rim of the minimum RTL score location. The similarities between Figures 6.4b and 6.4c might be because the earthquake in the case study occurred at a comparable time and place.

Figure 6.4c displays the Q_s parameters for 2014.08-2014.31, during which an anomaly was formed in a 200 km^2 region north of Chiang Mai, Thailand. The M_L -6.3 earthquake that struck on May 5th, 2014, occurred northeast of Chiangmai, Thailand. It occurred along the rim, where the minimal RTL area is located.

The quiescent time calculated from temporal investigation for the 5.1 M_L earthquake that struck on June 9th, 2014, at the east of Mong Pan, Myanmar, along the Thailand-Laos-Myanmar boundary, was in the range of 2013.35-2013.74, with the spatial distribution of the RTL, score shown in Figure 6.4d. In the area of the Thailand-

Laos-Myanmar boundary. The earthquake's epicenter, on the other hand, was near the center of the anomaly.

In Figure 6.4e, covering the quiescent period of 2012.93-2013.12, a prominent anomaly occurred in two portions: a weak anomaly in Chiangmai, Thailand, and a strong anomaly in the north of Mong Pan, Thailand. In addition, the epicenter of the 5.1 M_L earthquake that occurred on May 24th, 2015, was located on the rim of the defined strong RTL anomalies (Figure 6.4d).

Figure 6.4f illustrates an anomaly in two locations: a weak anomaly in the south of Chiangmai, Thailand, and a significant anomaly in the northeastern part of Mong Pan, Myanmar. Additionally, the epicenter of the 5.1 M_L April 18th, 2017, earthquake was located near the defined significant RTL anomalies (Figure 6.4f).

As illustrated in Figure 6.4g, the spatial distribution of the RTL score from 2012.74 to 2014.31 demonstrated that the seismic quiescence area covered about 200 km^2 along the Myanmar-Laotian border. The lowest RTL score, in particular, denotes the northeastern section of Mong Pan, Myanmar. The epicenter of the 5.1 M_L earthquake that struck on February 3rd, 2018, was located in the southern portion of the RTL anomaly (Figure 6.4g).

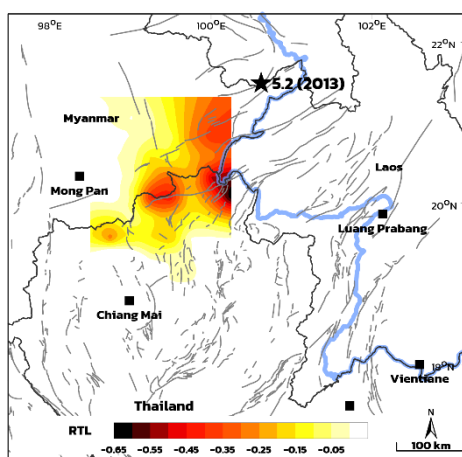
In Figure 6.4h, the distribution of the Q_s parameter averaged for 2014.24-2015.23 reveals seismic in two locations connected: strong anomalies are in the south of Mong Pan, Myanmar, and west of Luang Prabang, Laos, and a weak anomaly is around the substantial anomaly area. The epicenter of the M_L -5.9 earthquake that struck on November 20th, 2019, occurred within the minimum RTL score location in the west of Luang Prabang, Laos. The similarities between Figures 6.4h and 6.4i might be because the earthquake in the case study occurred at a comparable time and place.

Figure 6.4i displays the Q_s parameters for 2013.97-2015.23, during which an anomaly was formed in two locations connected. The strong anomaly is in the south of Mong Pan, Myanmar, and west of Luang Prabang, Laos. A weak anomaly is around

the strong anomaly area. The M_L -6.4 earthquake that struck on November 20th, 2019, occurred west of Luang Prabang, Laos. It occurred along the area where the minimal RTL area is located.

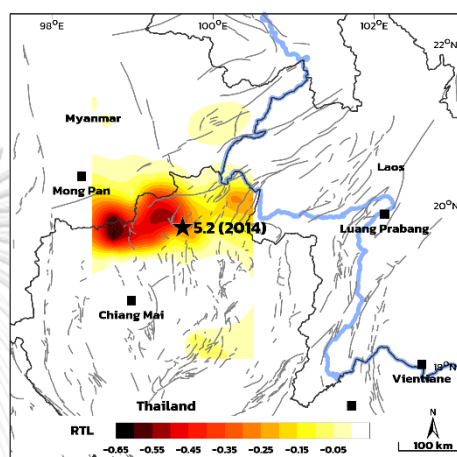
(a) 5.2 M_L , 22/09/2013

Q_s : 2013.70



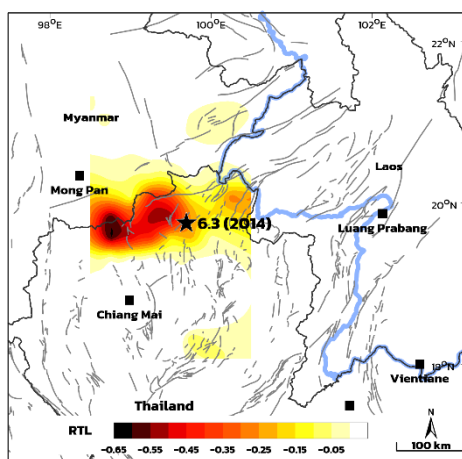
(b) 5.2 M_L , 05/05/2014

Q_s : 2014.24



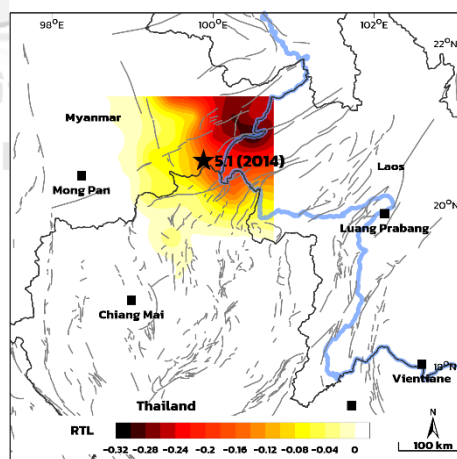
(c) 6.3 M_L , 05/05/2014

Q_s : 2014.31



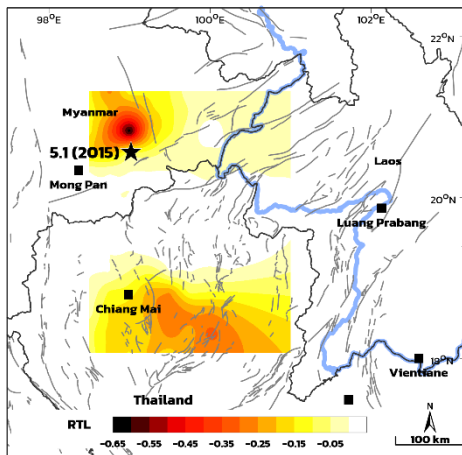
(d) 5.1 M_L , 09/06/2014

Q_s : 2013.70



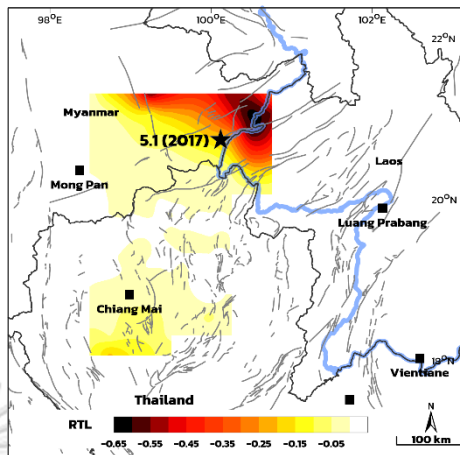
(e) 5.1 M_L , 24/05/2015

Q_s : 2013.01



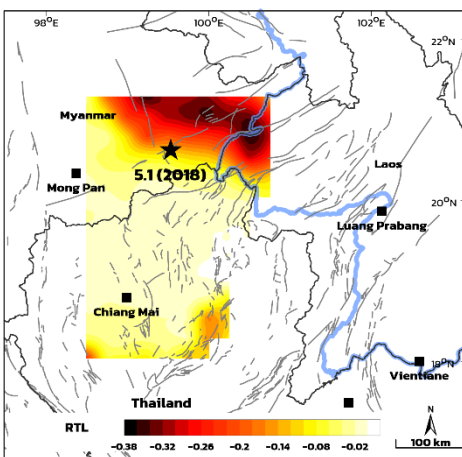
(f) 5.1 M_L , 18/04/2017

Q_s : 2013.70



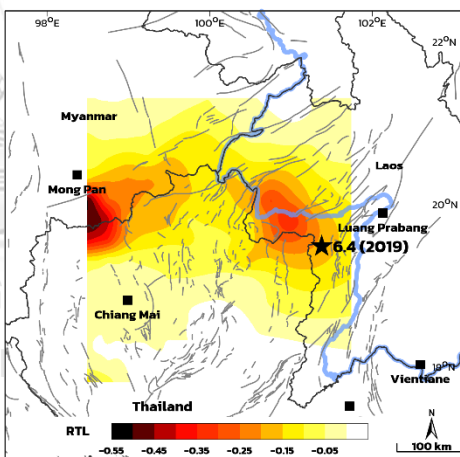
(g) 5.1 M_L , 03/02/2018

Q_s : 2013.70



(h) 6.4 M_L , 20/11/2019

Q_s : 2014.81



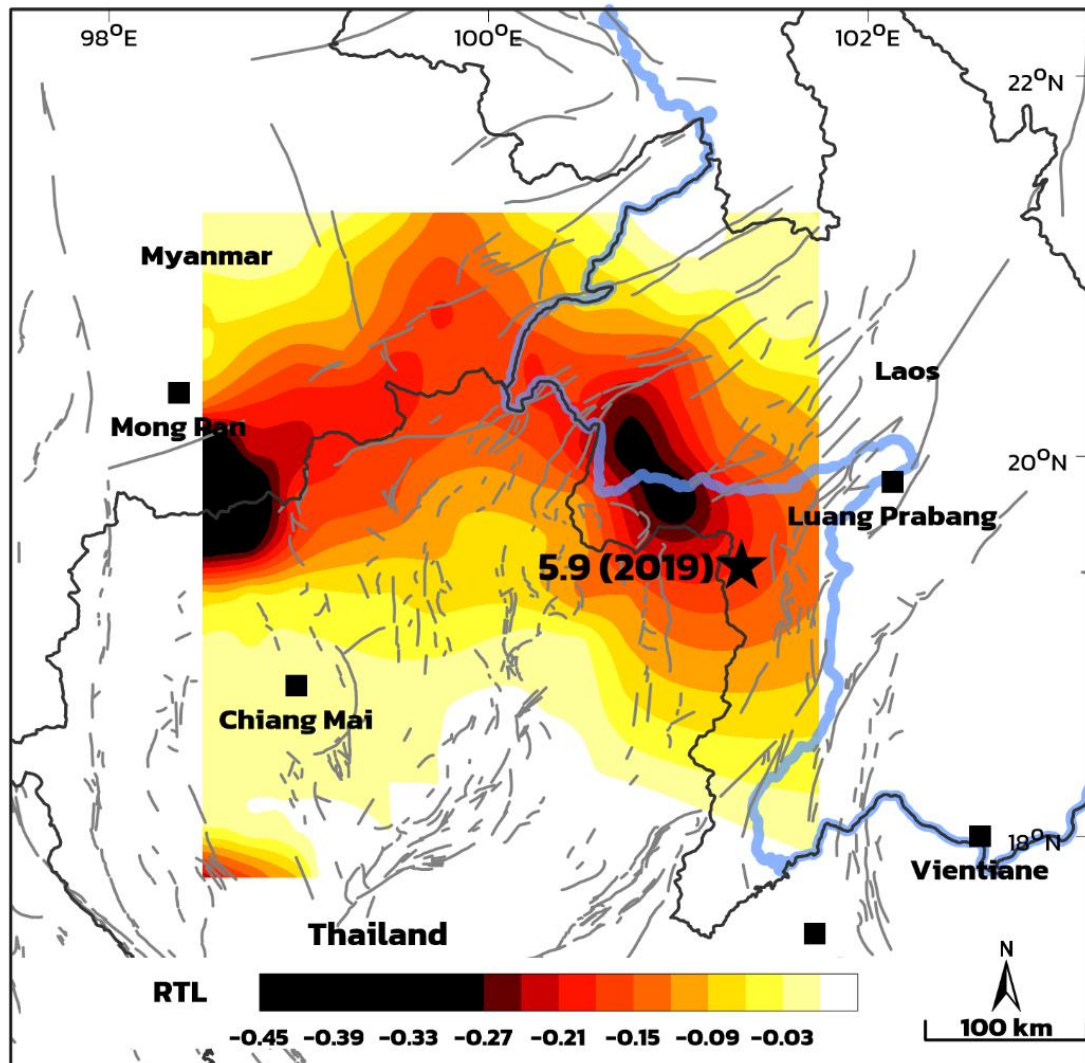
(i) 5.9 M_L , 20/11/2019 Q_s : 2014.81

Figure 6.4. (a-i) During each case study, the spatial distribution of RTL values along TLMB observed seismic quiescence. The epicenter of each earthquake is depicted as a black star.

CHAPTER 7

DISCUSSION

7.1 Earthquake Activity

The earthquake activity is shown in the term of the maps. Firstly, the spatial distribution of a and b values may had similar pattern. Low b values indicate high earthquake activity and a low ratio of minor to major earthquakes. In the spatial distribution of the b value map, the southwestern part of Luang Prabang, Laos, northward to Mong Pan, Myanmar shows low b values indicating high activity area. On the other hand Chiang Mai, Thailand, and north of Mong Pan, Myanmar show the area of high b values that indicate low activity area. Moreover, the standard deviation of b value and percent of the goodness of fit that derived a and b values are likely to be reliable with low variation.

Earthquake activity shows in the term of maximum magnitude. The east of Mong Pan, Myanmar, can generate a maximum magnitude of around 5.1 M_L in 5 years. The area from Mong Pan, Myanmar, extending to the western part of Laos, can generate a maximum magnitude of around 5.6 M_L in 10 years. The area west of Mong Pan, Myanmar, to the northeast of Myanmar, and South of Luang Prabang, Laos, can generate a maximum magnitude of around 6.3 M_L in 30 years. The area from west of Mong Pan, Myanmar, to the northeast of Myanmar and south of Luang Prabang, Laos, can generate a maximum magnitude of around 6.3 M_L in 30 years and 6.7 M_L in 50 years. To restrict the result of earthquake activity in terms of maximum magnitude.

Then, we compared it with Figure 7.1b from Pailoplee et al. (2013). This thesis is nearly identical to the previous work. Further, it expands coverage to include additional areas in the Pua fault zone in the Thai province of Nan and the Dien Bien Fu fault zone to the southwest of Luang Prabang. As a result, the results of prior research pinpoint the region that can generate the maximum magnitude in the northwest-to-southeast trend of the study area. Similarly, the result of this thesis determines the region capable of producing the maximum magnitude of the trend from the northwest to the south of the study area.

In terms of the return period, the border of three countries covering the northeastern part of Mong Pan, Myanmar, and the southwestern part of Luang Prabang, Laos, has the potential to generate an earthquake within a short period. For instance, the return periods of the earthquake with M_L of 4.0, 5.0, 6.0, and 7.0 were 1, 5, 20, and 75 years, respectively. In contrast, for the western part of Chiang Mai, the average time intervals of the earthquake occurrences were around 50-5,000 years for an earthquake magnitude of 4.0-7.0 M_L . We compared the results of earthquake activity to Figure 7.2b from Pailoplee et al. (2013) to constrain the return period. As a result, this thesis shows that the trend from the northwest to the south of the study area shows where the short return period is most likely to happen (Figure 7.2a). In the northwest-to-southeast direction of the study area of Pailoplee et al. (2013), the results of previous research point to the area that can generate a short return period.

In terms of the probability of occurrence, the border of three countries covering the eastern part of Mong Pan, Myanmar, the southwestern part of Luang Prabang, Laos covering the east of Chiangmai, Thailand is the high activity zone. The possibility of generating an earthquake. For instance, the probability of occurrence of the earthquake with M_L of 4.0, 5.0, 6.0, and 7.0 were 100%, 100%, 70-100%, and 20-60%, respectively. In contrast, in the eastern part of Chiang Mai, the probability of earthquake occurrence of the earthquake with M_L of 4.0, 5.0, 6.0, and 7.0 were 100%, 20-60%, 0-20%, and 0%, respectively. We compared the result of earthquake activity to Figure 7.3b from Pailoplee and Charusiri (2015) to define the result in terms of probability of occurrence. the outcome of this thesis identifies the region capable of generating a high probability of occurrence in the study area's northern region. (See Figure 7.3a.). The research area of Pailoplee and Charusiri (2015) covered in the preceding work is only a minor portion of the research area covered in this thesis. Prior research has identified the location in the northern half of the study area with a high probability of occurrence related to this study.

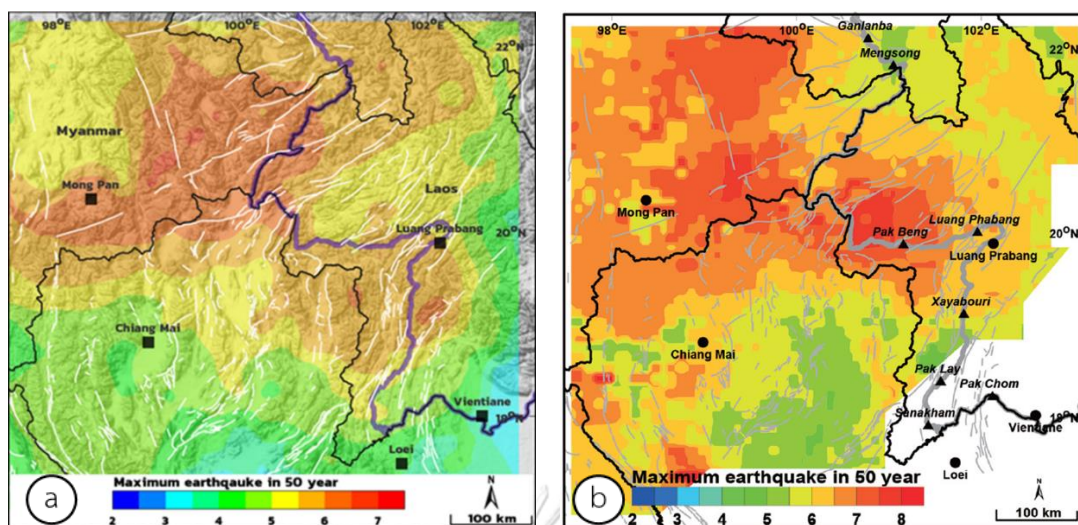


Figure 7.1. Comparative of (a) this study with (b) Pailoplee et al. (2013) showing maximum magnitude in 50 years in TLMB.

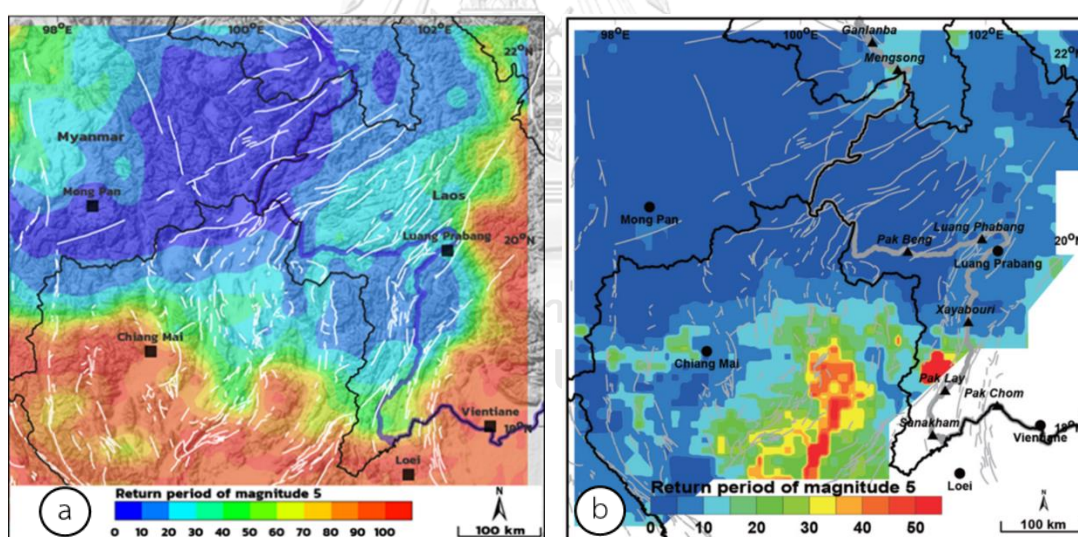


Figure 7.2. Comparative of (a) this study with (b) Pailoplee et al. (2013) showing the distribution of return period of 5.0 along the TLMB.

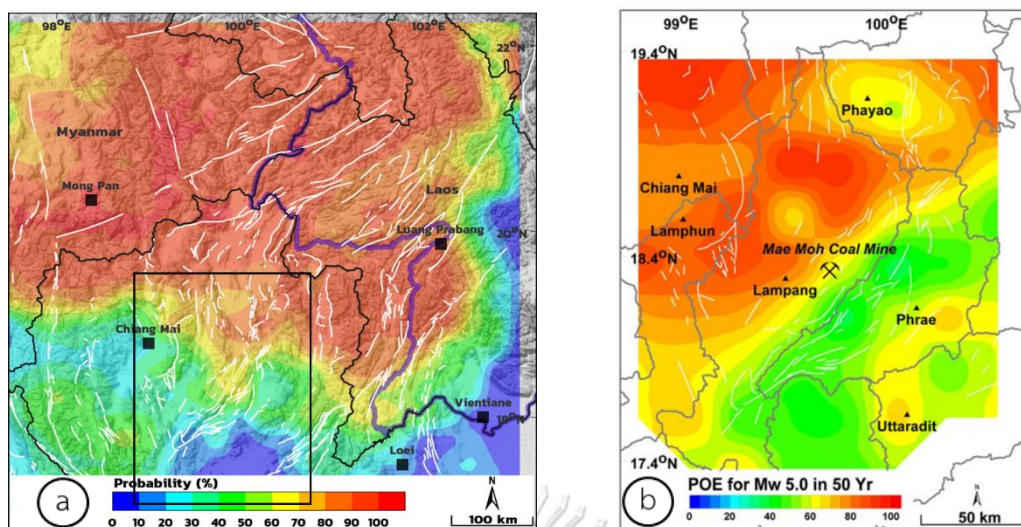


Figure 7.3 Comparative of (a) this study with (b) Pailoplee and Charusiri (2015) showing the distribution of the probability of occurrence of 5.0 along the TLMB.

7.2 Seismic Pattern

As mentioned in Chapter 2, the fractal dimension shows how much space the fractal takes up in the area around it. If we know the value of D , we can predict how the fracture will look. For example, a D_c value around 3 means that earthquake cracks are filling up a volume of the crust, a value near 2 means that a plane is being filled up, and a value near 1 means that line sources are the most common. Also, Tosi (1998) showed that, depending on the dimension of the embedding space, the range of possible fractal dimension values is between 0 and 2. The meaning of these limit values is that a set with D_c close to 0 means that all events are happening in one place, while a set with D_c close to 2 means that events are spread out randomly or evenly over a two-dimensional embedding space.

As a result, in Figure 5.4, the D_c value varied from 0.1 to 0.3, a D_c value close to 1 means that line sources are predominant (Aki, 1981) and with D_c near to 0 suggests that all events are concentrated at a single place. In addition, because of the geological setting in this location, the faults are geographically dispersed throughout the region, and the seismic pattern in the research area may be interpreted as a fault line based on the D_c value.

7.3 Evolution of Stress Transfer

In order to demonstrate the state of the dynamic evolution of seismic stress throughout the last ten years, four tests of sub-datasets were performed, consisting of the $M_L \geq 5.0$ earthquakes from 2010-2012, 2010-2014, 2010-2016, and 2010-2018 shown in Figure 7.4.

The spatial distribution of b value in 2010-2012 (Figure 7.4a). Indicate two regions with lower b values discovered: i) in the east of Mong Pan, Myanmar, along TLMB, ii) In the west of Mong Pan, and iii) surrounding Chiangmai, Thailand, extends the southeastern ward to Loei,

The spatial distribution of b value in 2010-2014 (Figure 7.4b). Three regions with low b values were discovered i) the east of Mong Pan, Myanmar, which is the same area as the previous paragraph, ii) the northwest to southeast trend from the TLMB boundary to Vientiane, Laos, which was developed in 2010-2012, and iii) south of Chiangmai which is the smaller portion compare with the same area in 2012.

The spatial distribution of b value in 2010-2016 (Figure 7.4c). The area with low b values discovered: i) west of Mong Pan, Myanmar, which developed from 2010 until the $M_L=5.0$ occurred in 2018, ii) from the east of Mong Pan, Myanmar, southward to Vientiane, Laos, iii) south of Chiangmai, and iv) Luang Prabang Laos. Five earthquakes with an M_L greater than 5.0 were recorded after this period. All the earthquakes are in the low b-value area except 5.1 M_L in 2021 in northwest of Mong Pan

The spatial distribution of b value in 2000-2018 (Figure 7.4a). Low b-value areas were found in the northwest-southeast trend from i) the eastern part of Mong Pan, Myanmar, ii) the southern part of Chiangmai, and iii) the northeastern-eastern part of Chiangmai, Thailand. Two earthquakes with an M_L greater than 5.0 were recorded after this period. All the earthquakes are in the low b value-area except 5.1 M_L in 2021 in the northwest of Mong Pan, which shows a high SD of b value and Low goodness fit

It can be concluded that the trend of the stress, in this case, the low b-value area, may shift from the west to the east of TLMB.

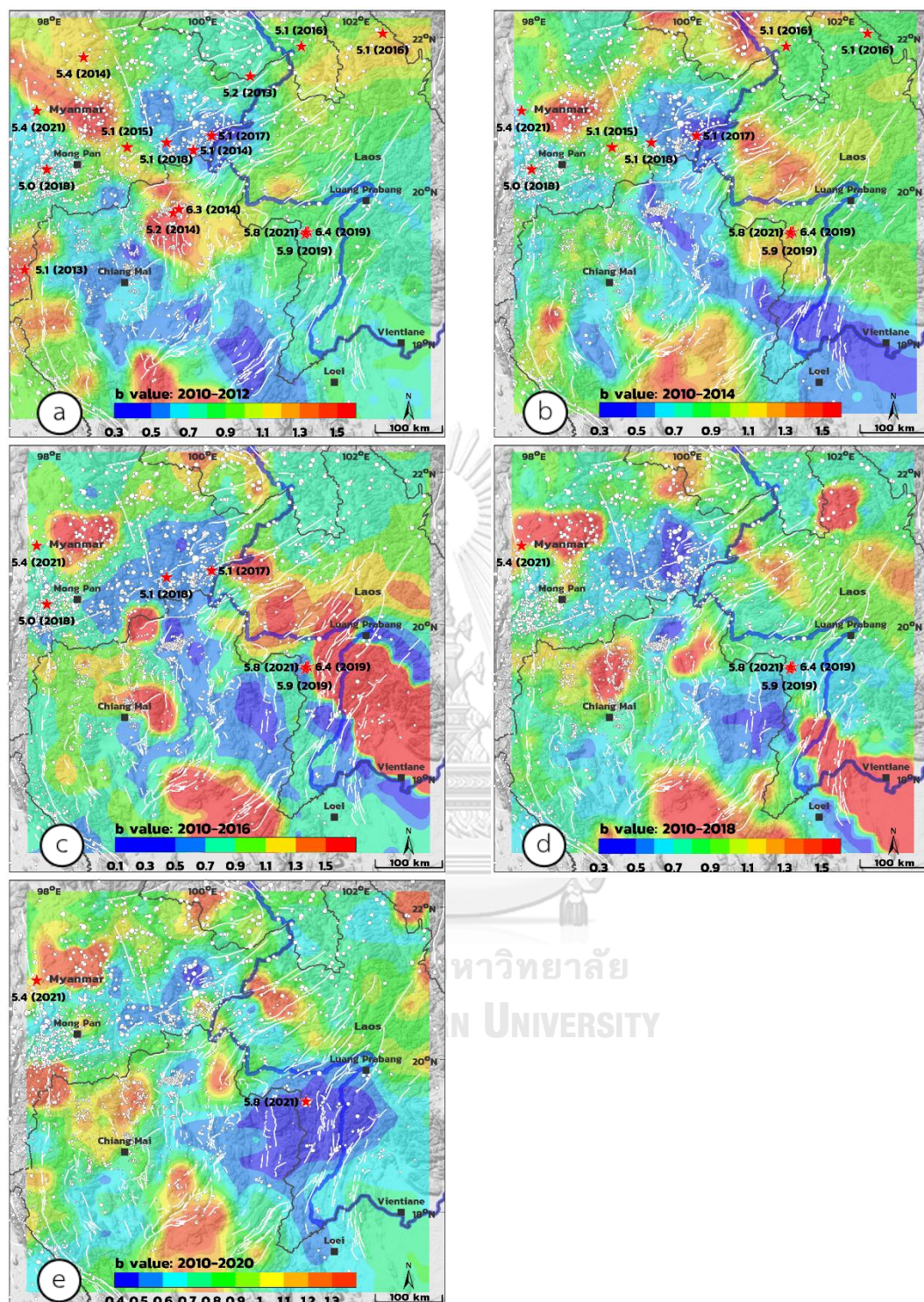


Figure 7.4. Distribution of b value along the TLMB from (a) 2010-2012, (b) 2010-2014, (c) 2010-2016, (d) 2010-2018, and (e) 2010-2020. The red star indicates earthquakes with a magnitude $\geq 5.0 M_L$ that occurred after the data collection.

7.4 Tectonic Stress in Present Day

After looking at how tectonic stress has changed over time in the last topic, we will now talk about the details of tectonic stress today and compare them to what Pailoplee et al. (2013) found in Figure 7.5b. the result of this thesis determines the prospective area in the northwest to the southeast of the study area. (Figure 7.5b)

Similarly, the previous study examined the b value for 1984 to 2010 and suggested the prospective areas with the low b value, which are the northern region of Mong Pan and the Pak Beng-Luang Prabang dams, similar to this thesis. Moreover, This thesis further expands coverage to include an additional area in the Pua fault zone in the Thai province of Nan to the southwest of Luang Prabang, covering the Dien Bien Fu fault zone.

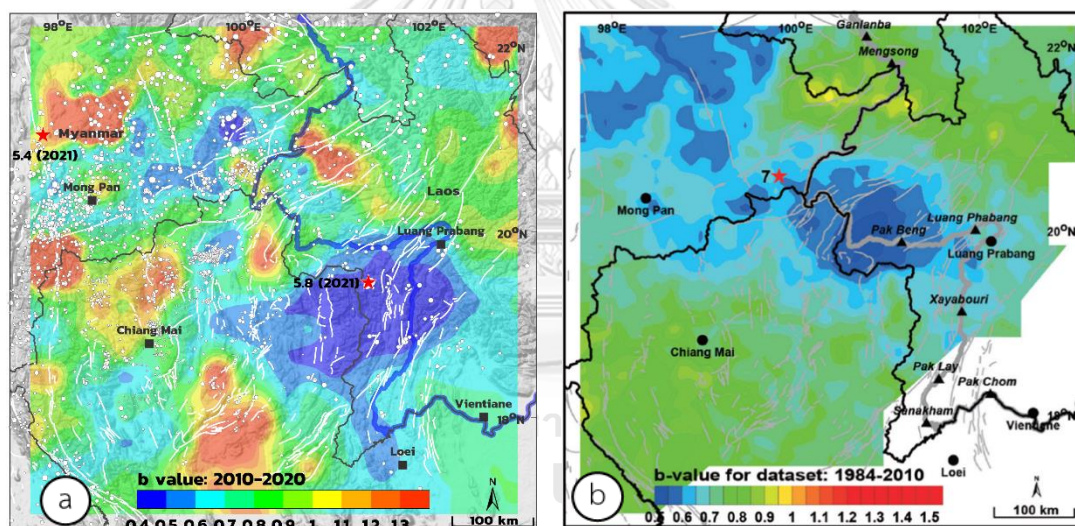


Figure 7.5. Comparative the spatial distribution of b value along the TLMB border of (a) the spatial distribution of b value this study from 2000-2020 with (b) the spatial distribution of the b value of Pailoplee et al. (2013) in 1984-2010. The red star indicates earthquakes with a magnitude ≥ 5.0 that occurred after the data collection.

7.5 Quiescence Time Span of Z value

Next, we focused on seismicity rate change in terms of temporal variation as a precursor (Z value). Now we will discuss the specifics of the time of seismic quiescence (Z_{\max}) graph and compare them to what Puangjaktha and Pailoplee (2016) discovered in Figure 7.6b. This thesis establishes that the highest Z value of 4.7 happened in 2015.42, and 7.9 years later, on November 11th, 2019, the M_L -6.4 earthquake happened west of Xyabouri dam in Laos. Previous research analyzed the graph of the time of seismic quiescence (Z_{\max}) and determined that the final Z peak at 1997.07 is the precursory peak of an M_L -6.8 earthquake generated in the TLMB. Therefore, it can be concluded that we can be considered seismic quiescence as a precursor that existed prior to the occurrence of the earthquake.

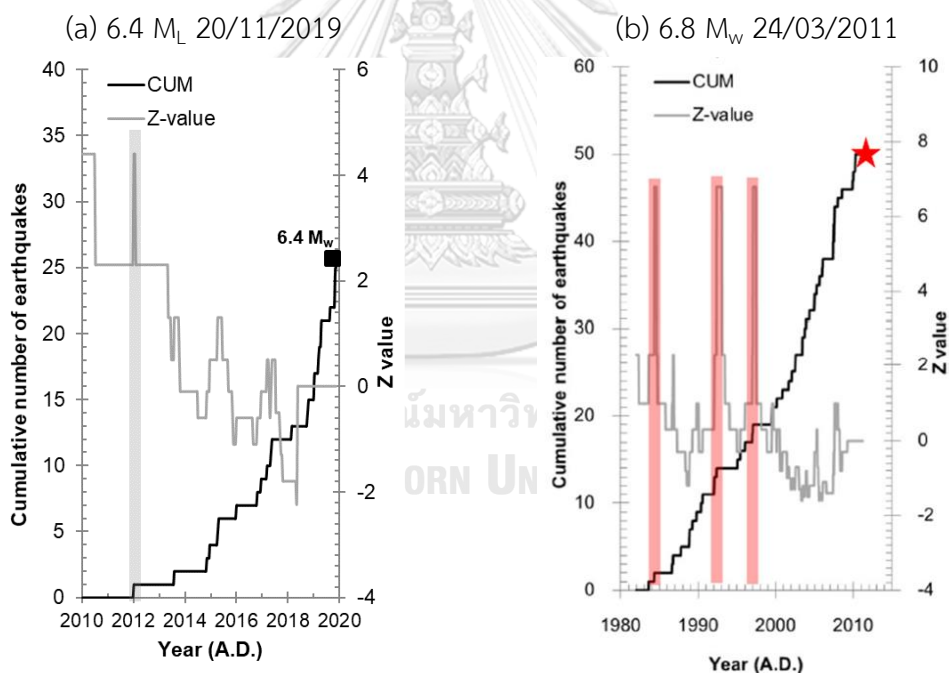


Figure 7.6. Comparative of Puangjaktha and Pailoplee (2016) with this study showing the graph of time of seismic quiescence (Z_{\max}) to the time of the major earthquake. The cumulative number of earthquakes (grey line) and Z value (black line) are plotted versus time for earthquakes. The red stars and black squares are the occurrence time of each earthquake. A transparent grey and red strip illustrates the anomalous Z value recognized as the quiescence stage

7.6 Present Quiescence Map from Z value

Next, we focused on seismicity rate change in spatial distribution as a precursor (Z value). We will now talk about the details of the prospective area and compare them to what Puangjaktha and Pailoplee (2016) found in Figure 7.7. The result of this thesis determines the prospective area, including the eastern portion of Mong Pan, Myanmar; Chiang Rai province, Thailand, in the Mengxing fault zone and the Mae Chan fault zone; Nan province, Laos, that includes the Pua and Dien Bien Fu fault zones; and Chiangmai and Tak provinces. The previous study analyzed the spatial distribution of Z values and suggested that the prospective areas in which the Z values, which were mapped in 1997.07, a strip of anomalously high Z values, delimited in an east-west direction at the TLMB juncture. Then, on March 24th, 2011, approximately 14.2 years later, the epicenter of a magnitude 6.8 earthquake occurred, located within the high Z-value zone occupied by the Mengxing fault zone. Therefore, this study's positive Z-value area conforms with the Puangjaktha and Pailoplee (2016), and it can be concluded that the seismic quiescence might be a precursor to the forthcoming earthquakes.

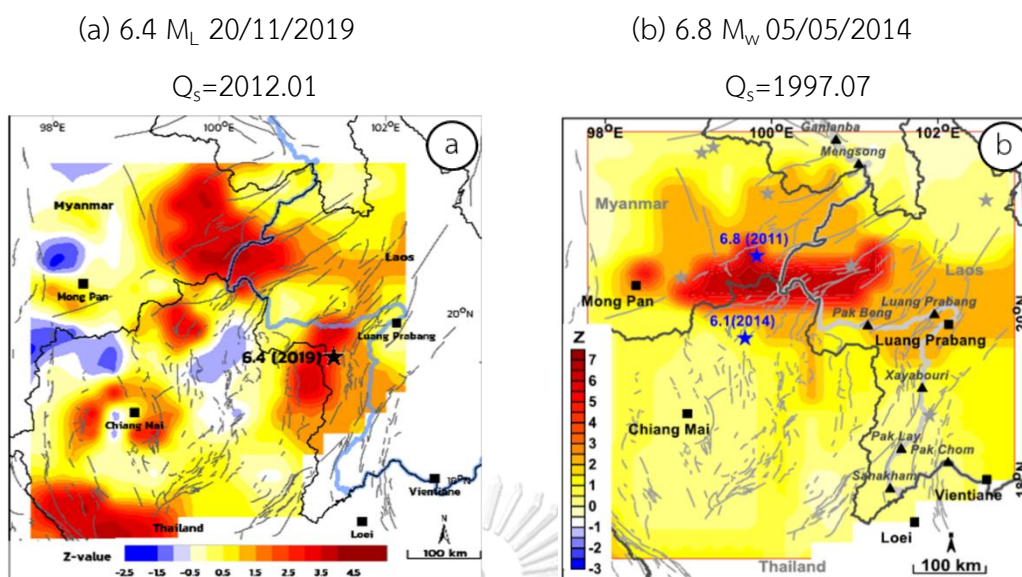


Figure 7.7. The maps of the TLMB area illustrate the spatial distribution of the Z values of (Puangjaktha and Pailoplee, 2016) with this study. Red and blue colors denote decreased (+Z) and increase (-Z) in the seismicity rate, respectively. Black stars represent the epicenter of the earthquake case study.

7.7 The Starting of Seismic Quiescence from Seismicity Rate Change(Z value)

To strengthen the Z value investigation and the RTL algorithm. Both can potentially evaluate seismic precursors in the intermediate-term earthquake forecast before the earthquake's occurrence. This work also compared the calculable duration time between the start of seismic quiescence and the occurrence of the main shock (Q-time) calculated using both techniques to previous research.

After examining previous research on Z value investigation shown In Figure 7.8, it can be divided into two categories: intermediate-term investigation (from months to 10 years) and long-term investigation (over ten years). The first group suggests that Q-time ranged between 0.75-7 years which are Wiemer and Wyss (1944), Murru et al. (1999); Chouliaras and Stavrakakis (2001); Öztürk and Bayrak (2009); Chouliaras (2009), Wu and Chiao (2006), and Katsumata, (2011a); The second group shows that Q-time is more extended than twenty years (Katsumata, 2011b). However, when the Z value investigation in the TLMB was conducted, the Q-time of thirteen earthquake

retrospective tests was in the range of 1.6-7.9 years, suggesting that the method might be somewhat valuable for intermediate-term forecasting (months–10 years).

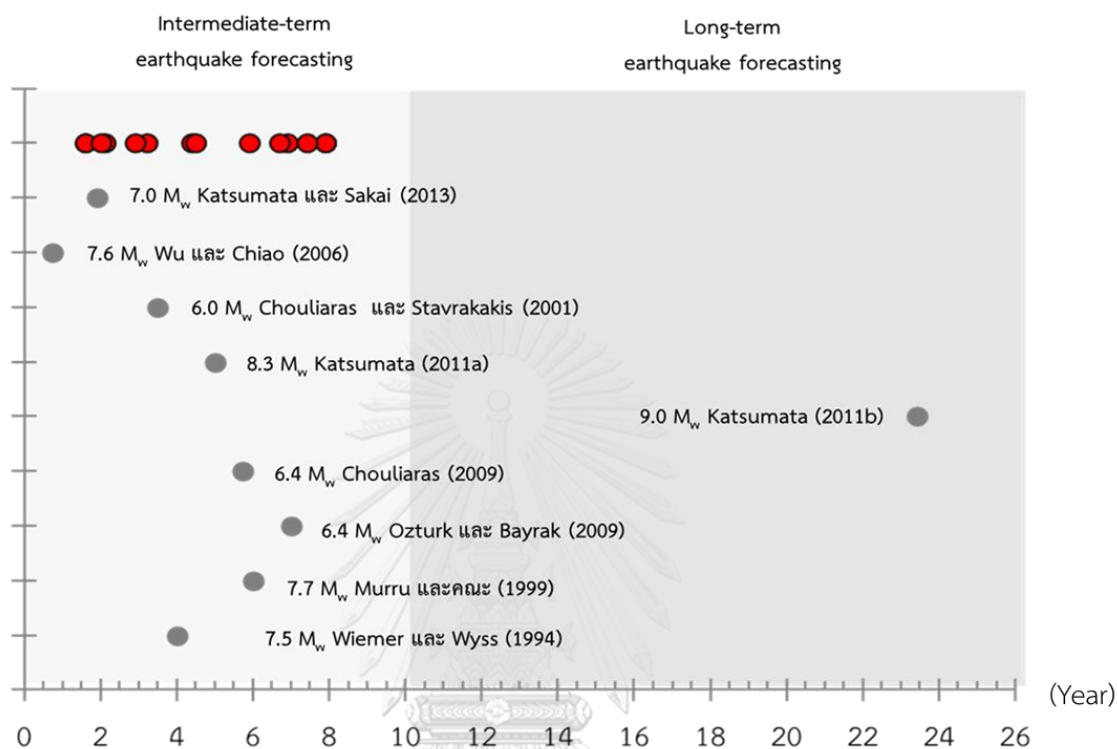


Figure 7.8. The Graph shows the time of Z-value's seismic quiescence (Q time) to the time of a major earthquake. Black dots show the result from previous work, and red dots show this study's results. (Modified from Puangjaktha and Pailoplee (2016)).

7.8 Stochastic of Z value

The stochastic test (Huang, 2006) was used to ensure that the Z values obtained in this investigation were not due to random events. Initially, 10,000 earthquake catalogues were stochastically synthesized within the same study area, and the entire earthquake catalogue recording time was utilized in this work (i.e., 2010-2020). Z values were calculated at the epicenter of the M_L -7.2 earthquake (No. 15 in Table 6.1) using free characteristic parameters $N = 90$ events and $T_w = 2.5$ years in each synthesized catalogue. The likelihood that the Z value corresponds to random phenomena is then added in Figure 7.9. The likelihood was estimated at 44.73% (Figure 7.9) based on the greatest Z value of 4.7 in the M_L -5.1 earthquake case study, showing

that the Z values obtained in this study are significant and not attributable to random events

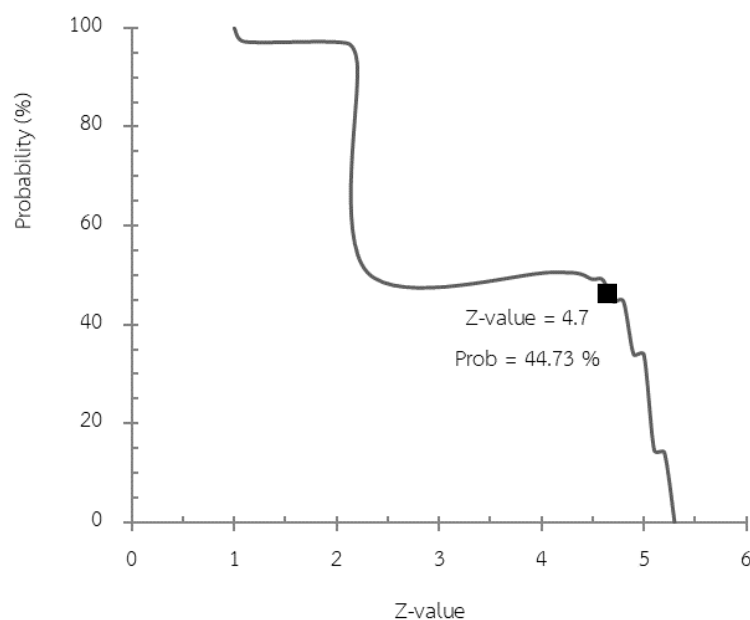


Figure 7.9. The probability percentage of various Z values accords to a random phenomenon calculated at the epicenters of the M_L 5.1 earthquake.

7.9 Quiescence time span of RTL Algorithm

Following that, we concentrated on seismic quiescence in terms of temporal variation as a forerunner (RTL score). Now we will analyze the characteristics of the period of seismic quiescence (RTL score) graph and compare them to what Puangjaktha and Pailoplee (2018) discovered in Figure 7.10b. The thesis results show that seismic quiescence began to drop in 2012.93 and peaked in 2014.81 (RTL score = -0.20). Furthermore, with a maximum RTL score of 0.94, the RTL score suggested an activation period between 2016.88 and 2019.87, even though on November 20th, 2018, a 6.4 M_L earthquake occurred during an activation stage. Previous research evaluated the graph of the time of seismic quiescence and determined that the variation in the RTL score represented the seismic quiescence. The RTL began to fall in 2007.38 and reached its lowest point in 2007.58 before reverting to the background rate in 2009.57. The M_L 6.8

earthquake occurred 3.7 years later, on March 24th, 2011. Therefore, it is possible to conclude that the seismic quiescence existed before the earthquake.

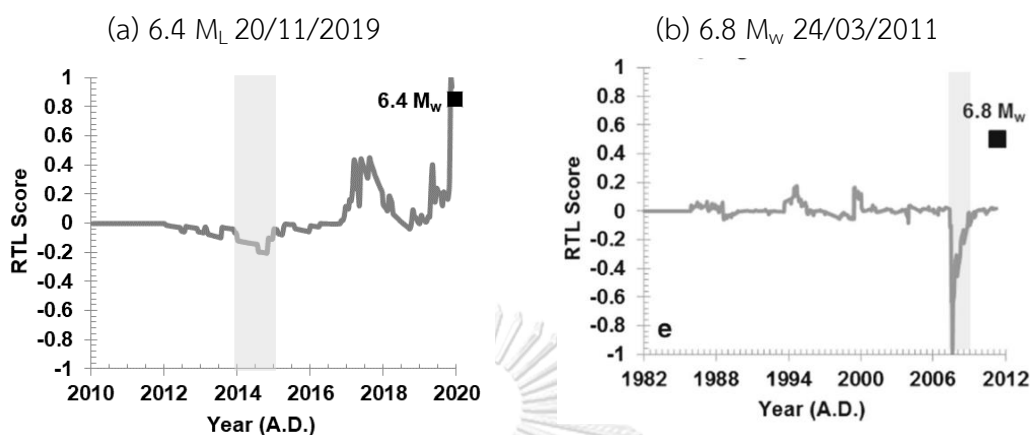


Figure 7.10. Comparative of (a) this study with (b) Puangjaktha and Pailoplee (2018) showing a temporal variation of the RTL score (grey line) of strong-to-major earthquakes (black square). A transparent grey and red strip illustrates the anomalous RTL recognized as the quiescence stage

7.10 Present Quiescence Map from RTL algorithm

As a precursor, we then concentrated on seismic quiescence in terms of spatial distribution (RTL score). We will now discuss the prospective area's details and compare them to what Puangjaktha and Pailoplee (2018) discovered in Figure 7.11b. This study finds almost the same area as the previous study and then covers southwest of Luang Prabang with the Dien Bien Fu fault zone and an extra area in Nan province of Thailand in the Pua fault zone. The previous study investigated the spatial distribution of Z values, and the spatial distribution of the RTL score from 2007.38 to 2009.57 revealed that the seismic quiescence spanned around 300 km² along the Thailand–Myanmar border. Specifically, the minimum RTL score defines the northern portion of Chiang Mai city, which is adjacent to the Mae Chan fault zone. Within five years of these anomalies (2010–2015), two dangerous earthquakes occurred nearby (Figure 7.11b): the M_L -6.8 Tarlay earthquake on March 24th, 2011 (Wang et al., 2014a) and the M_L -6.3 Mae Lao earthquake on May 5th, 2014 (Ornthammarath, 2015).

Therefore, this negative RTL score area conforms with the Puangjaktha and Pailoplee (2018), and it can be concluded that the seismic quiescence might be a precursor to the forthcoming earthquakes.

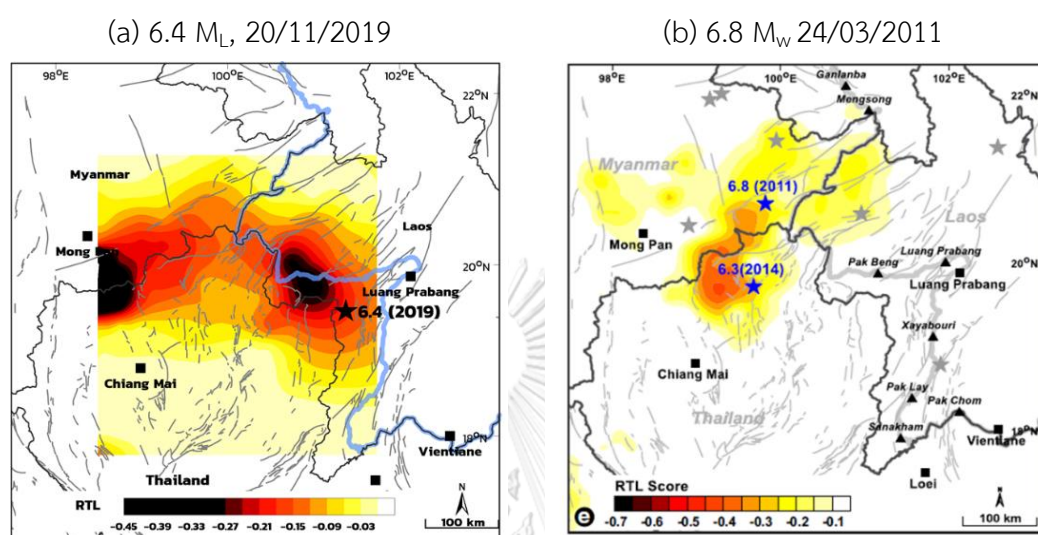


Figure 7.11. A comparative of this study with Puangjaktha and Pailoplee (2018) shows that the spatial distribution of RTL values along TLMB during each case study is observed in seismic quiescence. The epicenter of each earthquake defines as a black star.

7.11 The Starting of Seismic Quiescence of RTL Algorithm

After examining previous studies on the RTL algorithm shown in Figure 7.12, it was determined that the previous study indicated that RTL investigations are classified as an intermediate-term (ranging from months to 10 years). According to a prior study, the duration of Q-time ranged between from 1 to 5 years (Di Giovambattista and Tyupkin (2000), Huang et al. (2001), Huang and Sobolev (2002), Huang and Zhao (2004), Huang, Huang, and Chiu (2005), Chen and Wu (2006), Mignan and Di Giovambattista (2008), Nagao et al., (2011), and Gambino, Laudani, and Mangiagli (2014).

However, in the TLMB region for RTL algorithm research, the Q-time range of ten retrospective tests was 0-6.3 years, which might be pretty practical for intermediate-term forecasting (months–10 years) despite its relatively large range distribution. Consequently, the quiescence detection time determined in this study

similarly applies to intermediate-term forecasting, as previously addressed with Z-value research.

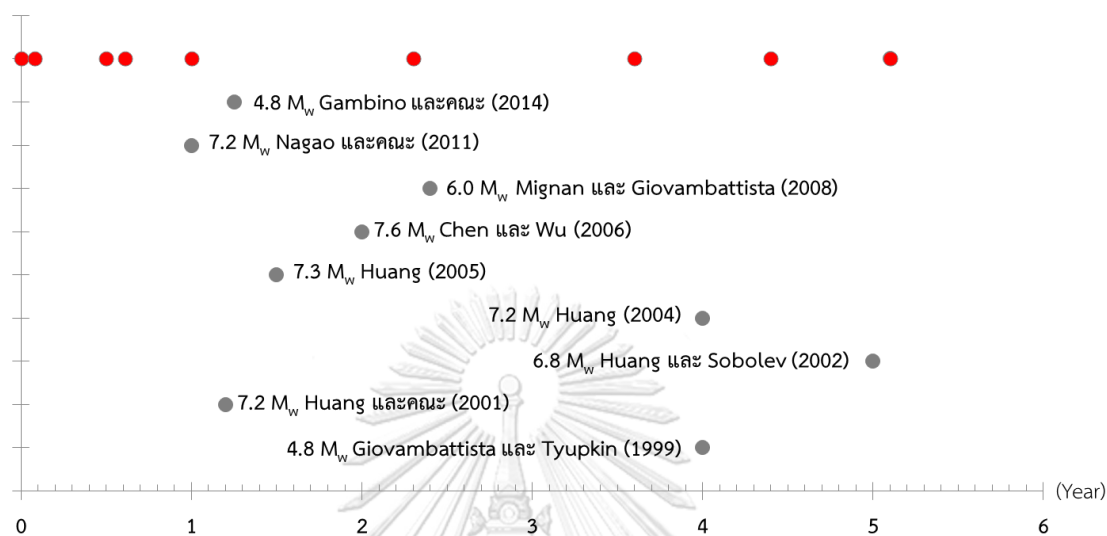


Figure 7.12. The Graph shows the time of the RTL algorithm's seismic quiescence (Q time) to the time of a major earthquake. Black dots show the result from previous works, and red dots shows the results from this study (Modified from Puangjaktha and Pailoplee (2018)).

7.12 Correlation Coefficient of RTL Score

To constrain the significance of the selected characteristic parameters ($r_0 = 90$ km and $t_0 = 2$ years), the temporal variations of the RTL scores were also examined by increasing/decreasing r_0 by 20 km (70 km and 110 km) and t_0 by 0.5 years (1.5 years and 2.5 years) from the parameters utilized in this study (Table 6.2). In addition, the correlation coefficient (Huang, 2006) was examined for the M_L -5.2 earthquake that occurred on May 5th, 2014, to assess the sensitivity of the free characteristic parameters given for the TLMB ($r_0 = 90$ km and $t_0 = 2$ years), (no. 8 in Table 6.2). In all situations, variations in RTL scores were explored over time and significantly associated with the Z value computed by $r_0 = 90$ km and $t_0 = 2$ years (Figure 7.3). The correlation coefficients in this RTL score analysis are 0.698-0.972 (Table 6.2), showing that free-parameter modifications have no meaningful influence. Therefore, the selected characteristic parameters were meaningful, and the quiescence found in the TLMB is

not due to the artifact of free parameter selection. P values are commonly utilized in hypothesis tests to evaluate whether or not the null hypothesis is rejected. A small p-value is indicative of the falsity of the null hypothesis. Commonly, the null hypothesis is rejected if the p-value is less than 0.05. In this thesis, the p-value of every case is less than 0.00001.

Table 7.1. Examples of correlation coefficients of the RTL scores obtained with different utilized r_0 and t_0 values for the M_L 5.2 earthquake on May 5th, 2014. Case A represents the parameters utilized in this study, whereas case B represents the other nearby parameters recognized for correlation.

Case 2	A	$r_0 = 90 \text{ km}, t_0 = 2 \text{ year}$			
	B	$r_0 = 70 \text{ km}$	$r_0 = 110 \text{ km}$	$t_0 = 1.50 \text{ year}$	$t_0 = 2.50 \text{ year}$
Correlation (R^2) between A and B		0.698	0.972	0.796	0.813
p-value		< 0.00001	< 0.00001	< 0.00001	< 0.00001

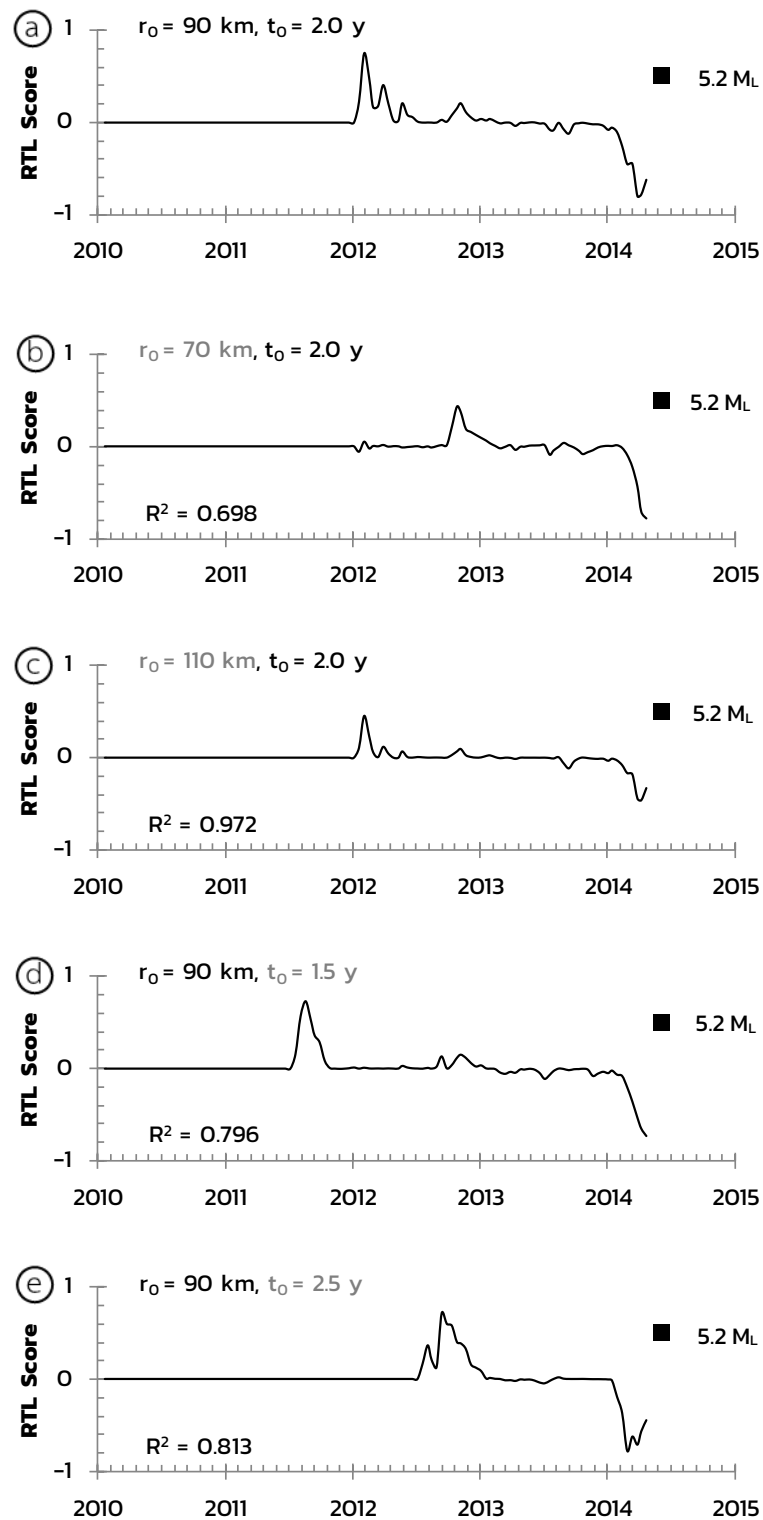


Figure 7.13. Temporal variation of the RTL score (grey lines) was evaluated from different characteristic parameters. Black squares denote the origin time of the M_L -5.2 earthquake generated on May 5th, 2014.

7.13 Forecasting Prospective Area

To discuss the prospective areas of this topic, we try to interpret results from all of the precursors, which are the anomalous b value from Seismotectonic stress, the anomalous Z value from a seismicity rate change and the RTL score from seismic quiescence were compared as shown in Figure 7.17. Additionally, it was observed that the seismicity rate varies with seismic quiescence. Seismotectonically, the lower b value indicates the potential prospective earthquake source. The positive and negative Z values correspond to the quiescence and activation stages in the particular location and time of interest. A lower or negative RTL score, on the other hand, indicated a higher level of seismic quiescence.

Figure 7.14 shows the results from the seismotectonic stress method, which is the spatial distribution of the b value indicates the potential prospective earthquake source. The blue line identifies the prospective area of an earthquake with a low b value. In this study, a b value of less than 0.6 is considered an anomalous b value. The prospective areas were found to be in the northwest-southeast trend of the study area, composed of (i) the eastern part of Mong Pan, Myanmar, located in the Mengxing fault zone, (ii) Chiang Rai Province, Thailand, is located south of the Mae Chan fault zone, (iii) Chiangmai's southern outskirts, Thailand, and (iv) a large area in Prae and Nan provinces, as well as the southwest of Luang Prabang, Laos, encompassing the Pua and Dien Bien Fu fault zones.

Figure 7.15 illustrates the spatial distribution of the Z value because of the seismicity rate change. The black line indicates the potential location for an earthquake with a positive Z value correspond to the quiescence stage. In this study, a Z value of more than 1.5 is considered an anomalous Z value. The prospective area of Z -value zones were discovered in (i) the eastern portion of Mong Pan, Myanmar, (ii) Chiang Rai province, Thailand, located in the Mengxing fault zone and the Mae Chan fault zone, (iii) A large area in Nan province, and the west of Luang Prabang, Laos includes the Pua and Dien Bien Fu fault zones, and (iv) Chiangmai and Tak province.

Figure 7.16 shows the results from the seismic quiescence, which is the spatial distribution of the RTL score. The red line identifies the prospective area of an earthquake with a negative RTL score indicated a higher level of seismic quiescence. In this study, a RTL score of less than -0.05 is considered an anomalous RTL score. The prospective area from RTL score areas were found on the boundary of Thailand-Laos-Myanmar with two portions of strong anomaly (i) the southeastern part of Mong Pan, Myanmar, encompassing the northern part of Thailand, including the provinces of Chiangmai and Chiang Rai, and located in the Mengxing and Mae Chan fault zones (ii) The northern part of Thailand, including the provinces of Chiang Rai, Phayao, and Nan, and (iii) the area west of Luang Prabang, Laos, which includes the Pua and Dien Bien Fu fault zones.

To limit the areas of interest from the three precursors, overlap the three maps shown in Figure 7.17 and then give the anomalous areas that overlap a grade of A, B, or C (Figure 7.18). The anomaly zones overlap with three precursors: b value, Z value, and RTL score, all considered grade A which indicates the high potential of prospective area and quiescence stage. The anomaly zones are in the same place as two of the three precursors considered grade B. The anomaly zones touch one of the three precursors considered grade C. The grade A region is the anomaly zone that overlaps with three precursors: b value, Z-value, and RTL score. This area, which is the most hazardous area, comprises three regions: (i) the border between Myanmar and Thailand in the Mengxing fault zone, (ii) The province of Chiang Rai, Thailand, is situated in the Phayao and Mae Chan fault zone, (iii) A large area in Nan province, Thailand, near the Pua fault zone and southwest of Luang Prabang, Laos, including the Dien Bien Fu fault zone. The grade B region is the anomaly zone that overlaps with two of the three precursors. This area, which is in secondary danger in this study area, is composed of: (i) northeast of Mong Pan, Myanmar, (ii) Thailand-Laos borders in Pua fault zone, (iii) east of Mong Pan, Myanmar in Mengxing fault zone, (iv) Chiang Rai, Thailand near Mae Chan fault zone, (v) Nan and Phayao province near Phayao and Pua fault zone, Thailand and west Luang Prabang, Laos near Dien Bien Fu fault zone, (vi) Thailand-Laos-Myanmar border in Nam Ma, Mae Chan, and Mae Ing fault zone, (vii) Chiang Rai province, Thailand in Mae Chan and Phayao fault zone. The grade C region is the

anomaly zone that overlaps with one of three precursors. This area, which is the least dangerous, is composed of: (i) Prae and Uttaradit province, Thailand, (ii) South of Luang Prabang, Laos, (iii) Northeast of Mong Pan, Myanmar, (iv) Myanmar-Laos border, near Mae Chan and Mae Ing fault zone, (v) Chiangmai province, Thailand, (vi) Tak and Chiang Mai, Thailand, (vii) Thailand-Myanmar border near Chiang Mai province, Thailand and Mong Pan, Myanmar in Mengxing fault zone, (viii) Thailand-Laos border near Chiang Rai, Thailand and west of Luang Prabang.

On the other hand, we attempt to discover more research in TLMB related to the prospective area. Boonchaisuk et al. (2017) investigate the three-dimensional magnetotelluric imaging of the Phayao fault zone in northern Thailand. Most of the epicenters of the earthquakes were found in the transition zone between the Mae Lao segment and the Pan segment of the Phayao fault zone. In addition, the shallow 3-D resistivity structure corresponds exceptionally well with the surface geology, while the deeper structures reveal numerous fascinating resistive and conductive anomalies. The seismogenic zone is located near the major conductive anomaly (ML) at a depth of 4 km to the mid-crust beneath the Mae Lao segment. The ML conductor has a highly linked aqueous fluid content and plays an essential role in the earthquake sequence of May 5th, 2014. The presence of fluid within a fractured fault would significantly weaken the strength of the fault. Therefore, the cumulative pre-existing tectonic stress from the north can reach the maximum frictional strength of the Mae Lao segment, causing it to slip and generate the primary shock. Wang, Zhao, and Yao (2013) also found that the low resistivity anomalies were linked to the low-velocity zone in the lower crust. It shows that fluids weaken the upper and middle crustal seismogenic layers and cause big earthquakes. Figure 7.19 depicts the ML conductor between the Mae Lao segment and Pan segment faults in the middle of their study area. They interpreted this conductivity anomaly beneath the Mae Lao segment and partially beneath the Pan segment from a depth of 4 km to the mid-crust as fluid-rich saline zones in which the presence of fluid within a fractured fault would considerably reduce the strength of the fault as well as cause large earthquakes. Compared to this thesis,

their prospective area overlaps with grades A and B in the province of Chiang Rai, Thailand in the south of Mae Chan fault zone and Phayao province in the Phayao fault zone.

In addition, it became noticeable that the most dangerous area, or grade A area, is indicated in the active fault zone that should be aware of, which are the Mangxing fault zone, Nam Ma fault zone, Mae Chan fault zone, and Mae Ing fault zone. Consequently, among the b value, the Z value, RTL score anomalies, and other methods mostly overlapped to confirm that increased potential areas, such as the border between Myanmar and Thailand, Nan province, Thailand, and west of Luang Prabang, Laos, all of them might act as precursors to the subsequent forthcoming earthquakes.



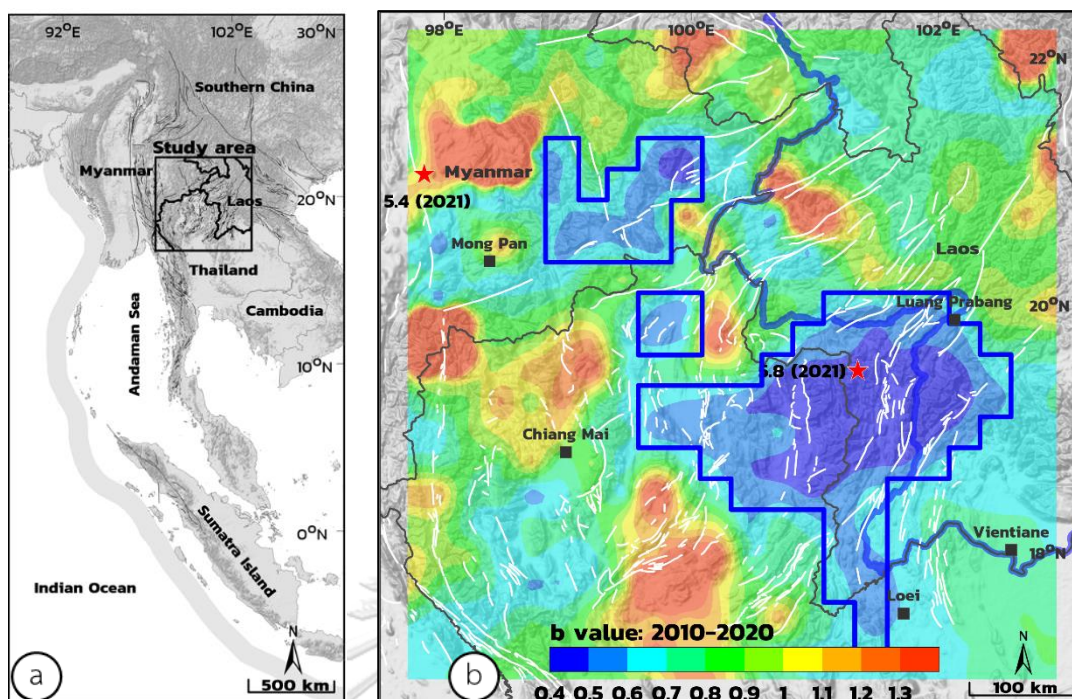


Figure 7.14. The photos show (a) a map of Mainland Southeast Asia. (b) The study area focuses on the TLMB overlay with the spatial distribution of the b value. The blue dashed line identifies the prospective area.

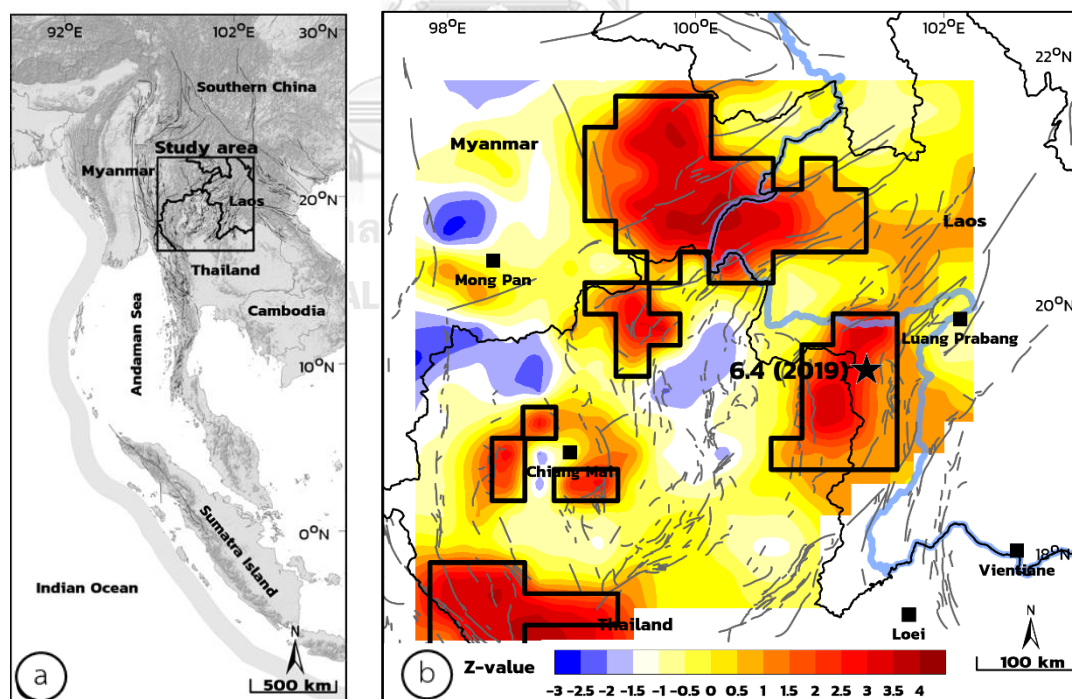


Figure 7.15. The photos show (a) a map of Mainland Southeast Asia. (b) The study area focuses on the TLMB overlay with the spatial distribution of the Z value. The black dashed identifies the prospective area.

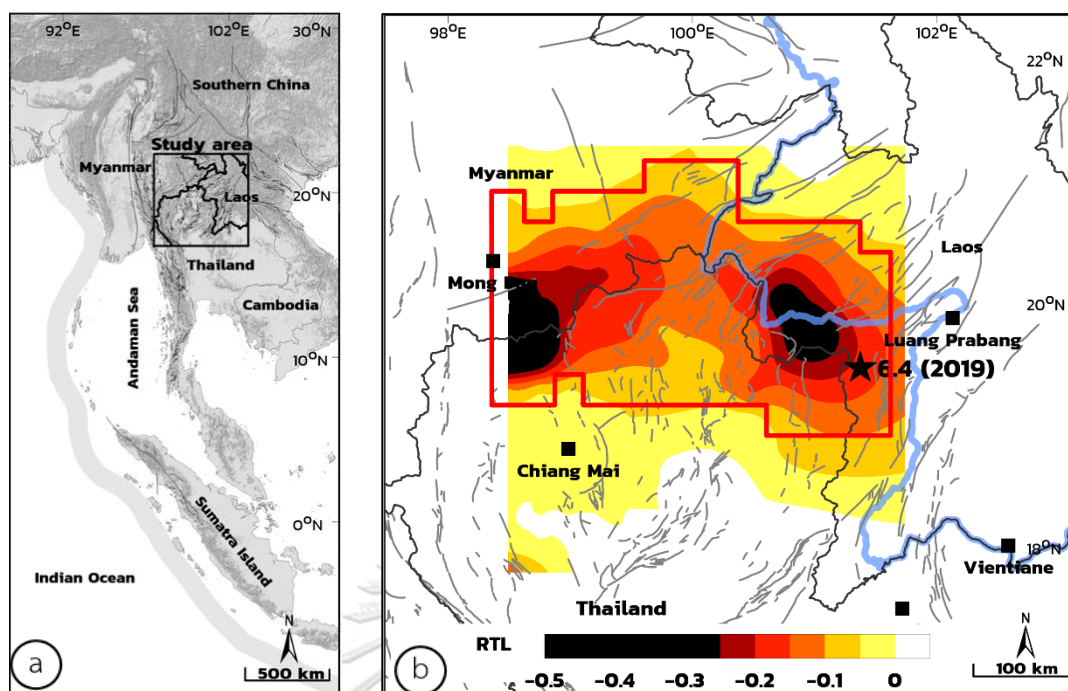


Figure 7.16. The photos show (a) a map of Mainland Southeast Asia. (b) The study area focuses on the TLMB overlay with the spatial distribution of the RTL score. The red line identifies the prospective area.

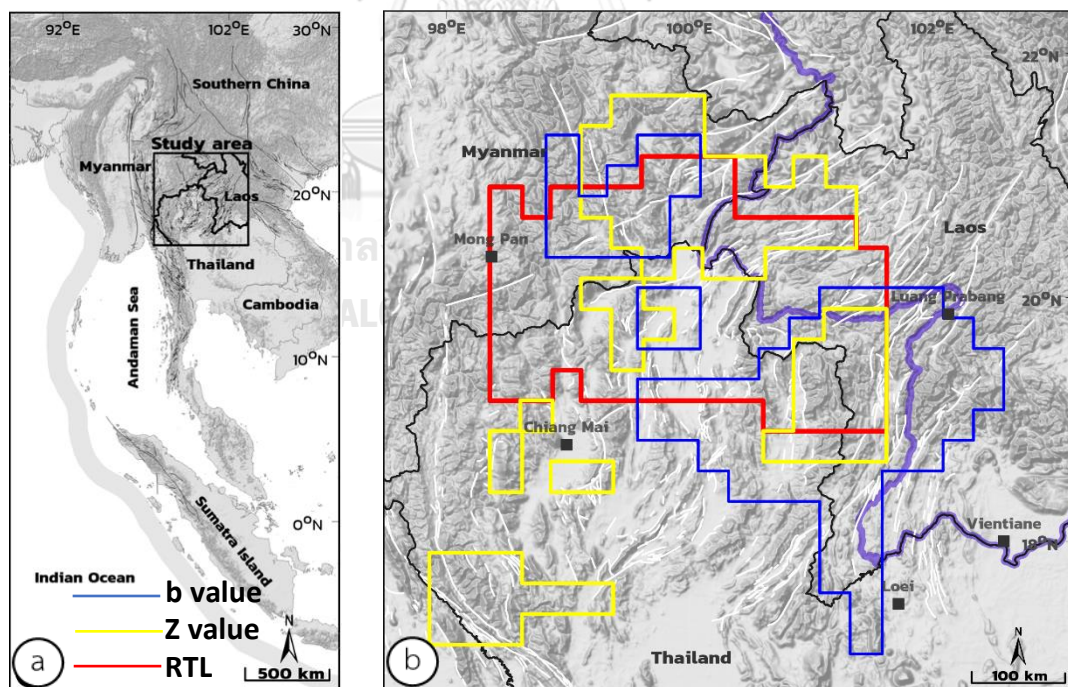


Figure 7.17. The photos show (a) a map of Mainland Southeast Asia. (b) The study area focuses on the TLMB overlay with the spatial distribution of the b value. The line identifies the prospective area of three precursors.

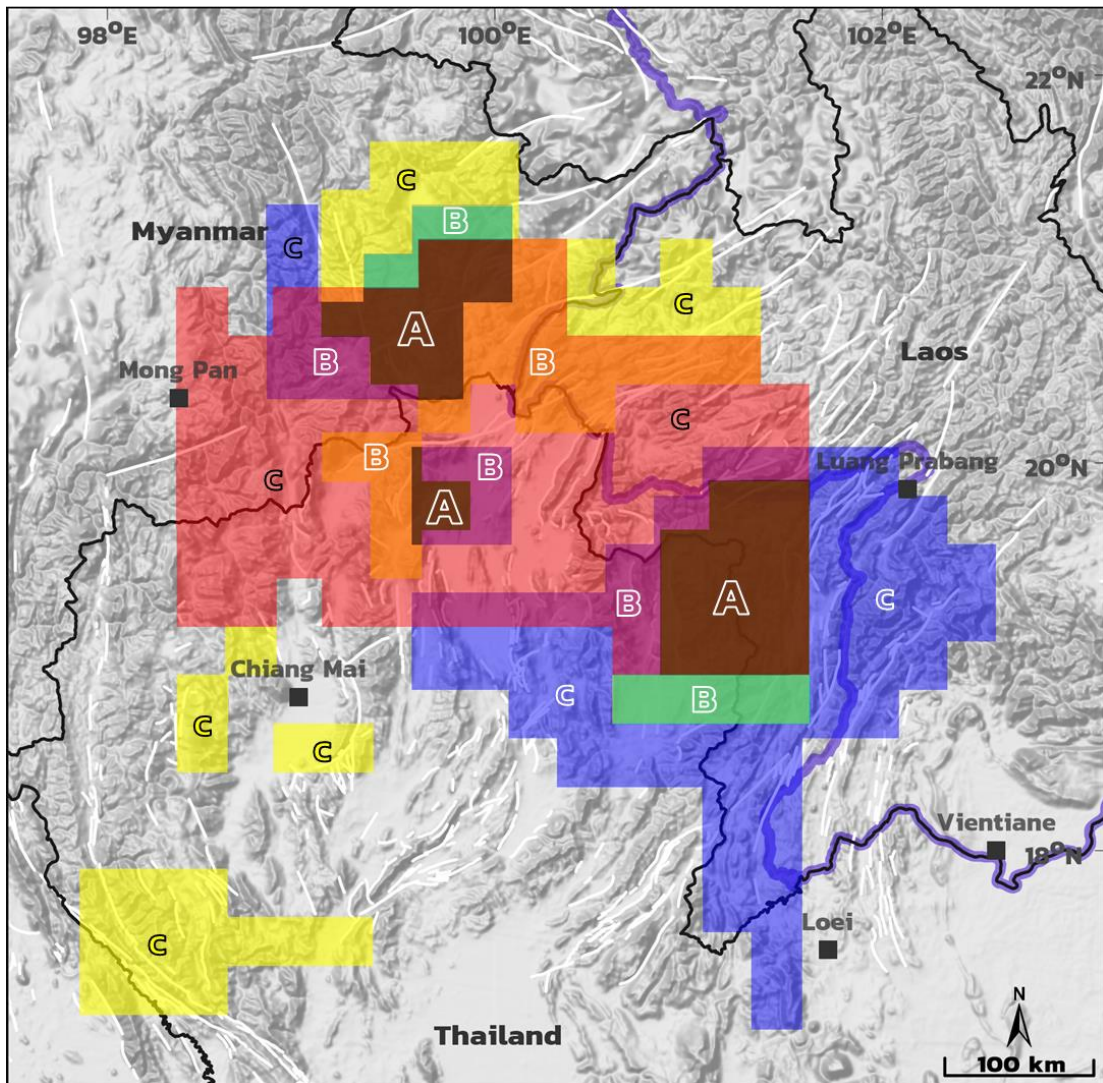








Figure 7.18. The study area focuses on the TLMB overlay with the spatial distribution of b value, Z value, and RTL score anomalies. The transparency color area identifies the prospective area of each precursors and describe the details in Table 7.2.

Table 7.2. Legend of the map in Figure 7.18 showing the prospective area in TLMB.

Grade	Legend	Prospective area
A		<ul style="list-style-type: none"> (i) Thailand-Myanmar border in Mengxing fault zone (ii) Chiang Rai province, Thailand near Mae Chan and Phayao fault zone (iii) Thailand-Laos borders in Nan province, Thailand in Pua fault zone and southwest of Luang Prabang, Laos, including the Dien Bien Fu fault zone
B		<ul style="list-style-type: none"> (i) Northeast of Mong Pan, Myanmar (ii) Thailand-Laos borders in Pua fault zone
B		<ul style="list-style-type: none"> (i) East of Mong Pan, Myanmar in Mengxing fault zone (ii) Chiang Rai, Thailand near Mae Chan fault zone (iii) Nan and Phayao province near Phayao and Pua fault zone, Thailand and west Luang Prabang, Laos near Dien Bien Fu fault zone
B		<ul style="list-style-type: none"> (i) Thailand-Laos-Myanmar border in Nam Ma, Mae Chan, and Mae Ing fault zone (ii) Chiang Rai province, Thailand in Mae Chan and Phayao fault zone
C		<ul style="list-style-type: none"> (i) Prae and Uttaradit province, Thailand (ii) South of Luang Prabang, Laos
C		<ul style="list-style-type: none"> (i) Northeast of Mong Pan, Myanmar (ii) Myanmar-Laos border, near Mae Chan and Mae Ing fault zone (iii) Chiangmai province, Thailand (iv) Tak and Chiang Mai, Thailand
C		<ul style="list-style-type: none"> (i) Thailand-Myanmar border near Chiang Mai province, Thailand and Mong Pan, Myanmar in Mengxing fault zone (ii) Thailand-Laos border near Chiang Rai, Thailand and west of Luang Prabang

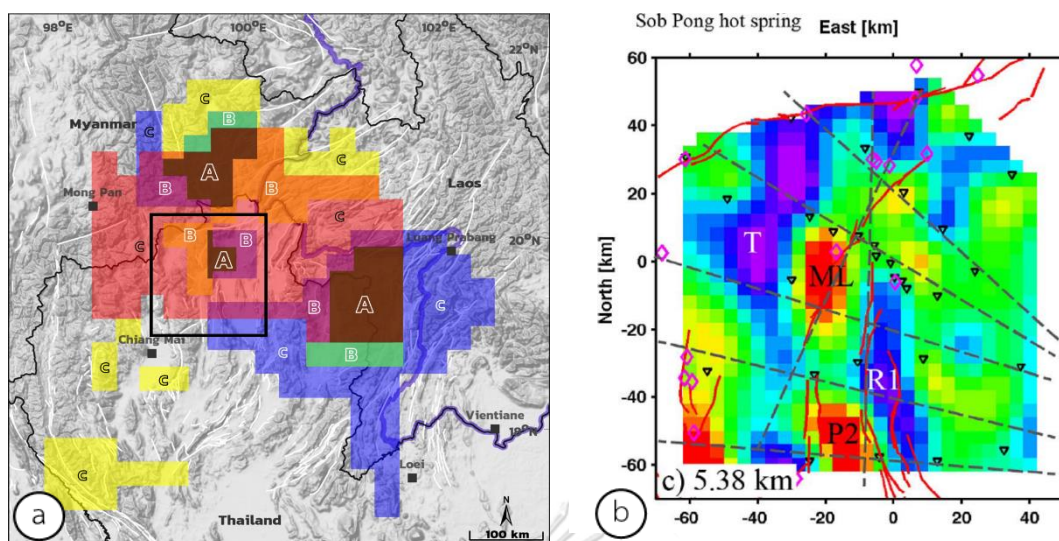


Figure 7.19. The photos show (a) the study area focuses on the TLMB overlay with the spatial distribution of b value, Z value, and RTL score anomalies. The transparency color area identifies the prospective area. (b) A photo of 3-D magnetotelluric imaging at 5.38 km depth slice of the final inverted model. The color bar is the \log_{10} resistivity in Ω m. (Boonchaisuk et al., 2017)

CHAPTER 8

CONCLUSION

The purpose of this study was to use the earthquake activity, seismotectonic stress, seismic pattern, seismicity rate change, and seismic quiescence methods to investigate the statistical seismology of the TLMB region prior to the occurrence of nineteen earthquakes and then to determine the prospective areas of upcoming earthquakes along the TLMB using the most recent seismicity data. The findings should aid in limiting the possible locations of future earthquakes. The acquired results and discussion contribute to the following conclusion:

i) After improving the earthquake catalogue from TMD by declustering and GENAS, the cumulative number rate trend is straighter and indicates the completeness of seismicity.

ii) From the earthquake activity, the maximum magnitude of around 6.3 M_L in 30 years and 6.7 M_L in 50 years can occur in the area from west of Mong Pan, Myanmar, to Northeast of Myanmar and South of Luang Prabang, Laos, and conform with the previous research.

iii) The return period of the earthquake with the M_L of 4.0, 5.0, 6.0, and 7.0 were 1, 5, 20, and 75 years at the border of three countries covering the northeastern part of Mong Pan, Myanmar, and the southwestern part of Luang Prabang, Laos which similar to previous research.

iv) The probability of occurrence of the earthquake with M_L of 4.0, 5.0, 6.0, and 7.0 are 100%, 20-60%, 0-20%, and 0%, respectively, at the border of three countries covering the eastern part of Mong Pan, Myanmar, the southwestern part of Luang Prabang, Laos covering the east of Chiangmai, Thailand and conform with the previous research.

v) The seismic pattern shows the D_c value is varied from 0.155-0.175, defined as an area source of an earthquake, indicating the fault plane following the tectonic setting in this area

vi) The tectonic stress in the present day shows the prospective areas in the northern region of Mong Pan and the Pak Beng-Luang Prabang dams. In this case, the low b-value area shows the seismotectonic stress that may shift from the west to the east of the TLMB.

vii) The Z-value investigation using the characteristic parameters the number of the earthquake (N) = 25 events and time window (T_w) = 1.5 years and discovered thirteen seismicity precursors, which is a time duration between the detection quiescence stage with the strong-to-major earthquake occurrences during the retrospective temporal investigation

viii) Moreover, the Z-value retrospective spatial investigation shows that the prospective area in the eastern portion of Mong Pan, Myanmar; Chiang Rai province, Thailand, in the Mengxing fault zone and the Mae Chan fault zone; Nan province, Laos, which includes the Pua and Dien Bien Fu fault zones; and Chiangmai and Tak provinces. Moreover, the distribution of Z anomalies related to the earthquake's epicentre in the case study.

ix) For the stochastic test of Z value, the calculated probability was 44.73%, indicating that the Z values obtained in this study are slightly significant and may not result from random events.

x) The RTL algorithm using the characteristic parameters distance r_0 of 90 km ($R_{max} = 180$ km) and time t_0 of 2 years ($T_{max} = 4$ years) and discovered nine seismicity precursors, which is a time duration between the detection quiescence stage with the nineteen strong-to-major earthquake occurrences during the retrospective temporal investigation

xi) Moreover, the RTL score retrospective spatial investigation shows that the prospective area is along the TLMB are the northern portion of Chiang Mai city, southwest of Luang Prabang with the Dien Bien Fu fault zone, as well as an extra area in Nan province of Thailand in the Pua fault zone.

xii) The correlation coefficient of the RTL parameters demonstrates that the RTL anomalies discovered before the earthquake are not an artifact caused by parameter selection showing the significance of the precursory of seismic quiescence.

xiii) It forecasted the prospective area from all of the precursors and defined it as the anomalous areas that overlap with each other with a grade of A, B, or C. The most dangerous area is grade A, which is (i) the border between Myanmar and Thailand in the Mengxing fault zone, (ii) The province of Chiang Rai, Thailand, is situated in the Phayao and Mae Chan fault zone, (iii) A large area in Nan province, Thailand, near the Pua fault zone and southwest of Luang Prabang, Laos, including the Dien Bien Fu fault zone.



REFERENCES

- Ahamed, A., and Bolten, J. D. 2017. A MODIS-based automated flood monitoring system for southeast asia. International Journal of Applied Earth Observation and Geoinformation 61: 104-117.
- Aki, K. 1981. A Probabilistic Synthesis of Precursory Phenomena. Earthquake Prediction, pp. 566-574.
- Bachmann, D. 2001. Precursory seismic quiescence: two methods of quantifying seismicity rate changes and an application to two northern Californian mainshocks. M. Sc. Thesis.
- Bayrak, Y., and Bayrak, E. 2012. Regional variations and correlations of Gutenberg–Richter parameters and fractal dimension for the different seismogenic zones in Western Anatolia. Journal of Asian Earth Sciences 58: 98-107.
- Boonchaisuk, S., Noisagool, S., Amatyakul, P., Rung-Arunwan, T., Vachiratienchai, C., and Siripunvaraporn, W. 2017. 3-D magnetotelluric imaging of the Phayao Fault Zone, Northern Thailand: Evidence for saline fluid in the source region of the 2014 Chiang Rai earthquake. Journal of Asian Earth Sciences 147: 210-221.
- Chen, C.-C., and Wu, Y.-X. 2006. An improved region-time-length algorithm applied to the 1999 Chi-Chi, Taiwan earthquake. Geophysical Journal International 166(3): 1144-1148.
- Chouliaras, G. 2009. Investigating the earthquake catalog of the National Observatory of Athens. Natural Hazards and Earth System Sciences 9
- Council, N. R. 1976. Predicting Earthquakes: A Scientific and Technical Evaluation, With Implications for Society. Washington, DC: The National Academies Press. [in English]
- Di Giovambattista, R., and Tyupkin, Y. 2000. Saptial and temporal distribution of seismicity before the Umbria-Marche September 26,1997 eartquakes. Journal of Seismology 4: 589-598.

- Felzer, K., Abercrombie, R., and Ekstrom, G. 2004. A Common Origin for Aftershocks, Foreshocks, and Multiplets. Bulletin of The Seismological Society of America - BULL SEISMOL SOC AMER 94: 88-98.
- Gambino, S., Laudani, A., and Mangiagli, S. 2014. Seismicity pattern changes before the M= 4.8 Aeolian Archipelago (Italy) earthquake of August 16, 2010. The Scientific World Journal 2014
- Grassberger, P., and Procaccia, I. 1983. Measuring the strangeness of strange attractors. Physica D: Nonlinear Phenomena 9(1): 189-208.
- Gutenberg, B., and Richter, C. F. 1944. Frequency of earthquakes in California. Bulletin of the Seismological Society of America 34: 185-188.
- Habermann, R. 1983. Teleseismic detection in the Aleutian Island arc. Journal of Geophysical Research: Solid Earth 88(B6): 5056-5064.
- Habermann, R. E. 1987. Man-made changes of seismicity rates. Bulletin of the Seismological Society of America 77(1): 141-159.
- Huang, H.-C., Huang, S.-W., and Chiu, H.-C. 2005. Observed evolution of linear and nonlinear effects at the Dahan downhole array, Taiwan: analysis of the September 21, 1999 M 7.3 Chi-Chi earthquake sequence. pure and applied geophysics 162(1): 1-20.
- Huang, J., and Zhao, D. 2004. Crustal heterogeneity and seismotectonics of the region around Beijing, China. Tectonophysics 385(1-4): 159-180.
- Huang, Q. 2006. Search for reliable precursors: A case study of the seismic quiescence of the 2000 western Tottori prefecture earthquake. Journal of Geophysical Research: Solid Earth 111(B4)
- Huang, Q., and Ding, X. 2012. Spatiotemporal variations of seismic quiescence prior to the 2011 M 9.0 Tohoku earthquake revealed by an improved Region–Time–Length algorithm. Bulletin of the Seismological Society of America 102(4): 1878-1883.
- Huang, Q., and Nagao, T. 2002. Seismic Quiescence before the 2000 M = 7.3 Tottori earthquake. Geophysical Research Letters 29(12): 19-1-19-4.

- Huang, Q., Öncel, A., and Sobolev, G. 2002. Precursory seismicity changes associated with the $M_w=7.4$ 1999 August 17 Izmit (Turkey) earthquake. Geophysical Journal International - GEOPHYS J INT 151: 235-242.
- Huang, Q., and Sobolev, G. A. 2002. Precursory seismicity changes associated with the Nemuro Peninsula earthquake, January 28, 2000. Journal of Asian Earth Sciences 21(2): 135-146.
- Huang, Q., Sobolev, G. A., and Nagao, T. 2001. Characteristics of the seismic quiescence and activation patterns before the $M=7.2$ Kobe earthquake, January 17, 1995. Tectonophysics 337(1): 99-116.
- Huang, R., Li, and WL. 2009. Analysis of the geo-hazards triggered by the 12 May 2008 Wenchuan Earthquake, China. Bulletin of Engineering Geology and the Environment 68(3): 363-371.
- Ishimoto, M. 1939. Observations of earthquakes registered with the microseismograph constructed recently. Bull. Earthq. Res. Inst. 17: 443-478.
- Kagan, Y., and Knopoff, L. 1980. Spatial distribution of earthquakes: the two-point correlation function. Geophysical Journal International 62(2): 303-320.
- Katsumata, K. 2011. Precursory seismic quiescence before the $M_w=8.3$ Tokachi-oki, Japan, earthquake on 26 September 2003 revealed by a re-examined earthquake catalog. Journal of Geophysical Research 116(B10): 1-16.
- McCann, W., Nishenko, S., Sykes, L., and Krause, J. 1979. Seismic gaps and plate tectonics: seismic potential for major boundaries. Earthquake prediction and seismicity patterns, pp. 1082-1147. Springer.
- Mignan, A., and Di Giovambattista, R. 2008. Relationship between accelerating seismicity and quiescence, two precursors to large earthquakes. Geophysical Research Letters 35: 15306.
- Nagao, T., Takeuchi, A., and Nakamura, K. 2011. A new algorithm for the detection of seismic quiescence: introduction of the RTM algorithm, a modified RTL algorithm. Earth, planets and space 63(3): 315-324.
- Nuannin, P. 2005. Spatial and temporal b-value anomalies preceding the devastating off coast of NW Sumatra earthquake of December 26, 2004. Geophysical Research Letters 32(11): L11307.

- Ornthammarath, T. 2015. The 5 May 2014 M W 6.1 Mae Lao (Northern Thailand) earthquake: Interpretations of recorded ground motion and structural damage. Earthquake Spectra
- Öztürk, S., and Bayrak, Y. 2011. Spatial variations of precursory seismic quiescence observed in recent years in the eastern part of Turkey. Acta Geophysica 60: 92-118.
- Pailoplee, S. 2014a. Earthquake Catalogue of the Thailand Meteorological Department — A Commentary. Journal of Earthquake and Tsunami 08(05)
- Pailoplee, S. 2014b. Mapping b-Value Anomalies Along the Indonesian Island Chain: Implications for Upcoming Earthquakes. Journal of Earthquake and Tsunami 08: 1-11.
- Pailoplee, S., Channarong, P., and Chutakositkanon, V. 2013. Earthquake Activities in the Thailand-Laos-Myanmar Border Region: A Statistical Approach. Terrestrial, Atmospheric and Oceanic Sciences 24(4-2): 721-730.
- Pailoplee, S., and Charusiri, P. 2015. Probabilistic analysis of the seismic activity and hazard in northern Thailand. Geosciences Journal 19
- Pailoplee, S., and Choowong, M. 2013. Probabilities of earthquake occurrences in Mainland Southeast Asia. Arabian Journal of Geosciences 6
- Pailoplee, S., and Choowong, M. 2014. Earthquake frequency-magnitude distribution and fractal dimension in mainland Southeast Asia. Earth, Planets and Space 66(1): 8.
- Pailoplee, S., Sugiyama, Y., and Charusiri, P. 2009. Deterministic and probabilistic seismic hazard analyses in Thailand and adjacent areas using active fault data. Earth Planets and Space 61: 1313-1325.
- Petersen, M. D., Dewey, J., Hartzell, S., Mueller, C., Harmsen, S., Frankel, A., and Rukstales, K. 2004. Probabilistic seismic hazard analysis for Sumatra, Indonesia and across the Southern Malaysian Peninsula. Tectonophysics 390(1-4): 141-158.
- Puangjaktha, P., and Pailoplee, S. 2016. Evolution of Precursory Seismic Quiescence of the Mw-6.8 Nam Ma Earthquake, Thailand-Myanmar Borders. Bulletin of Earth Sciences of Thailand 7: 1-15.

- Puangjaktha, P., and Pailoplee, S. 2018. Application of the region–time–length algorithm to study of earthquake precursors in the Thailand–Laos–Myanmar borders. Journal of Earth System Science 127
- Rudolf-Navarro, A., Diosdado, A., and Angulo-Brown, F. 2010. Seismic quiescence patterns as possible precursors of great earthquakes in Mexico. International Journal of the Physical Sciences 5: 651-670.
- Scholz, C. H. 1968. Mechanism of creep in brittle rock. Journal of Geophysical Research (1896-1977) 73(10): 3295-3302.
- Sobolev, G. 1995. Fundamentals of earthquake prediction.
- Sobolev, G. 1999. Precursory phases, seismicity precursors, and earthquake prediction in Kamchatka. Volcanology and Seismology 6: 615-627.
- Sobolev, G. A., and Tyupkin, Y. S. 1997. Low-seismicity precursors of large earthquakes in Kamchatka. Volcanology and Seismology 18(4): 433-445.
- Sorbi, M. R., Nilfouroushan, F., and Zamani, A. 2012. Seismicity patterns associated with the September 10th, 2008 Qeshm earthquake, South Iran. International Journal of Earth Sciences 101(8): 2215-2223.
- Sukrungsri, S., and Pailoplee, S. 2017. Precursory seismic quiescence along the Sumatra-Andaman subduction zone: past and present. Journal of Seismology 21
- Tosi, P. 1998. Seismogenic structure behaviour revealed by spatial clustering of seismicity in the Umbria-Marche Region (Central Italy). Annals of Geophysics 41(2)
- Wang, J., Zhao, D., and Yao, Z. 2013. Crustal and uppermost mantle structure and seismotectonics of North China Craton. Tectonophysics 582: 177-187.
- Wang, Y., Lin, Y. n., Simons, M., and Tun, S. T. 2014a. Shallow Rupture of the 2011 Tarlay Earthquake (Mw 6.8), Eastern Myanmar. Bulletin of the Seismological Society of America 104: 2904-2914.
- Wang, Y., Lin, Y. N. N., Simons, M., and Tun, S. T. 2014b. Shallow Rupture of the 2011 Tarlay Earthquake (Mw 6.8), Eastern Myanmar. Bulletin of the Seismological Society of America 104(6): 2904-2914.
- Wiemer, S. 2001. A Software Package to Analyze Seismicity: ZMAP. Seismological Research Letters 72(3): 373-382.

- Wiemer, S., and Wyss, M. 1994. Seismic quiescence before the landers ($M = 7.5$) and big bear ($M = 6.5$) 1992 earthquakes. Bulletin of the Seismological Society of America 84: 900-916.
- Woessner, J. 2005. Assessing the Quality of Earthquake Catalogues: Estimating the Magnitude of Completeness and Its Uncertainty. Bulletin of the Seismological Society of America 95(2): 684-698.
- Wyss, M. 1973. Towards a Physical Understanding of the Earthquake Frequency Distribution. Geophysical Journal of the Royal Astronomical Society 31(4): 341-359.
- Wyss, M. 1991. Evaluation of Proposed Earthquake Precursors. Eos, Transactions American Geophysical Union 72(38): 411-411.
- Wyss, M., Sammis, C., Nadeau, R., and Wiemer, S. 2004. Fractal Dimension and b-Value on Creeping and Locked Patches of the San Andreas Fault near Parkfield, California. Bulletin of the Seismological Society of America 94: 410-421.
- Zúñiga, F. R., and Wiemer, S. 1999. Seismicity patterns: Are they always related to natural causes? pure and applied geophysics 155(2): 713-726.



จุฬาลงกรณ์มหาวิทยาลัย
CHULALONGKORN UNIVERSITY

VITA

NAME Ms. Manunchaya Neanudorn

DATE OF BIRTH 4 June 1995

PLACE OF BIRTH Bangkok, Thailand

INSTITUTIONS ATTENDED 2007 Smithichote school
2010 Horwang school
2013 Horwang school
2017 Bachelor of Science in Geology, Chulalongkorn University

HOME ADDRESS 1124/5 Soi. Paholyothin 32, Chamkasem, Chatuchak, Bangkok 10300 Thailand

PUBLICATION Neanudorn, M., and Pailoplee, S. 2022. Simultaneous Analysis of Seismicity Rate Change and Quiescence in the Thailand-Laos-Myanmar Borders: An Updated Prospective Earthquake Source. Bulletin of Earth Sciences of Thailand 14(1): 97-109.